HUNGARIAN UNIVERSITY OF AGRICULTURE AND LIFE SCIENCES

ASSESSMENT OF NOVEL ADSORBENTS FOR THE SEQUETRATION OF POLLUTANTS FROM AQUEOUS SOLUTIONS – A SUSTAINABLE APPROACH TOWARD ENVIRONMENTAL MANAGEMENT

DOI: 10.54598/007380

A

Dissertation Submitted

In Partial Fulfilment of the Requirement

for the Degree of

DOCTOR OF PHILOSOPHY IN

ENVIRONMENTAL SCIENCES

By

Ibrahim Ghaleb Al-Labadi

Under the Guidance of

Assoc. Prof. Dr. Márk Horváth

Assistant prof. Alaa Ghidan

Institute of Environmental Sciences

Hungarian University of Agriculture and Life Sciences (MATE), Gödöllő, Hungary

2025

Hungarian University of Agriculture and Life Sciences, Hungary

Magyar Agrár- és Élettudaományi **Egyetem (MATE)**

The Ph.D. School

Name: Ibrahim Ghaleb Al-Labadi

Discipline: Environmental Engineering Chemistry

Doctoral School: Ph.D. School of Environmental Sciences

Head: Professor Dr. Michéli Erika Csákiné
Head of Doctoral School, DSc
Corresponding Member of Hungarian Academy of Sciences
MATE, Institute of Environmental Sciences

Supervisor (s): Dr. Márk Horváth
Associate Professor, Ph.D.
MATE, Institute of Environmental Sciences
Department of Environmental Analysis and
Environmental Technology.

Dr. Alaa Ghidan/External Co-advisor
Assistant Professor, Ph.D. Assistant Professor of Nanotechnology
& Microbiology Department of Pharmacy Aqaba University of Technology.

…….
Approval of Head of Doctoral School

…….
Approval of Supervisor (s)

DECLARATION

This dissertation is my original work and has not been presented for a degree at any other university. No part of this dissertation may be reproduced without prior permission of the author and/or the Hungarian University of Agriculture and Life Sciences**.**

_____ Date_____

Ibrahim Ghaleb Al-Labadi

DECLARATION BY SUPERVISORS

This dissertation has been submitted with our approval as supervisors.

_____ Date_____

Dr. Márk Horváth

Associate Professor, Ph.D

MATE, Institute of Environmental Sciences

Department of Environmental Analysis and Environmental Technology

_____ Date_____

Dr. Alaa Ghidan

Assistant Professor, PhD
Aqaba University of Technology /Department of Pharmacy.

DEDICATION

First and foremost, I dedicate this work to our parents, whose unwavering belief in me, along with their continuous financial and emotional support, has sustained me through every challenge. They have been there through every hardship, never leaving my side when I felt like giving up and have planted and nurtured the seed of knowledge in my mind. I also dedicate this work to my loving wife Alaa, whose unconditional support and profound inspiration have been my guiding light.

To my son Omar, the light of my life and to my daughter Masa, who fills my heart with joy every day.

To my brothers and sisters, for their endless encouragement and support.

To myself, for facing each challenge with patience and courage, and for relentlessly pursuing my life's dream until, by the will and support of God, it finally came true.

To you, dear reader, for making this journey worthwhile.

And to everyone who helped make this journey possible.

TABLE OF CONTENTS

LIST OF FIGURES

LIST OF TABELS

LIST OF ABBREVIATIONS

Abbreviations	Item Means
AAS	Atomic Absorption Spectrometry
AES	Atomic Emission Spectrometer
AFS	Atomic Fluorescence Spectrometry
AFM	Atomic Force Microscopy
AG	Gibbs Free Energy
AI	Artificial Intelligence
ANNs	Artificial Neural Networks
APDP	Atmospheric Pressure Discharge Plasma
ARE	Average Relative Error
AS	Entropy
BET	Brunauer-Emmett-Teller
BJH	Barrett-Joyner-Halenda
BOD	Biochemical Oxygen Demand
CNCs	Cellulose Nanocrystals
CNFs	Cellulose Nanofibrils
COD	Chemical Oxygen Demand
D-R	Dubinin-Radushkevich
DLS	Dynamic Light Scattering
DSC	Differential Scanning Calorimetry
DTA	Differential Thermal Analysis
EABS	Sum Of Absolute Errors
EDS	Energy-Dispersive X-Ray Spectroscopy
ERRSQ	Sum Square Error
FESEM	Field Emission Scanning Electron Microscopy
EU	European Union
FTIR	Fourier Transform Infrared Spectroscopy
GIS	Geographic Information Systems
HPLC	High-Performance Liquid Chromatography
HYBRID	Hybrid Fractional Error Function
ICP-AES	Inductively Coupled Plasma-Atomic Emission Spectrometry
ICP-OES	Inductively Coupled Plasma-Optical Emission Spectrometry
IDP	Intraparticle Diffusion Model
InKc	Natural Logarithm Of Kc
IPD	Intra-Particle Diffusion
IUPAC	International Union Of Pure And Applied Chemistry
Kc	Equilibrium Constant
K_{dr}	Dubininâ€“Radushkevich Constant
K_f	Freundlich Constant
Kp	Intraparticle Diffusion Rate Constant

LCR	Lifetime Carcinogenic Risk
LCB	Lignocellulosic Biomass
LIBS	Laser-Induced Breakdown Spectrometry
LNP	Lignin Nanoparticles
LSB	Lignocellulosic Biomass
MBR	Membrane Bioreactor
ML	Machine Learning
MLR	MLR Modelling
MPSD	Marquardt's Percent Standard Deviation
NF	Nanofiltration
NS	Nano Cellulose
OES	Optical Emission Spectrometry
PFO	Pseudo-First Order
pH_{pzc}	Point Of Zero Charge Ph
PSO	Pseudo-Second Order
PV	Photovoltaic
Qe	Adsorption Capacities
R^2	Coefficient Of Determination
RBC	Rotating Biological Contactor
RO	Reverse Osmosis
RS	Remote Sensing
RT	Gas Constant * Temperature
SEM	Scanning Electron Microscopy
SRE	Standard Deviation Of Relative Errors
SSE	Sum Of the Errors Squared
TDS	Total Dissolved Solids
TEM	Transmission Electron Microscopy
TG	Thermogravimetry
THQ	Target Hazard Quotient
TPR	Temperature Programmed Reduction
TPO	Temperature Programmed Oxidation
UASB	Upflow Anaerobic Sludge Blanket
UV	Ultraviolet
UV-vis	Ultraviolet-Visible Spectroscopy
VSM	Vibrating Sample Magnetometry
XRD	X-Ray Diffraction
XPS	X-Ray Photoelectron Spectroscopy

INTRODUCTION OF THE WORK AND ITS AIMS

This introductory chapter establishes the foundational context for the present investigation. It commences by articulating the significance of the research and delineating the central problem, which is substantiated with relevant supporting data. Subsequently, the primary aim and principal objectives of the study are precisely formulated. The chapter concludes with an overview of the dissertation organizational structure, followed by a concise review of the foundational literature pertaining to the core topics under examination.

1. Introduction

The remediation of heavy metals and pharmaceutical compounds from industrial wastewater is a subject of considerable environmental significance, attributable to their persistence within aquatic systems and the resultant detrimental impacts they exert on the environment. Population growth and its associated anthropogenic effects is the fundamental reasons for this global issue. The enduring presence of heavy metals and pharmaceutical contaminants within aquatic ecosystems, coupled with the adverse consequences they precipitate, underscores the critical environmental importance of their removal from industrial wastewater streams.(Li et al., 2023). On the other hand, Potential Toxic Elements (PTEs) such as Zn, Pb, Cu, and Cd are known for their hazardous and detrimental effects on human health and various ecologies. PTEs on the other hand, are characterized by their bioaccumulation, toxicity, nonbiodegradability, Uncontrolled release of these harmful pollutants into water resources and/or insufficient pretreatment of wastewater along with global warming and shortage of available freshwater resources have all contributed to make the problem much worse especially in developing countries. Indeed, over 40% of the world's lakes and rivers have been contaminated by PTEs (Zamora-Ledezma et al., 2021). Moreover, a recent investigation by WHO reveals that around 2.2 M individuals die each year due to illnesses caused by the ingestion of contaminated drinking water (Rind et al., 2024). To tackle this issue, many technologies have been applied for the removal of these famous types of pollutants such as chemical precipitation, membrane filtration, ion exchange, electrocoagulation. and adsorption. Nevertheless, several researchers have acknowledged the potential disadvantages of the aforementioned methods, including their expensive nature, generation of hazardous sludge, and their potential inability to effectively remove PTEs at low metal concentrations (K. Mishra et al., 2024).

In contrast to these limitations and obstacles, adsosorption has been identified as a very effective and easily implementable approach for the bioremediation of polluted water bodies by eliminating PTEs and CFX (Bukhari et al., 2023). The general global research trend is now focused on the elaboration of applying inexpensive, ecofriendly, available, efficient and pollutant-selective adsorbents.

In this dissertation, two different adsorbents have been used namely: Norway Spruce Wood Residue (NSWR) for the removal of four heavy metals (Pb,Zn,Cu, Cd) and modified coal with (H_2SO_4 and HNO_3) for the removal of Ciproflaxacin (CFX).These two adsorbents are characterized by destinctive properties made them potentially good options.

he treatment of laundry water presents a pertinent example of these wastewater challenges. Laundry wastewater, originating from industrial laundries and commercial establishments, is characterized by significant levels of turbidity, COD, BOD, anionic surfactants, and high pH, making it unsuitable for direct discharge or reuse without treatment (Kitte et al., 2019). The complex composition, influenced by various cleaning products and textile types, contributes to potential aesthetic losses and ecosystem toxicity (Crini et al., 2024). Public health aspects, including the presence of xenobiotic organic compounds and heavy metals, further complicate its management and potential reuse (Kitte et al.,

2019). For instance, laundry greywater can contain heavy metals, nitrogen, and phosphate, potentially causing toxic effects and biodiversity changes. In regions like Jordan, where water scarcity is a concern, the reuse potential of such wastewater is often overlooked despite its significant contribution to available water resources. This highlights the critical need for effective and sustainable treatment technologies capable of addressing such complex wastewater streams.

Both of these adsorbents were characterized qnd tested under various influencing factors, and kinetically thermodynamically and isothermally modelled. Furthermore,NSWR was used as a precursor of nanocrystal material which was used for the treatment of real sample taken from laundry wastewater shop in Jordan .In addition, Madaba landfill`s- soil was evaluated for its cadmium content and for the assessment of the vulnerability of groundwater Simplified Groundwater Vulnerability Index (SGVI) method, which depends on the affecting weighs of 7 various influencing parameters was applied.

Aim of the study

This research was designed to achieve two principal goals. The primary objective was to synthesize a novel bio sorbent, conduct its comprehensive characterization, and subsequently assess its performance as a viable adsorbent for eliminating specific heavy metal ions [Pb (II), Cd (II), Cu (II), and Zn (II)] from aqueous solutions. A second, parallel objective involved the synthesis and characterization of a modified version of this biosorbent. The efficacy of this modified material was then evaluated for the purpose of removing ciprofloxacin, which was investigated as a representative example of a pharmaceutical pollutant. My preference for CFX as the target adsorbate was due to their broad use and prevalence in wastewater, particularly in developing countries. The reason behind choosing the forementioned metals because they normally found together in nature. Additionally, this dissertation provides a preliminary assessment for the contamination level by Cd in a local landfill soil and presents an evaluation of the hydrological vulnerability by adopting proposed sustainable environmental management based on green chemistry approach.

1.1. Study objectives

Based on the problem statement, the following objectives were identified:

1. To experimentally determine the chemical composition and physical characteristics of the NSWR sample.
2. To evaluate the efficacy of untreated, sustainable, cost-effective, and widely available wood-based materials, functioning as biosorbents, for sequestering four specific potable heavy metals (Cd, Cu, Pb, Zn) within a competitive multi-element aqueous environment.
3. Twofold aim :first to put forward an eco-friendly way for capturing of PTEs and second to reduce the accumlation of the bio-waste “NSWR” resulted from agriculture .This research work represents part of project.
4. To investigate the impact of various operational factors—specifically pH, equilibrium duration, initial metal ion concentration, particle size distribution, temperature, adsorbent dosage, agitation speed, and sorbent loading—in order to identify the optimal conditions for achieving the highest possible removal of heavy metal ions using the novel biosorbent materials.
5. Investigate of adsorption kinetics and isothermal thermodynamics of the NSWR.
6. Explore the efficiency of a synthesised nano-absorbent from NSWR for the remediation of a real wastewater laundry sample collected from a laundry shop in Madaba city- Jordan.
7. Evaluate the usefulness of applying AI regression models for predicting adsorption performance and elucidating underlying mechanisms.

8. Evaluate the economic and adsorption potential of using modified coal with H_2SO_4 and HNO_3 to remove ciprofloxacin from industrial effluent.
9. To fully characterize the modified adsorbent i.e. coal and modified coal with H_2SO_4 and HNO_3
10. To undertake a comprehensive performance evaluation of the synthesized adsorbents by benchmarking the removal efficiency of heavy metals by NSWR and ciprofloxacin by the modified coal against other adsorbents reported in the literature. This evaluation includes the application of advanced isotherm models to elucidate the drug's adsorption mechanism and an assessment of the modified coal's potential for regeneration and cyclical reuse.
11. To conduct an environmental site assessment of a landfill in Madaba, Jordan, by utilizing Geographic Information Systems (GIS) and Remote Sensing (RS). This investigation will quantify the extent of Cadmium (Cd) soil contamination, evaluate the potential risk to groundwater resources relative to international standards, and subsequently, propose a detailed management and remediation strategy for the contaminated site (ex. applying NSWR as liner material).

The objective is to ascertain the influence of diverse process parameters, including but not limited to solution pH, adsorption equilibrium time, the initial concentration of metal ions, variations in particle size, thermal conditions, sorbent mass, mixing velocity, and the concentration of the adsorbent itself, to establish the most favourable operational settings for maximizing the uptake of heavy metal ions by the newly developed bio sorbents. Another possible advantage is that this dissertation will provide insight into the utilization of modified coal for the removal ciprofloxacin from wastewater with emphasis on applying along with full characterization of modified coal as an adsorbent. Moreover, the dissertation provides a possible environmental management approach to enhance the performance of a local landfill.

1.2. Research hypotheses and questions

Hypothesis 1: Acid-modified coal has superior efficacy in the removal of ciprofloxacin from aqueous solutions compared to traditional adsorbents.
Hypothesis II: Norway spruce wood residue (NSWR) exhibits a high adsorption capacity for the selective removal of heavy metals (Zn, Cu, Pb, Cd) from water.
Hypothesis 3: NSWR is effective in decontaminating actual wastewater samples from washing operations that contain various heavy metal pollutants.
Hypothesis 4: Nano-NSWR will exhibit markedly superior adsorption capabilities relative to raw NSWR for the removal of heavy metals.
Hypothesis 5: NSWR can be effectively employed as a landfill liner material to inhibit heavy metal leaking into groundwater (**currently working on this issue, results are still unpublished**).
Hypothesis 6: Artificial intelligence models can precisely predict adsorption kinetic behaviour than conventional mathematical models.

Hypothesis 7: Modifying coal with H_2SO_4 is economically viable compared to conventional adsorbent (activated carbon).

- **Structure of the Dissertation**

This dissertation is methodically structured into six detailed chapters; each focusing on unique but interrelated facets of new adsorbent creation and use for sustainable environmental management. The study advances from foundational principles to the production of novel materials, culminating in practical applications, as illustrated in the below diagram.

Chapter 1: Introduction and Research Foundation

Defines the research context, rationale, and aims. Evaluates the environmental effects of heavy metals and ciprofloxacin. Analyzes contemporary therapeutic technology and identifies significant research deficiencies.

Chapter 2: Literature Review and Theoretical Framework

Offers an exhaustive analysis of adsorption-based remediation technologies. Comprehensive theoretical framework encompassing adsorption theory, surface chemistry, and mass transfer mechanisms.

Chapter 3: Materials and Methods

Details the synthesis of raw and nanocrystalline-enhanced NSWR for the removal of heavy metals, as well as acid-modified coal for the adsorption of ciprofloxacin. Describes characterization techniques (XRD, FTIR, SEM-EDS, BET) and presents the integration of machine learning.

Chapter 4: Results and Discussion

Analyze parameter optimization. Introduces nanocrystalline technology that attains a 1.8-fold increase in capacity. Exhibits a significant advancement in AI integration.

Chapter 5: Conclusions and Recommendations

Integrates research contributions, limits, recommendations, and outlines future views.

Chapter 6: New Scientific Results

Presents the new contributions to the scientific community

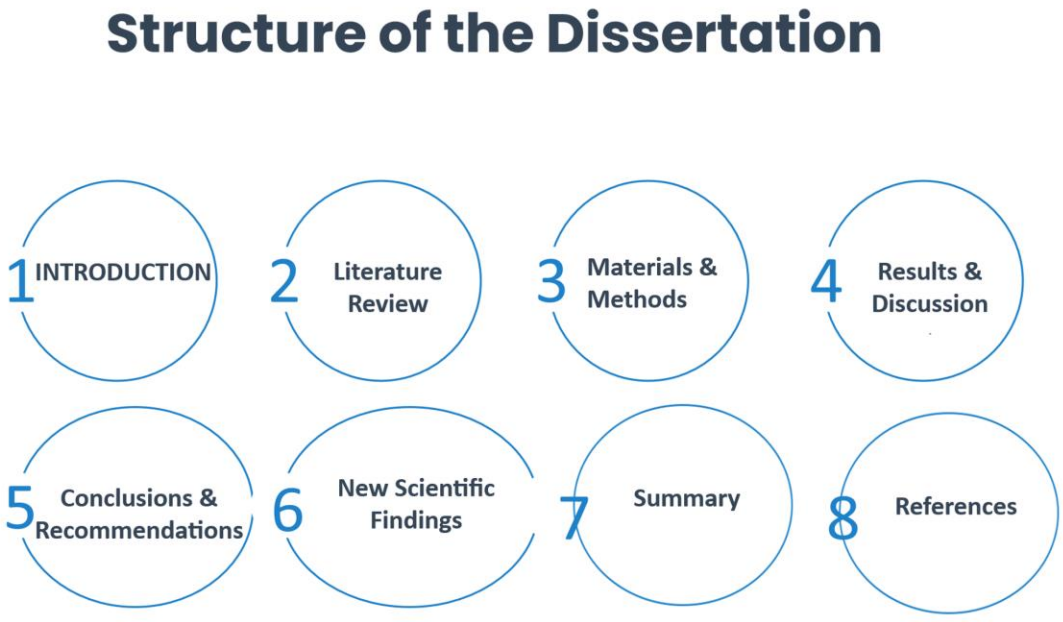

2. Literature Review

2.1. A closer Look at Global Water Resources

The Earth's hydrologic cycle, often referred to as the water cycle, is a fundamental biogeochemical process that tracks the movement of water molecules across the atmosphere, terrestrial surfaces, subsurface strata, and oceanic bodies. The planet's total water endowment is fixed, with the freshwater component essential for agricultural, industrial, and domestic applications representing a mere 2.5% of the global water volume. Given that the predominant fraction of this freshwater is sequestered in polar ice caps and glaciers, the proportion readily accessible for human consumption as surface or groundwater at any given moment is critically limited to approximately 0.8% of the Earth's total water mass (Van Brahana, 2020). Water is an extremely important substance for all life (including humans) on our planet. Water exists in large amounts, as there are aroundan estimated 1.386 billion km³ (1.386 x 10^9 km³) (Council et al., 2007) km^3 of water on Earth in three of its three physical states: solid, liquid, and gas. It differs in its abundance across the following contexts: seas and oceans (97.24%), glaciers and icecaps (2.14%), groundwater (0.61%), freshwater lakes (0.009%), inland seas (0.008%), soil (0.005%), atmosphere (0.001%), and lotic systems (0.0001%).Water may seem bountiful, but only under 1% of the Earth's water can be used to meet human demands (Bănăduc et al., 2022)**.**

Types of Water Pollutants

Pollutants, broadly categorized into inorganic, organic, biological, pharmaceutical, and heavy metal types (as depicted in **Figure 2-1**), command significant environmental concern owing to the detrimental effects they impose. The correlation between escalating global populations and environmental contamination is demonstrably and directly proportional; as the human population surges, so too does the quantity of potentially toxic substances introduce into ecosystems. Consequently, pollution has emerged as a critical environmental challenge confronting the planet.

Figure 2-1. Different types of pollutants in wastewater.

2.2.Environmental Impact of Pharmaceutical Pollutants

Recently, everyone knew that the pharmaceutical residues, which usually enter water bodies, cause environmental destruction and raise several human health concerns. The challenge, in this case, is that the pollutants are not only widespread, but they are also numerous, eventually harming the ecosystems' functions. Along with consumers and companies in the pharmaceutical sector, directly or indirectly, contaminating the environment by discharging active compounds of medicines back to the atmosphere during their life cycle is partly the problem These pharmaceutical pollutants intrude into oceans, inland territories, and even the atmosphere due to human activities, leading to ecosystem disturbance (**Figure 2-2**) (Alobaidi et al., 2024).Once in the air, these pollutants can be deposited back into aquatic and terrestrial ecosystems through processes such as precipitation, contributing further to the pollution load . Additionally, pharmaceutical residues can also contaminate interstitial spaces in soils, affecting the soil microbiome and altering soil chemistry. This contamination can hinder plant growth and disrupt the natural soil filtration processes, further exacerbating environmental degradation. The pollutants affect habitats of invertebrates and vertebrates. As organisms accumulate these substances at different steps through the food chain, the affected organisms suffer, and the complexity of formulating policies to deal with the drug menace includes establishing rehabilitation aims that accommodate the harmful effects of drugs. The ecological parameters such as pH of the water, soil compositions, temperature, persisting chemicals, and co-occurring pharmaceuticals are key factors accountable for expanding the compounds' persistence in the environment. The microbial consortia are one of the main microbes that will aid bioremediation processes if they enter the attenuation mechanisms via natural attenuation pathways. Human and animal health problems due to the logic activity of pharmaceutical pollutants are the long-term consequences that occur in the bodies of the animals. Mucosal microbes' participation in inducing, degrading, and transforming these compounds is essential for microbial degradation. A key impact of concomitant pollutants in the environment is that they promote the biodegradation of other pharmaceutical contaminants. Scientists have found that the combination of other pollutants, like metals, nanoparticles, pesticides, and multiple pharmacological compounds, can make naturally occurring bacteria less active or accelerate the population of microorganisms, which can produce other unexpected effects on the microbial world (Alobaidi et al., 2024).

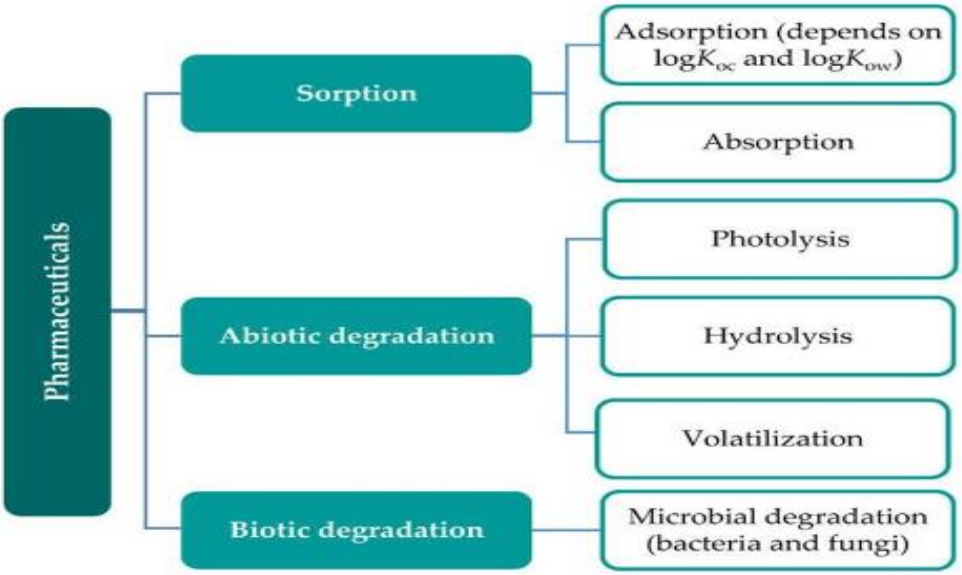

Figure 2-2. Illustrating the diverse environmental remediation pathways for pharmaceuticals.

2.2.1. Ciprofloxacin as an Example of Pharmaceutical Pollutants: Its Definition, Characteristics & Potential Health Impacts

The proliferation of pharmaceutical production facilities and the emergence of novel infectious diseases have substantially amplified the prevalence of antibiotics within aquatic environments over time. Ciprofloxacin (CFX), a distinctive second-generation fluoroquinolone antibiotic, is presently extensively utilized in both human and veterinary medicine due to its wide-spectrum efficacy against a range of microorganisms. Research indicates that approximately 80% of ingested ciprofloxacin is ultimately discharged into the environment without undergoing prior treatment. The presence of these antibiotics in water bodies exerts an adverse influence on microbial populations, and the improper disposal of surplus medications can degrade water quality. Consequently, the implementation of efficacious strategies for the removal of CFX from aquatic systems is imperative. (Shankar et al., 2024). Ciprofloxacin (CFX), a fluoroquinolone antibiotic with the chemical formula $C_{17}H_{18}FN_3O_3$, is extensively utilized for treating various infectious diseases, including those affecting the respiratory system, bones, and gastrointestinal tract, and serves as a potent antibacterial agent against both Gram-positive and Gram-negative bacilli. A significant challenge associated with CFX is its low metabolic stability; approximately 75% of an administered dose is excreted from the human or animal body as unchanged parent compounds. Consequently, CFX is frequently detected in urban and hospital sewage systems at concentrations reaching up to 150 μg/L, and in the effluent from pharmaceutical manufacturing plants at levels as high as 30 mg/L. The persistence of CFX in water, soil, and the food chain is linked to severe adverse health effects in humans, such as kidney failure, fatty liver, nausea, and headaches. Furthermore, residual CFX critically contributes to the proliferation of antibiotic resistance among common pathogens. Its ecological impact is also profound, as CFX has been shown to disrupt the aquatic nitrogen cycle and inhibit both the photosynthetic process and chloroplast replication, which in turn suppresses algal growth. Therefore, developing effective methods for the complete removal of antibiotics like CFX from aqueous environments and water supplies constitutes a formidable environmental challenge and a priority area for current research (S. M. Ibrahim et al., 2021)**.**

Ciprofloxacin (CFX) functions as a broad-spectrum antimicrobial agent, and notably, antibiotics represent the most frequently administered Prescription and Consumer Pharmaceutical Products (PCPPs). An analysis of antibiotic consumption patterns and influencing factors across 76 nations between 2000 and 2015 revealed a substantial increase. Specifically, the report indicated approximately a 65% rise in antibiotic consumption, quantified by 34.8 trillion defined daily doses, during this interval. Furthermore, this research projected a potential doubling of global antibiotic consumption by 200% in comparison to 2015 levels.

2.2.2. HPLC: Analytical Method for Ciprofloxacin Determination

High-performance liquid chromatography, or HPLC, is a sophisticated analytical instrumentation technique employed for the separation of sample constituents. This process facilitates the identification and quantification of individual components within a mixture, finding broad utility across diverse sectors such as medicine, polymer science, coatings, pharmaceuticals, and various other commercial and industrial arenas. As an established industry standard, HPLC analysis is integral to product validation, particularly for goods regulated by the FDA or subject to industrial specifications and is applicable for both qualitative and quantitative assessments. Consequently, HPLC is the

selected analytical methodology for the measurement and assay of ciprofloxacin. (Elgendy et al., 2023).

2.3. Environmental Impact of Heavy Metals

2.3.1. Definition of Heavy Metals, Types & Properties

The designation of "heavy metals" lacks a universally standardized definition, with varying criteria applied across different contexts. When density is considered, these are metallic substances possessing a density exceeding 4 or 5 g cm^{-3}. From an atomic perspective, heavy metals are often identified as those with atomic numbers greater than 20 and atomic masses exceeding 40 atomic mass units (amu), as exemplified by Calcium (Fei & Hu, 2023).A total of 35 metals warrant attention due to residential or occupational exposure, 23 of which are classified as heavy metals. Despite the absence of a definitive definition, literature generally characterizes a heavy metal as a metallic element possessing a high atomic weight and a density at least five times that of water, with atomic weights typically falling within the range of 63.5 to 200.6 amu. These metals are naturally occurring components of the Earth's crust and are ubiquitously present in varying concentrations across all ecosystems. A defining characteristic of heavy metals is their inherent resistance to biodegradation, which leads to their long-term persistence in natural settings. These elements are generally categorized into two distinct groups. The first group comprises highly toxic metals, including lead (Pb), cadmium (Cd), and arsenic (As), which are designated by regulatory bodies such as the United States Environmental Protection Agency (EPA) and the Agency for Toxic Substances and Disease Registry (ATSDR) as being among the top 20 most hazardous substances. The second group consists of essential metals such as copper (Cu), zinc (Zn), manganese (Mn), iron (Fe), nickel (Ni), and chromium (Cr) which can also become toxic above certain thresholds. A significant danger of all heavy metals is that they can be carcinogenic and exert hazardous effects even at minute, trace-level concentrations. They are prone to rapid bioaccumulation within living tissues and cannot be intrinsically degraded. Exceeding critical threshold levels, they can exert significant adverse effects on human health and various aquatic environments. Consequently, heavy metals have emerged as a prominent issue in contemporary water pollution, fostering widespread public apprehension regarding environmental and human health, and are currently recognized as a major global concern. Therefore, a comprehensive understanding of their origins, chemical transformations, leaching mechanisms, and deposition patterns is essential for mitigating the risks they present to both the environment and public well-being (Rai et al., 2019).

2.3.2. Sources, Toxicity Levels, Routes of Exposure, Health Impacts and Maximum Allowable Limits of Zn, Cu, Pb and Cd.

The presence of heavy metals in the environment is a result of their release from a wide spectrum of sources. These sources are broadly categorized as either **natural** or **anthropogenic** (human-induced), a distinction that is visually represented in **Figure 2-3**. Natural sources stem from fundamental geological and atmospheric processes, encompassing volcanic activity, the weathering of mineral-bearing rocks, and soil formation. Conversely, anthropogenic contributions, which have drastically increased the environmental burden of these elements, are primarily linked to industrial, agricultural, and urban activities such as mining, fossil fuel combustion, waste disposal, and the application of fertilizers and pesticides. This section will further elucidate the specific sources, toxicity levels, routes of exposure, and significant health impacts associated with four key heavy metals of environmental and public health concern: lead (Pb), cadmium (Cd), copper (Cu), and zinc (Zn).

Lead (Pb): Lead (Pb) is an elemental metal that persists in the environment, resistant to biodegradation, and is naturally present in comparatively low concentrations. However, atmospheric concentrations of lead are progressively escalating due to anthropogenic activities, including industrial manufacturing, mining operations, and the combustion of fossil fuels. Exposure to lead in amounts exceeding physiological optima poses a significant risk to human health. Vulnerable populations, particularly children, face a heightened susceptibility to lead poisoning; contact with dust contaminated by environmental lead exacerbates the severity of intoxication (Loh et al., 2016). Pb (II) ions are detrimental to human health through bioaccumulation, leading to damage of the central nervous system, with children and pregnant women representing the most at-risk demographic.

Cadmium (Cd): Cadmium (Cd) is introduced into the atmosphere through both natural geological processes and anthropogenic activities, leading to varied exposure routes for humans and animals. Aquatic environments become contaminated with cadmium via absorption processes, industrial effluent discharge, and surface runoff that transports it into soil and sedimentary layers. Human exposure to cadmium can occur through the consumption of contaminated food, inhalation of polluted air, or ingestion of water containing elevated concentrations of this metal. Cadmium exhibits no beneficial attributes for plant development or metabolic functions. Exposure to Cd (II) ions is associated with the causation of reproductive, cardiovascular, pulmonary, and gastrointestinal disorders.

Copper (Cu): Ions are released in substantial quantities from various industrial sectors, particularly metal-related fields like electroplating, mining, and metallurgical processing. Other significant sources of environmental contamination include petroleum refining, agricultural runoff containing fertilizers and fungicides, and the corrosion of copper-based pipes and packaging, which can contaminate water and food products. Human exposure to excessive copper is associated with severe health consequences, including neurotoxicity that can manifest as Wilson's disease due to copper accumulation in the brain. Furthermore, copper toxicity is linked to kidney and liver damage, while occupational exposure via fungicidal sprays has been correlated with an increased incidence of lung cancer.

Zinc (Zn) is extensively utilized across numerous industries, including galvanization, paint production, battery manufacturing, smelting, the formulation of fertilizers and pesticides, fossil fuel combustion, pigment production, and as a polymer stabilizer. Consequently, the wastewater generated by these sectors is frequently contaminated with significant quantities of zinc. Electroplating, a critical process for surface finishing and metal deposition to enhance durability and aesthetics, also contributes to zinc pollution. Substantial amounts of metal ions, including zinc, find their way into effluents during the washing of electroplating tanks. While zinc is essential for human health in trace amounts, excessive exposure can still precipitate significant health issues (Mitra et al., 2022; Parmar & Thakur, 2013)**.** Comparative toxicity levels of several selected metals for humans, from least to most toxic, are documented as: Cobalt < Aluminum < Chromium < Lead < Nickel < Zinc < Copper < Cadmium < Mercury(Nnaji et al., 2023). The World Health Organization (WHO) has established maximum permissible limits for heavy metals in drinking water, specifying 0.01 mg/L for lead (Pb), 0.05 mg/L for copper (Cu) and zinc (Zn), and 0.03×10^{-1} mg/L (or 0.3 mg/L) for cadmium (Cd) (Zhang et al., 2023)**.**

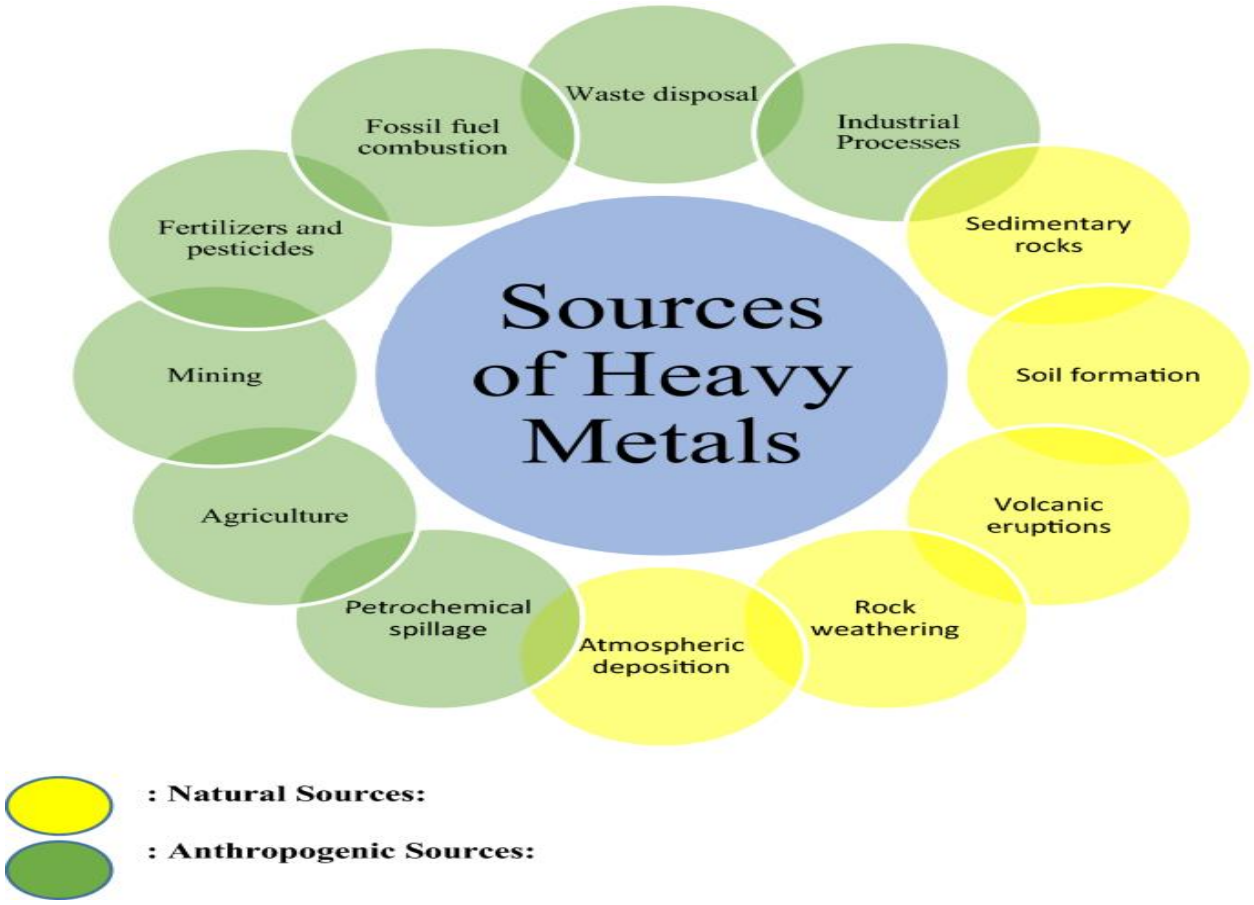

Figure 2-3. Sources of Heavy Metals.

A diverse range of geogenic, agricultural, industrial, and domestic activities, as well as atmospheric deposition, contribute to the presence of various metals in the environment. Significant metal contamination is often concentrated around point sources, which include mining operations, smelters, foundries, and other facilities involved in metal-based manufacturing. Furthermore, heavy metal pollution arises from numerous other factors, such as the expansion of industrial zones, disposal of high-metal-content waste, and runoff from mine tailings. Additional sources include the use of leaded gasoline and paints, the application of fertilizers, pesticides, animal manures, and sewage sludge, along with wastewater drainage, coal combustion residues, and petrochemical spills. As illustrated in Figure 1-3, these varied origins of metal contaminants are broadly classified by scientists into natural and anthropogenic categories. In recent decades, the scale of this issue has been highlighted by estimates of annual global emissions, which were reported to be 939,000 metric tons of copper, 1,350,000 metric tons of zinc, 22,000 metric tons of cadmium, and 783,000 metric tons of lead (Abdolali et al., 2017).

While a considerable number of treatment methods for remediating heavy metal contamination have been established over the years (Guo et al., 2024), the practical application of these technologies is often limited. A primary constraint is that most research has concentrated on the purification of water containing only a single metallic contaminant. This focus renders many existing techniques unsuitable for real-world applications, as industrial wastewater typically features a mixture of coexisting heavy

metals. Consequently, a significant and escalating demand exists for the development of advanced technologies and products capable of the simultaneous removal of multiple such pollutants from water.

2.3.3. Detection Methods for Heavy Metals Determination

The quantification of heavy metals is reliably achieved using a suite of established analytical methodologies. These include techniques such as inductively coupled plasma mass spectrometry/atomic emission spectrometry (ICP-MS/AES/OES), atomic absorption spectrometry (AAS), atomic fluorescence spectrometry (AFS), and laser-induced breakdown spectrometry (LIBS). Among these options, atomic fluorescence spectrometry (AFS) is particularly noteworthy for its capacity to overcome the intrinsic limitations associated with both atomic emission spectrometry (AES) and atomic absorption spectrometry (AAS). Nevertheless, inductively coupled plasma atomic emission spectrometry (ICP-AES) is widely regarded as a benchmark analytical technique for the routine analysis of heavy metals within a laboratory environment. For environmental metal pollutants, laser-induced breakdown spectrometry (LIBS) is particularly suitable for real-time and on-line detection. Concurrently, low-cost and portable atmospheric pressure discharge plasma (APDP) technology has garnered significant expert attention, emerging as a promising approach for trace element analysis. Plasma, fundamentally the fourth state of matter, is constituted by various particles, neutral atoms, molecular structures, free electrons, positive ions, and metastable particles. Within a plasma environment, heavy metal compounds or ions undergo atomization and excitation, leading to the emission of characteristic radiation (AES). This radiative process forms the core detection principle for methods like ICP-AES and LIBS. APDP technology enables plasma generation at atmospheric pressure, even in open-air conditions, thus presenting potential applications for elemental analysis. A notable advantage of ICP-Optical Emission Spectrometry (ICP-OES) is its capacity to cover an extensive wavelength range, typically from 165 nm to beyond 800 nm. This broad spectral coverage allows for the simultaneous analysis of multiple elements within a single experimental run, rendering it a valuable tool for environmental monitoring, geology, and biology. ICP-OES is particularly recommended for detecting trace elements at low concentrations, when simultaneous multi-element analysis is critical, or when dealing with complex sample matrices that are susceptible to interference, especially within environmental, geological, or biological research contexts. In contrast, ICP-AES is the preferred option when high precision and accuracy are paramount, matrix effects can be effectively managed through sample preparation protocols, or when sequential measurements of individual elements are acceptable, such as in the analysis of metals within alloys or for industrial quality control purposes (Song et al., 2024).

2.4.Conventional and Advanced Methods for Heavy Metal Removal

A determined challenge in the field of water treatment is the creation of technologies capable of eradicating heavy metal contaminants from wastewater in a manner that is concurrently effective, economically viable, and environmentally sustainable. To achieve this, a variety of conventional methodologies are commonly applied, including chemical precipitation, ion exchange, electrocoagulation, electrodialysis, photocatalysis, solvent extraction, and adsorption. The following section provides a critical assessment of these diverse techniques, specifically evaluating their respective merits and drawbacks about their practical application on an industrial scale (Oladimeji et al., 2024).

- **Physical-chemical treatment**

1) Coagulation and flocculation
2) Chemical precipitation
3) Sedimentation
4) Filtration

- **Tertiary treatment**

1) Adsorption
2) Ion exchange
3) Membrane process

- **Other advanced methods**

1) Chemical oxidation
2) Electrochemical precipitation
3) Crystallization and distillation
4) Photocatalysis

A comprehensive overview of these diverse treatment strategies, alongside the key performance indicators used for their evaluation—such as removal capacity, removal efficiency, and recyclability is illustrated in **Figure 2-4**. When these various methods are critically assessed against such criteria, adsorption consistently emerges as a highly advantageous approach. In comparison to other techniques that may be limited by high operational costs, incomplete removal, or the generation of toxic secondary pollutants like chemical sludge, adsorption is frequently recognized for its superior efficiency, economic viability, operational simplicity, and the potential for adsorbent regeneration (Burakov et al., 2018; Hoang et al., 2022) .

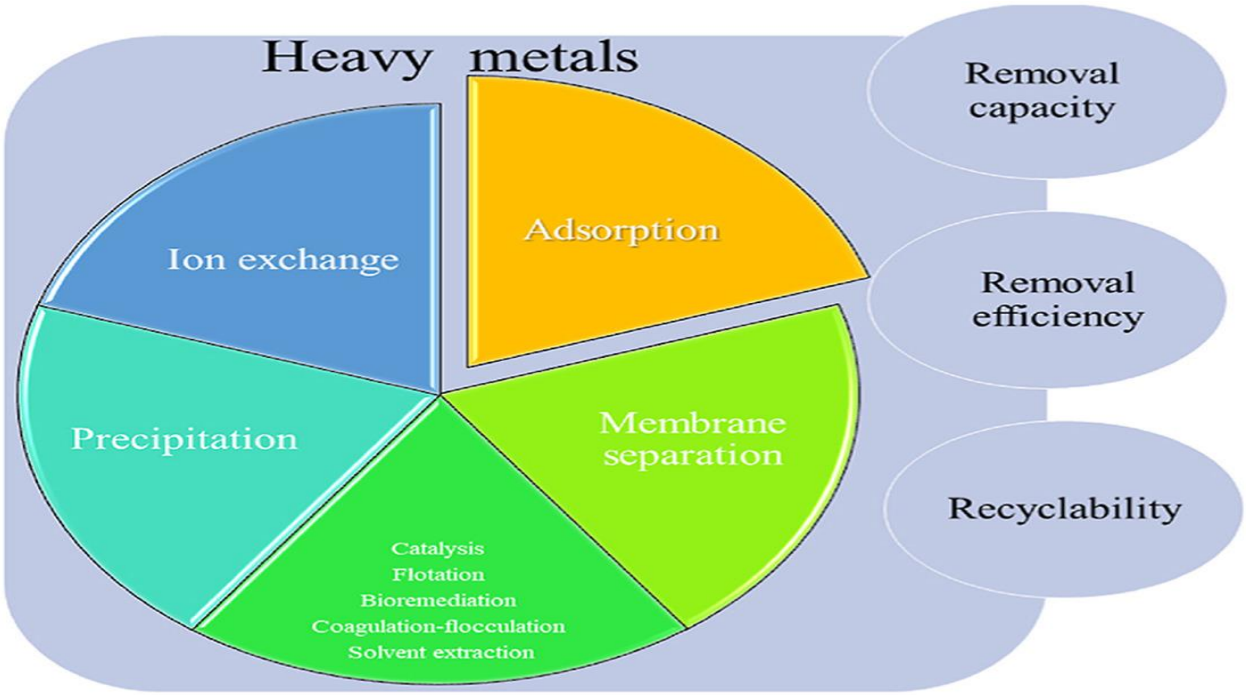

Figure 2-4. Conventional and advanced Methods for heavy metal removal**.**

2.5. Cost and Feasibility Analysis of Different Water Treatment Methods

While technical efficacy is paramount, the economic feasibility of a treatment technology is often the deciding factor for its implementation. A comparative cost analysis for several principal water treatment technologies reveals significant financial variations. For instance, the total cost per million liters of treated water can range from €20-400 for reverse osmosis to €15-340 for nanofiltration and electrodialysis. In contrast, adsorption (€45-130) and ion exchange (€45-170) often represent more cost-effective approaches for heavy metal removal, indicating their potential for industrial applications like EoL PV module recycling(Song et al., 2024).

However, a simple operational cost analysis does not capture the full economic picture. The long-term viability of these methods is intrinsically linked to their primary technical limitations, which can lead to indirect costs. **Figure 2-5** provides a summary of these main drawbacks and highlights the innovative solutions being developed to address them. For example, the high energy demand of membrane processes directly translates to higher operational costs, while the challenge of regenerating contaminant resins in ion exchange adds to maintenance and disposal expenses. The development of solutions, such as using by-products as efficient adsorbents, is therefore not just a technical enhancement but a direct strategy to improve the cost-effectiveness and overall sustainability of these treatment methods.

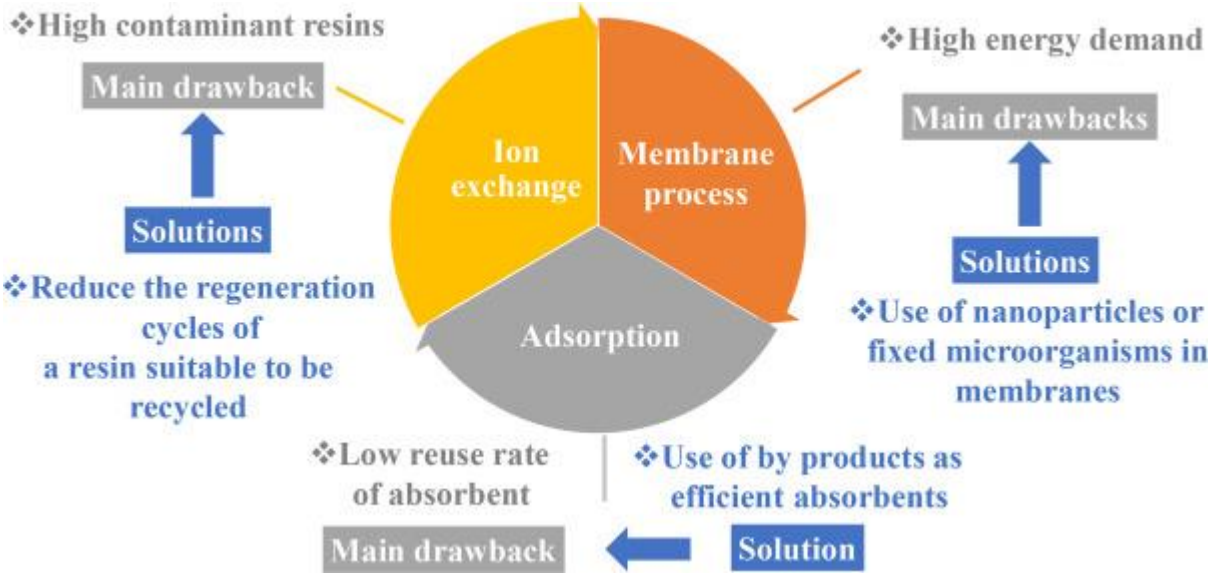

(Song et al., 2024)

Figure 2-5. A summary of primary limitations and potential enhancements for various water treatment methods concerning their practical application in heavy metal removal.

2.6. Greywater: Sources, Characteristics, Quantities and Advantages of Treatment and Reuse

The diminishing availability of global freshwater resources necessitates the reuse of water, a practice increasingly adopted not only in arid regions but also in European countries like Germany and the United Kingdom (Mandal et al., 2011). A significant source for water reclamation is greywater, which originates from washbasins, showers, kitchen sinks, and laundry, and can represent 50–80% of all wastewaters from households. It is distinct from sewage in that it excludes toilet water, resulting in a lower load of organic matter and harmful pathogens. This characteristic makes greywater safer to

handle and simpler to treat for non-potable reuse, such as for crop irrigation, toilet flushing, garden watering, or discharge into water bodies. While established biological processes, including Membrane Bioreactors (MBR), Rotating Biological Contactors (RBC), and Up flow Anaerobic Sludge Blankets (UASB), are highly effective at removing contaminants, their mechanized nature makes them more appropriate for centralized treatment facilities. Consequently, the push towards a circular economy in the water sector over the last two decades has intensified the search for sustainable, on-site treatment technologies. In contrast to centralized systems, localized solutions like the use of biosorbents are distinguished by lower capital investment and energy consumption, reduced operational and maintenance demands, and greater affordability, often stemming from the use of locally sourced materials (Quispe et al., 2022).

2.7.Adsorption Principles and Mechanisms

2.7.1. Definition of Adsorption Process

Adsorption is a mass transfer phenomenon characterized by the movement of substances from a liquid phase to the surface of a solid material, where they accumulate due to physical or chemical interactions. These substances, known as adsorbates, can be organic or inorganic in nature and may exist in either soluble or insoluble forms. Within the literature on wastewater treatment, the sportive capabilities of various natural biomasses are extensively studied, especially for applications involving low pollutant concentrations (less than 100 mg L^{-1}), where alternative treatment methods may be inefficient or prohibitively expensive. The reverse process, desorption, involves the transfer of the adsorbate from the adsorbent surface back into the liquid solution. The reversibility of the adsorption process is judged by the amount of adsorbate that can be desorbed; a higher degree of desorption corresponds to a more reversible process (Burakov et al., 2018). The most common types of adsorbent materials and adsorption processes investigated by researchers are depicted in **Figures 2-6 and 2-7.** To ensure clarity throughout this document, the term “cellulose-based” will henceforth be used to encompass all materials containing cellulose, including nanocellulose and any materials derived from them through mechanical or chemical means.

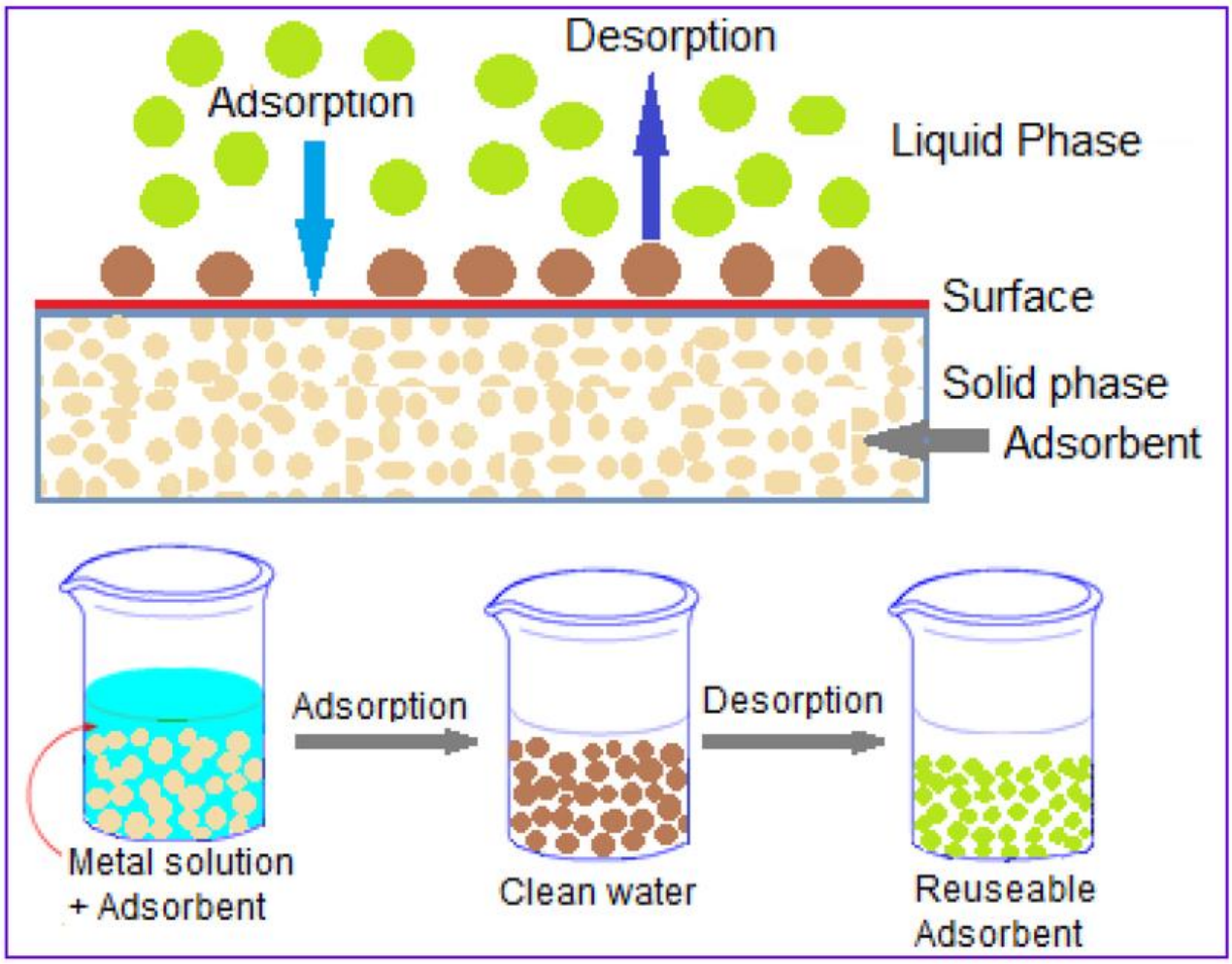

Figure 2-6. Schematic diagram of the adsorption-desorption process. (Zaimee et al.,2021)

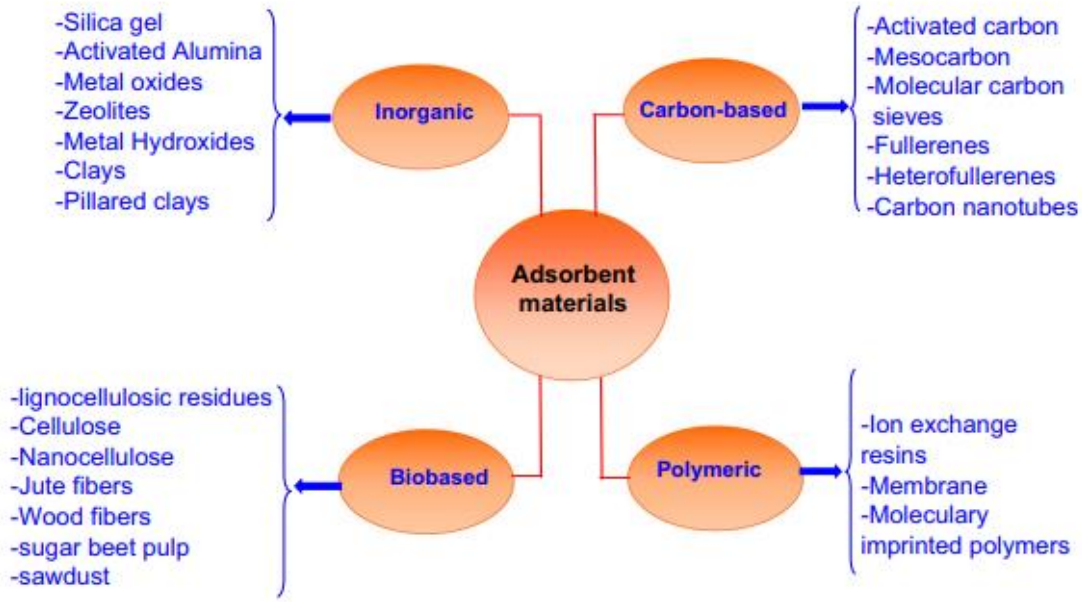

(Mahfoudhi & Boufi, 2017)

Figure 2-7. The most frequently used adsorbent materials.

2.7.2. Adsorption Regimes

A- Static Regime (batch) Adsorption

In the static or batch adsorption regime, a precisely measured amount of sorbent material is introduced into a fixed volume of a liquid solution. This mixture is then agitated, typically at a constant speed ranging from 100 to 250 rpm. The solution contains the adsorbate at a known initial concentration (expressed in units such as ppm, $mg \cdot L^{-1}$, or $mmol \cdot L^{-1}$). The process is monitored over a predetermined period, often by measuring the concentration of the adsorbate at various time intervals until equilibrium is achieved.

B- Dynamic Regime (Fixed-bed Column)

Adsorption can be conducted under a dynamic regime within a fixed-bed column, a configuration where the liquid solution containing a solute of interest is passed continuously through a stationary bed of sorbent material. This methodology is broadly implemented for the sequestration of both inorganic and dissolved organic contaminants from diverse water and wastewater streams. Within the column, the prolonged interaction between the liquid and solid phases facilitates the approach toward a state of thermodynamic equilibrium. By its nature, this is a rate-controlled, unsteady-state process, given that conditions at any discrete point within the bed fluctuate over time (John et al., 2024). The performance optimization of fixed-bed columns hinges on the analysis of breakthrough curves. These curves are generated by methodically varying critical operational parameters including initial solute concentration, pH, bed height, column diameter, and flow rate—to identify the optimal conditions for efficient operation.

2.7.3. Physisorption vs. Chemisorption

The phenomenon of physisorption arises from physical forces of attraction existing between the adsorbent and adsorbate, a process that is most effective at low temperatures and high pressures. Chemisorption, conversely, is distinguished by the formation of chemical bonds connecting the adsorbate to the adsorbent. This chemical bonding mechanism is characterized as being slow and frequently irreversible, leading to a defining outcome: the formation of a single molecular layer, or monolayer, of the adsorbate upon the adsorbent surface (Hoang et al., 2022). **Figure 2-8** illustrates the physisorption and chemisorption processes.

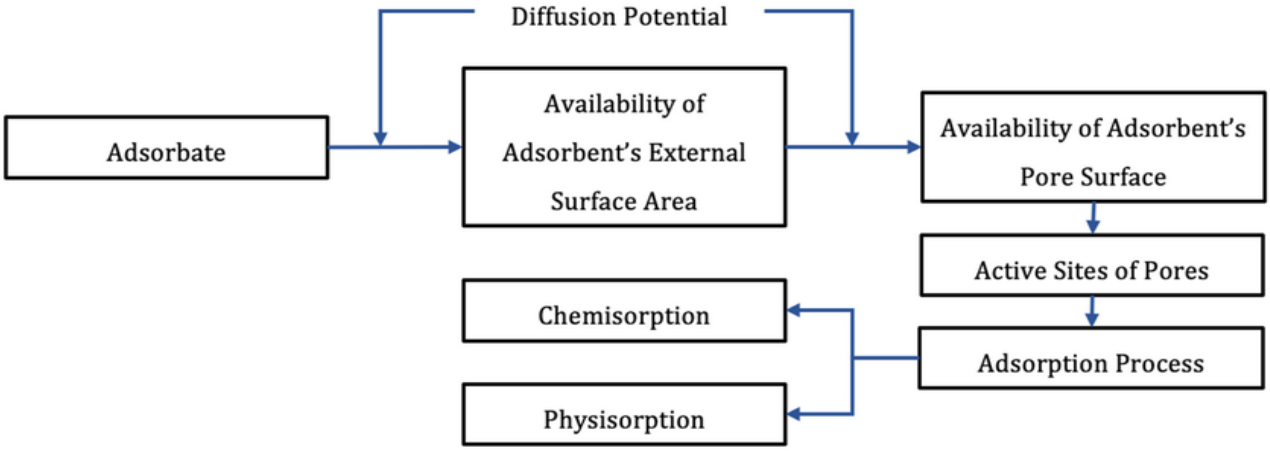

Figure 2-8 Biosorption pathway that leads to physisorption or chemisorption (Zaimee et al., 2021).

2.8.Types of Biosorbents for the Removal of Heavy Metals

An extensive range of materials, collectively known as biosorbents, has been evaluated for its potential in the sequestration of heavy metals from aqueous environments. These biosorbents can be grouped into several major categories based on their origin. One significant category includes agricultural products and byproducts, for which numerous studies have tested metal-binding capabilities. Examples of these materials include rice straw, coconut husks, waste coffee powder, dried plant leaves, wool, cotton seed hulls, waste tea, and cork biomass. Another major group consists of microbial cells—such as bacteria, fungi, algae, and yeast—along with other natural materials like peat moss and sewage sludge. Additionally, industrial waste, like the residual *Saccharomyces cerevisiae* biomass from the fermentation and food industries, as well as other polysaccharide materials, are utilized. These biosorbents, often used as native biomass, are further classified in **Tables 2-1 and 2-2**. Within this broad category, lignocellulosic materials of agricultural origin have received considerable scientific attention. Prominently reported examples in the literature include materials derived from fruit and vegetable waste, rice straws, wheat bran, and soybean hulls.

Table 2-1. A Comparative Overview of Physisorption and Chemisorption Characteristics**.**

Characteristic	Physisorption	Chemisorption
Binding Force	Governed by weak, non-specific Van der Waals forces.	Involves the formation of strong, specific ionic or covalent bonds.
Specificity	Non-specific interaction between adsorbent and adsorbate.	Highly specific interaction, dependent on chemical compatibility.
Adsorbed Layers	It can form multiple layers on the adsorbent surface (multi-layer).	Restricted to the formation of a single (mono) layer.
Reversibility	Generally, a reversible process.	Typically, an irreversible process.
Effect of Temperature	Favored by lower temperatures, efficiency decreases as temperature rises.	Favored by higher temperatures; efficiency often increases with temperature.
Influence of Surface Area	Adsorption capacity increases with greater available surface area.	Adsorption capacity increases with greater available surface area.
Influence of Pressure	Adsorption capacity generally increases as pressure rises.	Adsorption capacity generally increases as pressure rises.
Activation Energy	Requires little to no activation energy.	Requires significant activation energy to proceed.

Table 2-2. Classification and Examples of Common Biosorbent Materials.

Category	Illustrative Examples
Bacteria	This category features Gram-positive genera (*Bacillus sp., Corynebacterium sp.*), Gram-negative genera (*Escherichia sp., Pseudomonas sp.*), and Cyanobacteria (*Anabaena sp., Synechocystis sp.*).
Fungi	Comprises various molds (*Aspergillus sp.*, *Rhizopus sp.*), mushrooms (*Agaricus sp.*, *Trichaptum sp.*), and yeasts (*Saccharomyces sp.*).
Algae	Includes both micro-algae (*Chlorella sp.*, *Chlamydomonas sp.*) and macro-algae, the latter of which is subdivided into green seaweeds (*Enteromorpha sp.*, *Codium sp.*), brown seaweeds (*Sargassum sp.*, *Ecklonia sp.*), and red seaweeds (*Gelidium sp.*, *Porphyra sp.*).
Industrial Wastes	Consists of byproducts from fermentation processes, food and beverage manufacturing, as well as activated and anaerobic sludges.
Agricultural Wastes	Includes residues from fruits and vegetables, rice straws, wheat bran, and soybean hulls.
Natural Residues	Composed of various plant-based matter, sawdust, tree barks, and common weeds.
Other Materials	Includes materials derived from chitosan and cellulose.

Adapted from (Abbas et al., 2014)

2.8.1. Cellulose-Based Adsorbents

The primary constituents of all plant materials are three major biopolymers: cellulose, hemicellulose, and lignin. The term "cellulose" was first introduced in 1838 by the French chemist Anselme Payen, who created the word by merging the French "cellule" (cell) with "glucose" to signify the material's

biological origin and fundamental chemical structure (Rocky et al., 2023). Lignocellulosic materials, a category that encompasses agricultural wastes, forestry residues, grasses, and various woody materials, are noted for their considerable potential in the production of biofuels. As illustrated in **Figure 2-9**, the typical composition of agricultural lignocellulosic biomass is approximately 40–50% cellulose, 20–30% hemicellulose, and 10–25% lignin.

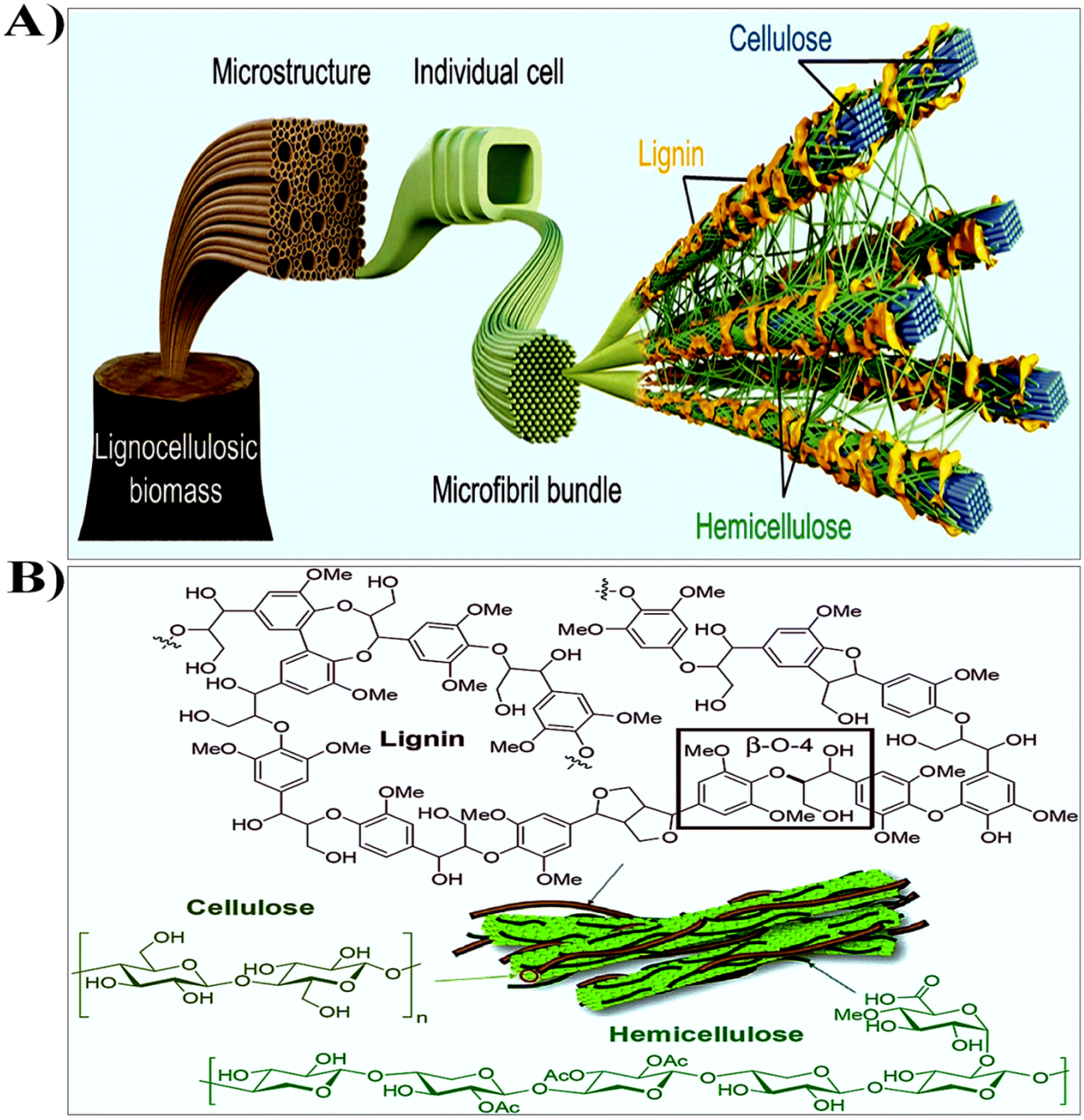

Figure 2-9. Multiscale architecture of lignocellulosic biomass, from cell wall to microfibrils (A). Key chemical motifs of cellulose, hemicellulose, and lignin (B).

Lignocellulosic materials represent a highly promising and renewable natural resource, essential to the functioning of modern industrial societies. Significant quantities of these materials are generated as waste byproducts from agricultural and agro-industrial activities, positioning them as a versatile and eco-friendly solution for various applications, including wastewater treatment. Although literature reports a wide diversity in the biosorption capacities of different lignocellulosic materials, making direct comparisons challenging, a consensus highlights their potential for industrial-scale metal removal due to their low cost and high effectiveness in binding metallic ions (Salman et al., 2015). The inherent abundance, biocompatibility, and renewability of lignocellulose make it a particularly appealing option for sustainable water remediation. The use of such renewable resources is critical for advancing sustainable social development goals related to wastewater cleanup. However, the fabrication of advanced lignocellulose-based adsorbents can be constrained by complex, expensive, and environmentally detrimental synthesis processes, as well as the generation of secondary byproducts. Despite these challenges, biosorption utilizing unprocessed lignocellulosic wastes and byproducts has been identified as a suitable alternative to conventional technologies for removing hazardous pollutants from wastewater streams. These materials have demonstrated high efficacy in adsorbing heavy metals such as arsenic (As), cadmium (Cd), copper (Cu), chromium (Cr), and lead (Pb). In addition to metals, their application extends to the capture of various organic pollutants, including dyes (e.g., methylene blue, methyl orange, malachite green), pharmaceutical residues, and pesticides.

Lignocellulosic materials, including forestry byproducts like pine bark and various agricultural wastes such as nut shells, serve as effective biosorbents for heavy metal remediation. The primary removal mechanism is passive biosorption, a non-metabolic process where metal ions are bound to functional groups on the non-living biomass surface via physicochemical interactions like ion exchange and complexation (Das et al., 2020). This passive uptake is distinct from metabolically driven bioaccumulation in living organisms. The overall efficiency of this process is governed by variables such as the biomass type, the chemistry of the metal solution, and environmental conditions (Lindholm-Lehto, 2019). Consequently, materials ranging from banana peels to wood-based sorbents like spruce sawdust (NSWR) have been successfully employed, either in their natural state or with modifications, to treat aqueous media contaminated with heavy metals (Das et al., 2020). Sawdust of Pinus Sylvestris (Taty-Costodes et al., 2003); Beech (*Fagus orientalis* L.) Sawdust of Deciduous Trees (Sawdust of Beech, Linden and Poplar trees) (Božić et al., 2009);Meranti Sawdust (Rafatullah et al., 2009);Untreated Pinus halepensis Sawdust (Semerjian, 2018); Modified Oak Sawdust Sawdust (Argun et al., 2007); Mansonia Wood Sawdust (Ofomaja, 2010);Wood Sawdust and Sugarcane Bagasse Modified with EDTA dianhydride (EDTAD) (Pereira et al., 2010); Pine (Pinus densiflora) Sawdust (Yang et al., 2010);By-product of *Lentinus edodes* (Chen et al., 2006); Hevea Brasilinesis sawdust (Karthikeyan et al., 2005);Sawdust of Lam Tree (Cordia africana);Beech Sawdust (Božić et al., 2009); Beech Sawdust (Anna, 2013);Pine bark (Cutillas-Barreiro et al., 2014);Citric Acid Modified Pine Sawdust (Y. Zhou et al., 2015);White Pine (*Pinus durangensis*) Sawdust (Salazar-Rabago et al., 2017); *Eucalyptus sheathiana* Bark (Afroze et al., 2016); Peat and sawdust of various types (Balintova et al., 2016) ;Pine (*Pinus halepensis*) Sawdust (Semerjian, 2018b);Schleichera oleosa Bark (Khatoon et al., 2018);Sawdust/MNP/PEI Nanocomposite (Ghasemi et al., 2018);alkaline treatment of Wooden Sawdust (Demcak et al., 2019); Wooden Sawdust Treatments (Kovacova et al., 2020); Albizia lebbeck Sawdust (Nurnabi et al., 2020); Raw and Chemically Activated Dibetou Wood (El Hajam et al., 2020); Pine bark (*Pinus radiata* D. Don)(Montes-Atenas & Schroeder, 2015); Eastern Spruce Sawdust (Turkey) (Bilgin & Ateş, 2021);Sawdust and Wheat Straw (Božić et al., 2009); Cedar Sawdust (Forgionny et al.,

2022));Sawdust of Oak Wood (N. A. Ibrahim et al., 2022) ; Fir sawdust (G. Zhou et al., 2023) etc. While many biosorbents have demonstrated a notable capacity for binding heavy metals, a true assessment of their practical applicability for treating polluted water requires more rigorous investigation. To properly evaluate an adsorbent, it is essential to study its performance across a broad spectrum of parameters that closely simulate the conditions found in actual wastewater effluents. The primary focus of such investigations must be on the biosorbent's behavior and effectiveness in complex aqueous mixtures that contain multiple toxic metal species simultaneously. This approach is critical because performance in single-metal ion solutions often fails to predict behavior in real-world scenarios. Addressing the challenge of simultaneous multi-metal removal from water remains one of the most formidable tasks in the field of water purification.

2.8.2. *Picea abies* (L.) H. Karst. (Norway spruce) as a Proposed Adsorbent

Picea abies (L.) H. Karst., commonly known as Norway spruce, is a coniferous tree from the Pinaceae family that grows wild throughout the Northern Hemisphere. In Romania, spruce constitutes approximately 23% of the nation's forests and is typically found at altitudes between 600 and 1700 meters. This species possesses high economic value, serving as a crucial raw material for the production of cellulose, paper, and various wood products. More recently, its use has expanded into alimentary products like syrups, jams, and beverages. A significant quantity of spruce biomass, estimated at 6 to 8 million tons annually, is generated as a byproduct of forestry operations. As indicated in **Figure 2-10** and **Table 2-3**, research has shown that this Norway Spruce Wood Residue (NSWR) biomass is capable of binding certain pollutants, including cationic dyes and metal ions. This adsorption capacity is attributed to the various functional groups present on the surface of the biosorbent material (Sandulovici et al., 2024).

Figure 2-10. Norway spruce *Picea abies* (L.) H. Karst. branch with mature, pendulous seed cones.

https://orleansconservationtrust.org/norway-spruce-picea-abies

Table 2-3. The main functional groups found in natural bio-adsorbent.

Functional group	Name	Atom	Class of compound
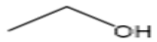	Hydroxyl	O	Alcohols, carbohydrates, phenols
	Etheric	O	Polysaccharides, Ethers
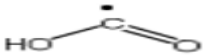	Carboxylic	O	Organic acids, proteins, Fatty acids.
	Carbonyl group	O	Carbohydrates, Aldehydes
	Amide	N	Proteins
	Thiols	S	Cysteine, amino acids

* (Priya et al., 2024)

2.9. Coal as A Potential Adsorbent for Ciprofloxacin: its Definition and Properties

Coal is defined as a sedimentary rock with a high concentration of organic material, primarily consisting of various macerals like lignite, cellulose, and resin, in addition to inorganic impurities. From a chemical standpoint, natural coal is structured as a matrix of polycyclic aromatic hydrocarbons. Attached to these aromatic rings are several types of oxygen-containing functional groups, notably carboxyl, phenolic, hydroxyl, and carbonyl groups. These specific chemical moieties are recognized for their pronounced activity and crucial role in facilitating adsorption processes (S. M. Ibrahim et al., 2021).

2.10. Mechanisms of adsorption

The sequestration of metal ions via adsorption is predominantly controlled by a set of primary mechanisms, which include ion exchange, complexation, chelation, surface sorption, and precipitation. The complete biosorption mechanism, however, remains to be fully elucidated because it is subject to the influence of numerous factors. As illustrated **in Figure 2-11**, The overall process is affected by variables such as: (1) the specific characteristics of the lignocellulosic material being utilized, (2) the distinct chemical properties of the metal solution, and (3) the prevailing environmental conditions.

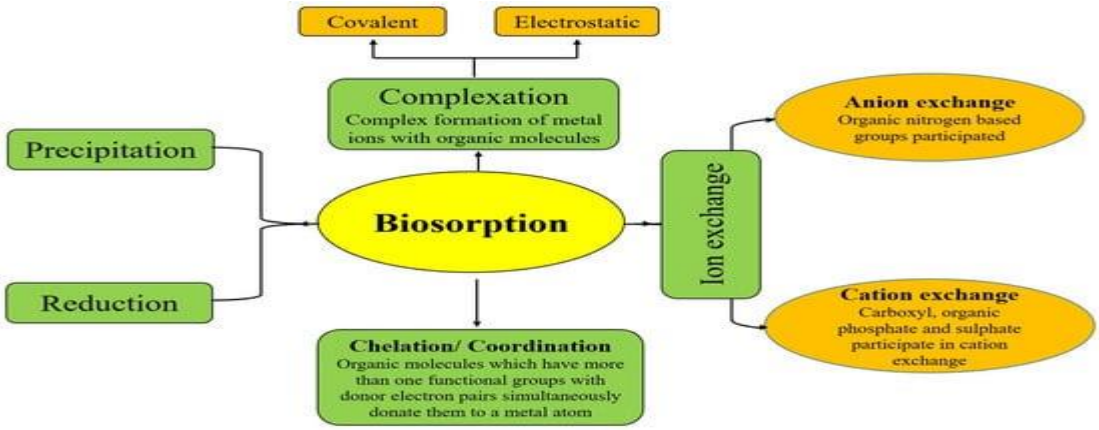

Figure 2-8. An Overview of General Adsorption Mechanisms (Zhang et al., 2023).

2.11. Characterization Analysis of Adsorbents

A broad array of analytical techniques is available to investigate adsorbent materials, allowing researchers to evaluate a sample's physical, chemical, and thermal properties with varying levels of detail. While it is common practice for studies to include at least one chemical and one physical characterization method to provide foundational information, a significant portion of the literature on new adsorbents often presents analyses that are not sufficiently comprehensive. To obtain a complete understanding, characterization should be performed at several key stages. This includes analysis of (I) the initial raw or precursor materials, (II) the final synthesized, composite, or modified adsorbent to confirm successful preparation, (III) the adsorbent after it has been loaded with the adsorbate to identify the mechanisms of uptake, and (IV) the material following adsorption/desorption cycles to assess its stability and potential for reuse. The selection of specific analytical techniques is necessarily guided by the nature of the adsorbent material, the properties of the adsorbate, the medium in which it will be applied, and the resources available to the research team. It is anticipated that ongoing technological development will make these methods more accessible and enhance the quality and accuracy of their results. Such improvements are critical for advancing adsorbent research, as they can help overcome the persistent challenge of scaling up new materials from controlled laboratory conditions to real-world applications. A new material that has been extensively studied and thoroughly characterized provides the scientific community and industry with high-quality, reliable information, thereby potentiating future development and practical implementation.

2.11.1. Chemical Characterization

A range of analytical methods can be employed for the chemical characterization of adsorbent materials, yielding crucial information regarding their elemental composition, including the identification, location, and quantification of chemical constituents. This type of analysis extends beyond simply determining the material's composition; it also provides vital insights into the nature of the functional groups present on the adsorbent's surface. These groups are directly involved in the binding process and govern the adsorption mechanisms, which can include hydrogen bonding, complexation, coordination/chelation, electrostatic attraction, hydrophobic interactions, and π-π stacking. The most utilized techniques for the chemical characterization of adsorbents include Fourier transform infrared spectroscopy (FTIR), ultraviolet-visible spectroscopy (UV-vis), Raman

spectroscopy, X-ray photoelectron spectroscopy (XPS), energy-dispersive X-ray spectroscopy (EDX), and zeta potential analysis.

2.11.2. Physical Characterization

Evaluating the physical attributes of an adsorbent—such as its crystalline structure, surface topography, morphology, particle size, and magnetic properties—is critical for assessing its potential performance. Several key techniques are utilized for these assessments. X-ray diffraction (XRD) analysis is used to determine the material's crystal structure and phase. The examination of surface morphology and topography is conventionally performed using analytical techniques such as scanning electron microscopy (SEM), field emission scanning electron microscopy (FESEM), transmission electron microscopy (TEM), and atomic force microscopy (AFM). Additional characterization is achieved through surface area and porosimeter analyses, which yield critical data regarding a material's porosity and specific surface area. To determine other physical properties, techniques like vibrating sample magnetometry (VSM) are employed to assess magnetic characteristics, while dynamic light scattering (DLS) is utilized to measure the particle size distribution.

2.11.3. Thermal Characterization

Thermal analysis can be carried out through several techniques in which the physical properties of a material and/or reaction products are evaluated as a function of temperature. The evaluated materials are subjected to a controlled temperature program and under a specified atmosphere. These analytical methods are based assessment of a physical property as a function of temperature, and include thermogravimetry (TG), differential thermal analysis (DTA) and differential scanning calorimetry (DSC), Temperature Programmed Reduction/Oxidation (TPR/TPO), among others (Pellenz et al., 2023)

2.12. The Impact of Influencing Factors on Adsorption

The efficiency and overall performance of an adsorption process are not static but are governed by a complex interplay of various physicochemical and operational parameters. Optimizing these factors is critical for maximizing contaminant removal, ensuring economic viability, and understanding the underlying removal mechanisms. The most significant parameters that influence adsorption include the contact time, adsorbent dose, solution pH, temperature, initial contaminant concentration, adsorbent particle size, and the inherent surface chemistry of the adsorbent material. A comprehensive overview of these key factors and their specific effects, such as influencing equilibrium state, active site availability, and mass transfer rates, is illustrated in **Figure 2-12**.

A detailed investigation into these parameters is essential for process design. For instance, analysing the effect of temperature provides crucial thermodynamic insights. This is often accomplished through thermal characterization, a suite of techniques that measure changes in a material's physical properties in response to a controlled temperature program. During analysis, the material under investigation is subjected to a precise heating schedule within a specified atmosphere. These analytical methods are founded on the assessment of a physical property as it varies with temperature. Prominent methods in this category include thermogravimetry (TG), which measures mass change, as well as differential thermal analysis (DTA) and differential scanning calorimetry (DSC), which measure temperature and heat flow differences. Other relevant techniques include Temperature Programmed Reduction/Oxidation (TPR/TPO), among others (Abas et al., 2013).

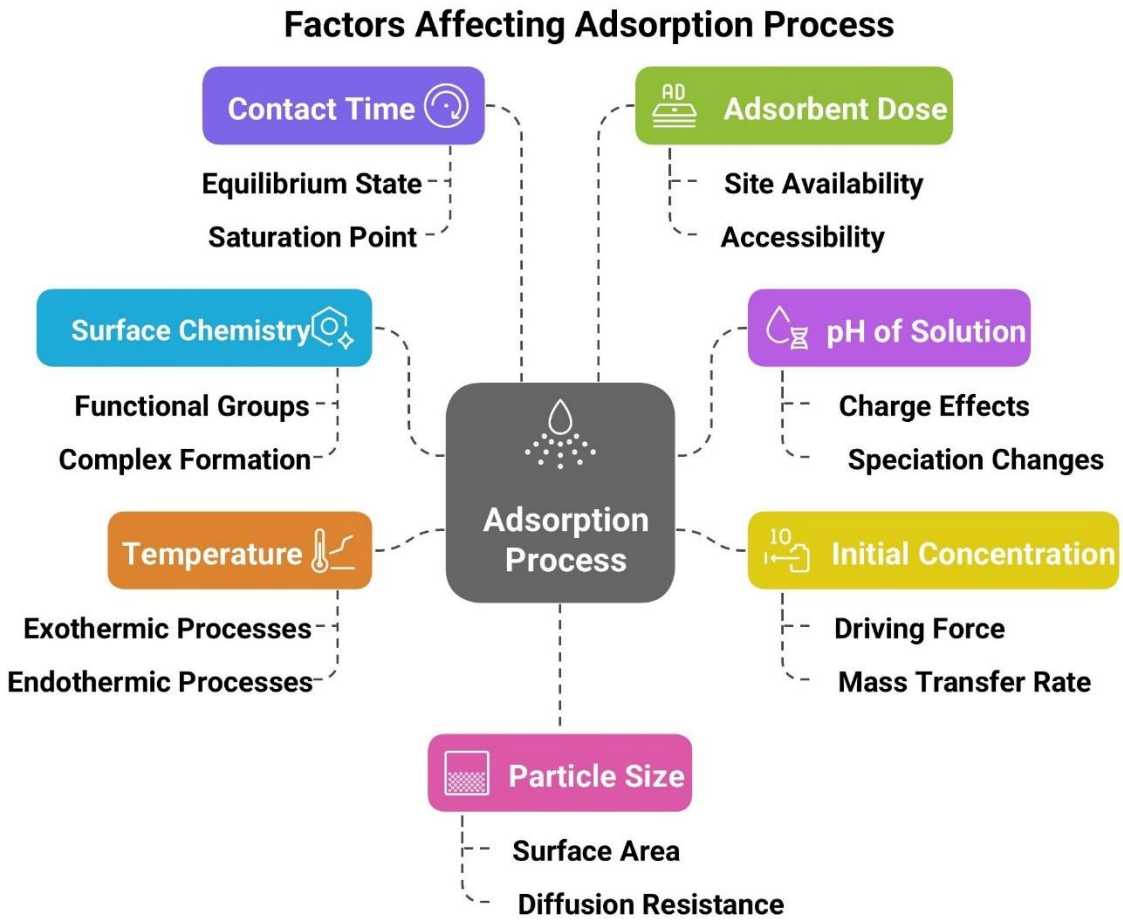

Figure 2-12. A schematic overview of the key operational and physicochemical factors that influence the performance of an adsorption process.

2.13. Methods of Adsorbent Modification

The performance of adsorbent materials can be enhanced through various physical, chemical, and biological modification methods. These treatments alter key physicochemical characteristics—such as surface area, porosity, charge, and the density of functional groups—to improve pollutant uptake. Advanced analytical techniques are essential for characterizing these modified materials and elucidating the underlying adsorption mechanisms and kinetics (Satyam & Patra, 2024).

For cellulose-based materials, chemical modifications like carboxylation, amination, or the incorporation of graphene can significantly improve sorption capacity for toxic ions such as Pb^{2+}, Cd^{2+}, and Cr^{3+}. These alterations often concurrently increase the material's chemical stability and durability, which is vital for long-term use in wastewater treatment. However, any single modification method typically has limitations, such as targeting only specific properties or having insufficient stability under extreme conditions.

To overcome these individual drawbacks, combined modification approaches are increasingly utilized to create materials with optimized and synergistic characteristics. For example, coupling a chemical treatment with a subsequent plasma or thermal process can produce sorbents with high activity

towards a broad range of pollutants. Studies indicate that such combined treatments can be more effective than chemical modification alone, as they often create additional surface microporosity and increase the number of active binding sites (Darmenbayeva et al., 2024).

2.14. Potential Advantages and Drawbacks of the Biosorption Process

Adsorption is widely recognized as an effective and practical process for removing various pollutants from water. Its primary advantages include low operational costs, simplicity in design and maintenance, and rapid treatment times. The method offers high efficiency and flexibility, supported by the availability of diverse and highly effective adsorbents, many of which can be produced from low-cost agricultural wastes (John et al., 2024) A summary of the key benefits and limitations of the adsorption process is provided in **Table 2-4**.

Table 2-4. Advantages and disadvantages of adsorption method.

Advantages	Disadvantages
High efficiency for removing pollutants, especially at low concentrations.	The disposal of pollutant-laden (spent) adsorbent requires careful management.
Operational simplicity, low cost, and design flexibility.	The regeneration of adsorbents can be expensive and may not fully restore original capacity.
Potential for adsorbent regeneration and reuse through suitable desorption methods.	Adsorption can be reversible, posing a risk of pollutant leaching if conditions change.
Produces high-quality treated effluent without generating large volumes of chemical sludge.	Performance can be less effective than chemical precipitation for certain high-concentration inorganic effluents.

Adapted from (Fouda-Mbanga et al., 2021)

2.15. Classification of Adsorption Isotherm Models

Adsorption isotherms are defined as mathematical models that represent the equilibrium partitioning of a solute between a liquid phase and a solid adsorbent surface under isothermal conditions. The nature of this equilibrium relationship is contingent upon the intrinsic properties of both the adsorbent and the adsorbate, and it is also influenced by ambient solution parameters, including pH, ionic strength, and temperature (Al-Ghouti & Da'ana, 2020). Consequently, these models are indispensable tools for the effective characterization of porous solids and for the design and optimization of industrial-scale adsorption systems

Isotherm models can be categorized based on several criteria:

- **Mathematical Form:** Models are classified by their mathematical structure as either linear or nonlinear.
- **Number of Parameters:** Models are grouped by the number of adjustable fitting parameters they contain. This includes two parameter models (e.g., Langmuir, Freundlich), three-parameter models (e.g., Sips, Toth), and more complex multi-parameter models.
- **IUPAC Classification:** The International Union of Pure and Applied Chemistry (IUPAC) classifies isotherms into six distinct types based on their characteristic shapes, which reflect different physical adsorption mechanisms.

- **Operational Mode:** Models can be specific to the experimental setup, distinguishing between those suited for batch (static) systems and those developed for continuous flow (fixed-bed column) systems, such as the Thomas and Yoon-Nelson models.
- **Physical Assumptions:** Advanced models derived from statistical physics provide a more detailed description, accounting for factors like monolayer or multilayer adsorption on surfaces with varying energy distributions.

2.16. Adsorption Kinetics

The study of adsorption kinetics is a critical parameter for determining the overall performance and efficiency of a sorption process. Fundamentally, kinetic analysis elucidates the rate of solute uptake onto the adsorbent material and provides essential insights into the controlling mechanisms at the solid-liquid interface. This behaviour is mathematically described using various kinetic models, which include the Pseudo-first order (Lagergren) model, the Pseudo-second-order model, the Elovich model, and the intra-particle diffusion model (Musah et al., 2022).

2.17. Criteria for an Effective Adsorbent in Water Treatment

Utilizing solid wastes as precursors for low-cost adsorbents offers a dual environmental advantage: it reduces the volume of waste requiring disposal while providing an economical solution for wastewater remediation. The low cost of these waste-derived materials can also obviate the need for complex and expensive regeneration processes. Consequently, numerous agricultural and industrial byproducts have been successfully converted into effective adsorbents, representing a promising strategy for sustainable pollution control (Bhatnagar & Sillanpää, 2010).

2.18. Overview of Regression Models

Beyond traditional kinetic and isotherm analysis, modern computational methods such as machine learning regression models offer a powerful approach for predicting adsorption capacity and understanding complex variable interactions. In this study, a suite of six regression algorithms, spanning from simple baseline models to advanced, high-performance ensemble techniques, were implemented and evaluated. **Figure 2-13** provides a comprehensive comparative framework of these models, illustrating their underlying mechanisms, key characteristics, and a summary of their predictive performance as observed in this work. The following sections provide a detailed overview of each evaluated model.

2.18.1. Linear Regression

Linear Regression is a supervised learning algorithm that models a linear relationship between a dependent variable and one or more independent variables. Due to its simplicity, it serves as a common baseline for regression analyses. However, its assumption of linearity limits its ability to capture complex patterns, which resulted in suboptimal performance for predicting the adsorption capacities of most heavy metals in this study.

2.18.2. Decision Tree

A Decision Tree is a non-parametric supervised learning method that predicts outcomes by creating a tree-like model of decisions. By splitting the dataset based on feature values, it can effectively model

non-linear relationships. This approach yielded improved accuracy over linear regression for adsorption prediction but demonstrated a susceptibility to overfitting the training data.

2.18.3. Random Forest

Random Forest is an ensemble technique that constructs a multitude of decision trees during training and outputs the average prediction of the individual trees. This method enhances model robustness and stability, controlling for overfitting. In this work, Random Forest exhibited strong predictive accuracy, though its performance was surpassed by boosting-based ensemble models.

2.18.4. Support Vector Regressor (SVR)

Support Vector Regression (SVR) adapts the principles of Support Vector Machines for regression tasks by fitting a model that remains within a predefined error margin. While SVR can model non-linear data via kernel functions, it struggled to accurately predict heavy metal adsorption in this context, yielding poor R^2 values, particularly for copper and lead.

2.18.5. Gradient Boosting

Gradient Boosting is an ensemble method that builds models in a sequential manner, where each new model corrects the errors of its predecessor. By iteratively combining weak learners, this technique effectively captures complex data patterns. Gradient Boosting achieved high predictive accuracy across all metals, demonstrating its suitability for modelling intricate adsorption processes.

2.18.6. XG Boost

XG Boost (Extreme Gradient Boosting) is an optimized and regularized implementation of the gradient boosting framework, known for its high efficiency and performance. In this study, XG Boost consistently delivered superior predictive results, achieving the lowest error and highest R^2 scores for several metals. Its robust performance and computational speed make it a leading candidate for adsorption capacity prediction.

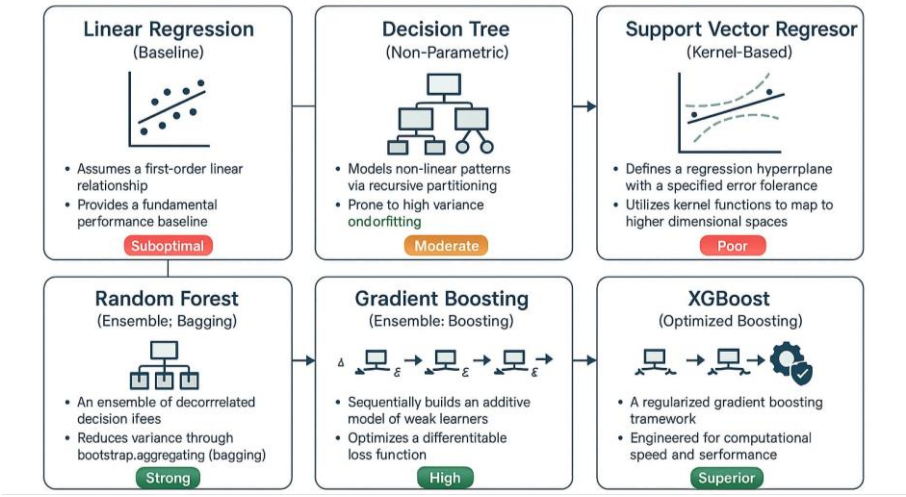

Figure 2-9. A comparative framework of the regression models evaluated in this study**.**

3. MATERIALS AND METHODS

3.1.Materials

3.1.1. Adsorbent Precursors

Two precursor materials were utilized for adsorbent preparation in this study. The first, a sub-bituminous coal, was obtained from the El-Maghara mine in Sinai, Egypt. This material was selected based on its high carbon content (68.4 wt.%), inherent porosity, and local availability, making it a suitable precursor for chemical modification. (Al-Labadi et al., 2023). The second precursor, Norway spruce wood residue (*Picea abies* (L.) Karst), was sourced as a forestry byproduct from Gödöllő, Hungary. This lignocellulosic biomass (composed of cellulose, hemicellulose, and lignin) was chosen due to its low cost, widespread availability, and natural affinity for binding heavy metal ions via its oxygen-containing functional groups(González-Feijoo et al., 2024).

3.1.2. Chemicals and Reagents

All experimental procedures were conducted using analytical-grade chemicals and reagents. The chemical modification of the sub-bituminous coal was performed using sulfuric acid (H_2SO_4, 98%, CorneLab Company) and nitric acid (HNO_3, 65%, Sigma-Aldrich). The model pharmaceutical pollutant investigated was ciprofloxacin (CFX; $C_{17}H_{18}FN_3O_3$; ≥98% HPLC purity, Sigma-Aldrich). For the heavy metal adsorption experiments, stock solutions (1000 mg/L) were prepared in a 0.01 M $NaNO_3$ matrix using the following salts from Merck (Germany): lead nitrate ($Pb(NO_3)_2$), copper nitrate trihydrate ($Cu(NO_3)_2 \cdot 3H_2O$), cadmium chloride hemi pentahydrate ($CdCl_2 \cdot 2.5H_2O$), and zinc nitrate ($Zn(NO_3)_2$). Throughout these experiments, sodium nitrate ($NaNO_3$, 99.9% purity, Merck) was used to maintain constant ionic strength, while sodium hydroxide (NaOH, 98% purity, Sigma-Aldrich) was used for pH adjustment. All chromatographic analyses utilized HPLC-grade methanol (Sigma-Aldrich). Ultrapure deionized water (ddH_2O), with a resistivity of 18.2 MΩ·cm and produced by a Merck Milli-Q system, was used for the preparation of all aqueous solutions and for all rinsing procedures to prevent background contamination.

3.2. Methods

3.1.1. Adsorbent Preparation

3.1.1.1. Acid-Modified Coal Synthesis

The synthesis of acid-modified coal adsorbents, namely Sulfuric acid-modified Coal (**S.C**) and Nitric acid-modified Coal (**N.C**), followed a standardized two-step chemical oxidation protocol. Raw sub-bituminous coal, obtained from the El-Maghara coal mine in Sinai, Egypt, was initially processed to reduce particle size. This involved grinding the coal using a conventional home blender until the coal fraction size was within the range of 20-70 μm. This particle size reduction was intended to maximize the effective surface area available for the subsequent acid modification process and to enhance homogeneity in the reaction. For the acid modification stage, 10 grams of the prepared ground coal were accurately weighed and dispersed separately into two 250 mL glass beakers. One beaker contained 100 mL of 95% sulfuric acid (H_2SO_4, CorneLab Company), while the second beaker contained 50 mL of 65% nitric acid (HNO_3, Sigma-Aldrich; Egypt). Both coal-acid mixtures were then homogenized using magnetic stirrers and heated to 150°C on Stuart CB162 hotplate stirrers for

a controlled reaction time of 60 minutes. This temperature and reaction time were optimized based on preliminary studies(Al-Labadi et al., 2025) to ensure effective oxidation without excessive degradation of the coal structure. Following the acid treatment, the modified coal samples (**S.C** and **N.C**) underwent rigorous washing with deionized distilled water (ddH_2O, Merck Milli-Q system) to remove any unreacted acid, soluble by-products, and residual salts generated during the oxidation. The washing process continued until the pH of the supernatant reached a neutral value (pH ≈ 7), confirming complete removal of free acid. The washed coal samples were then transferred to a digital dryer and dried at 65°C for 10 hours, a duration determined to be sufficient for removing all residual moisture while avoiding thermal alteration of the modified materials. The resulting dried acid-modified coal adsorbents were then carefully collected, labeled as S.C and N.C to denote the respective acid treatment, and stored in sealed containers to maintain their integrity and prevent moisture adsorption prior to characterization and adsorption experiments.

3.1.1.2.Biomass Processing

The preparation of two acid-modified adsorbents, designated as Sulfuric acid-modified Coal (S.C) and Nitric acid-modified Coal (N.C), was conducted using a standard two-step chemical oxidation method, beginning with a particle size reduction of the raw sub-bituminous coal sourced from the El-Maghara mine in Sinai, Egypt. Upon receipt, the raw *Picea abies* sample underwent an initial purification step to eliminate extraneous materials. This involved thorough rinsing of the biomass with deionized distilled water (ddH2O, Merck Milli- Q system) to remove any adhering soil particles, soluble salts, or other surface debris acquired from its agricultural source. The rinsing process was designed to minimize background interference and to ensure that the intrinsic adsorption properties of the Picea abies biomass were accurately assessed. Following purification, the rinsed biomass sample was subjected to a controlled two-stage drying process. Specimens of *Picea abies*, procured from an agricultural enterprise in Gödöllő, Hungary, were utilized to prepare the Norway Spruce Wood Residue (NSWR) biomass adsorbent. The second stage involved drying in a WTB binder 7200 oven (Tuttlingen, Germany) at a temperature of 85 °C for a period of 48 hours. This extended oven drying protocol was implemented to ensure complete removal of moisture and to inhibit microbial activity within the biomass, thereby preserving the material's structural integrity and adsorption characteristics during storage and experimentation. Post-drying, the Picea abies specimen was mechanically processed to enhance its surface properties. Following the initial drying, the specimen underwent comminution into a fine powder utilizing an IKA MF 10 basic Microfine grinder. These steps are shown in Fig.3-1. Subsequently, the pulverized material was carefully sieved to isolate a precise particle size fraction between 90 and 250 µm. This standardization of particle size was a critical step designed to ensure the uniformity of the adsorbent material across all batch adsorption experiments and to mitigate the influence of particle size variability during preliminary testing. Finally, the prepared NSWR biomass powder was preserved in hermetically sealed containers housed within a desiccator (Thermo Fisher Scientific - US). This storage protocol was implemented to prevent any reabsorption of atmospheric moisture, thereby maintaining the adsorbent's anhydrous state prior to its use.2.2.1.3. Synthesis of Nanocrystals from NSWR Biomass.

Figure 3-1. Schematic of NSWR biomass preparation steps for using as adsorbent. (Bayuo et. Al.,2023)

NSWR biomass powder obtained as described in **section 3.2.1.2** was further processed to synthesize nanocrystals via a modified acid hydrolysis procedure following the similar procedure of earlier work (Kaur & Pal, 2023). This process, illustrated schematically in **Figure 3-1**, involves dispersing the NSWR biomass powder in sulfuric acid, followed by acid hydrolysis to selectively break down amorphous regions and liberate crystalline domains. In a typical experiment, 5.0 g of the sieved NSWR biomass powder was dispersed in 50 mL of 64 wt.% sulfuric acid (H_2SO_4) under constant magnetic stirring at 45 °C. Acid hydrolysis was carried out for 2 hours to selectively break down the amorphous regions of the cellulose present in the biomass, thereby liberating crystalline domains. Upon completion of the reaction, the hydrolysis was terminated by slowly adding an excess of ice-cold deionized water, which diluted the acid and quenched further reaction. The resulting suspension was then subjected to centrifugation at 10,000 rpm for 15 minutes to separate the larger, unreacted fragments from the nanocrystal-rich supernatant. To ensure complete removal of acid and by-products, the sediment was re-dispersed in deionized water and the centrifugation cycle was repeated several times until the pH of the supernatant approached neutrality, as confirmed by pH measurement. Following centrifugation, the suspension was transferred into dialysis tubing (with an appropriate molecular weight cut-off) and dialyzed against deionized water for 48 hours, with frequent water changes, to remove any residual acid and low-molecular-weight impurities. After dialysis, the nanocrystal suspension was subjected to ultrasonication for 30 minutes using a probe sonicator to break any remaining agglomerates and obtain a uniform dispersion of nanocrystals. Finally, the well-dispersed nanocrystal suspension was freeze-dried to yield a dry nanocrystalline powder. The resulting product was stored in a desiccator until further characterization and subsequent use in adsorption experiments.

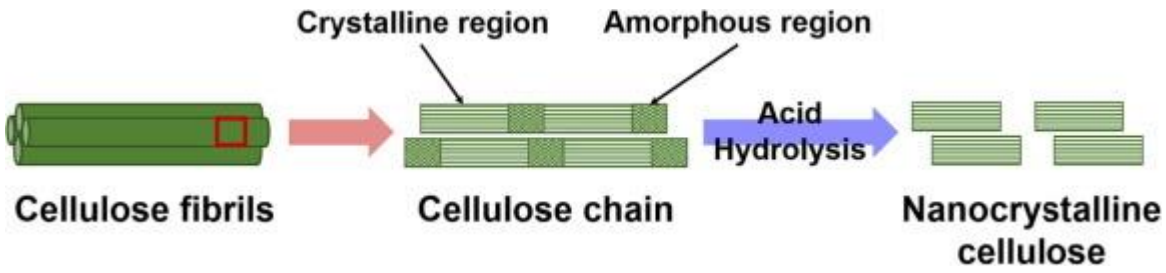

Figure 3-2. Schematic of nanocrystalline cellulose which can be extracted from cellulose

3.2. Adsorbent Characterization Techniques

Comprehensive characterization of the prepared adsorbents is crucial to elucidating their physicochemical properties and understanding the mechanisms governing their adsorption performance for both organic and inorganic pollutants. A suite of complementary techniques, commonly employed in materials science and environmental adsorption studies (Abukhadra et al., 2022), was therefore applied to characterize the coal-based adsorbents (Raw Coal, S.C, and N.C) and Picea abies biomass (NSWR). These techniques encompassed structural, spectroscopic, microscopic, and surface area/porosity analyses, as detailed in the subsequent subsections.

3.2.1. X-Ray Diffraction (XRD) Analysis

X-Ray Diffraction (XRD) analysis is a fundamental technique for determining the crystalline structure and phase composition of materials (Jenkins & Snyder, 1996). In this work, XRD analysis was conducted on raw coal, acid-modified coals (S.C and N.C), and Picea abies biomass (NSWR) (Al-Labadi et al., 2025) to assess the impact of chemical modification and biomass processing on their inherent structural properties. The XRD patterns were acquired using a PANalytical Empyrean X-ray diffractometer, employing Copper K-alpha (Cu-Kα) radiation. The crystallographic structure of the powdered samples was characterized using an X-ray diffractometer (PANalytical, Empyrean model). Diffraction patterns were recorded over a 2θ angular range from 5° to 80°. The instrument was equipped with a copper anode generating Cu-Kα X-ray radiation, which was used for the analysis at a characteristic wavelength (λ) of 1.5418 Å. The resulting diffraction patterns were analyzed to identify crystalline phases, determine the degree of crystallinity, and evaluate any structural alterations induced by acid treatments in coal and the inherent structural features of the Picea abies biomass.

3.2.2. Fourier Transform Infrared Spectroscopy (FTIR)

Fourier Transform Infrared Spectroscopy (FTIR) is an essential technique in materials characterization for identifying functional groups and chemical bonds within a sample. In this work, FTIR spectroscopy was employed to characterize the surface chemistry of raw coal, acid-modified coal derivatives (S.C and N.C) (Al-, and Picea abies biomass (NSWR). Spectra were recorded using a (FTIR-8400S, or Bruker Vertex 70v) mode, across a spectral range of 4000 to 400 cm^{-1}. For coal-based samples analyzed in transmission mode, samples were prepared as KBr pellets to achieve optimal signal quality, a standard protocol for solid-state FTIR analysis (Coates, 2010). The obtained spectra were analyzed to identify characteristic absorption bands corresponding to various functional groups, including hydroxyl, carbonyl, carboxyl, aromatic, and aliphatic groups, and to assess changes in surface functionality upon acid modification of coal and the inherent functional group composition of Picea abies biomass.

3.2.3. Scanning Electron Microscopy (SEM) and Energy-Dispersive X-ray Spectroscopy (EDS)

The surface morphology and elemental composition of the raw coal, acid-modified coals (S.C and N.C), and Norway spruce wood residue (NSWR) were examined using a Gemini Zeiss-Ultra 55 scanning electron microscope. The integrated Energy-Dispersive X-ray Spectroscopy (EDS) system was utilized concurrently to identify the elemental constituents of each material and to map their distribution across the adsorbent surfaces. The textural properties of the adsorbents were quantified by measuring nitrogen (N_2) adsorption-desorption isotherms at 77 K on a Beckman Coulter SA3100 surface area analyzer. Prior to analysis, all samples underwent degassing for 15 hours at 105°C. The specific surface area was calculated using the Brunauer-Emmett-Teller (BET) equation, while the total pore volume and pore size distribution were determined from the data using the Barrett-Joyner-Halenda (BJH) method.

3.2.4. Surface Area and Porosity Analysis

The surface area and porosity characteristics of the raw coal, the acid-modified coals (S.C and N.C), and the Picea abies biomass (NSWR) were quantified through the analysis of gas adsorption isotherm data. The specific surface area for each material was derived using the Brunauer-Emmett-Teller (BET) method, while the Barrett-Joyner-Halenda (BJH) method was employed to calculate the associated pore volume and pore size distribution (Brunauer et al., 1938; Barrett et al., 1951).

3.2.5. Determination of Point of Zero Charge (pH_{PZC})

To understand the pH-dependent adsorption mechanisms, the point of zero charge (pH_{PZC}) of the *Picea abies* biomass (NSWR) was determined. This critical parameter, which indicates the pH at which the adsorbent's net surface charge is zero, was identified using the pH drift method (Kosmulski, 2009). Following this procedure, the final equilibrium pH of the suspensions was measured with a calibrated pH meter. The pH_{PZC} value was then determined from the resulting pH drift curves, providing an essential basis for interpreting the heavy metal adsorption behaviour of the NSWR biomass under varying pH conditions (Fiol et al., 2006).

3.3. Batch Adsorption Experiments

Batch adsorption experiments were conducted to evaluate the efficacy of raw and acid-modified coal adsorbents for the removal of ciprofloxacin (CFX) from aqueous solutions, providing a controlled environment to assess the adsorption performance under varying experimental conditions. This batch method approach is a widely recognized and versatile technique for evaluating adsorbent materials, allowing for systematic investigation of key parameters influencing the adsorption process, including adsorbate concentration, temperature, contact time, and pH, crucial for understanding the adsorption behavior and optimizing the operational conditions for effective CFX sequestration in batch systems (Weber & DiGiano, 1996)

3.3.1. Batch Adsorption Experiments for Ciprofloxacin (CFX) Removal using Coal-Based Adsorbents

Batch adsorption experiments were conducted to assess the efficacy of three coal-based adsorbents raw sub-bituminous coal (R.C), sulfuric acid-modified coal (S.C), and nitric acid-modified coal (N.C)—for the removal of ciprofloxacin (CFX). To ensure a consistent basis for comparison, all experiments were performed using a fixed adsorbent dosage of 0.2 g/L in a 250 mL solution volume. The effects of key operational parameters were then systematically investigated.

- **Effect of Solution pH:** The impact of solution pH on CFX adsorption was investigated across a pH spectrum from 2 to 9. The pH of the solutions was modulated to the target values using dilute HCl and NaOH.
- **Adsorption Kinetics:** To ascertain the time required to achieve equilibrium, kinetic experiments were conducted by systematically varying the contact time over a period ranging from 30 to 1200 minutes (18 hours).
- **Effect of Initial Concentration:** To evaluate the maximum adsorption capacity, equilibrium isotherm experiments were performed using a range of initial CFX concentrations from 100 to 800 mg/L.

3.3.2. Batch Adsorption Experiments for Heavy Metal Removal using Picea abies Biomass Adsorbent

The efficacy of *Picea abies* biomass (NSWR) as a biosorbent was assessed in batch adsorption experiments for the simultaneous removal of Lead (II), Copper (II), Zinc (II), and Cadmium (II) ions from a quaternary aqueous solution. Following established methodologies (Marin & Ayele, 2002). these experiments were structured to determine the removal efficiency and adsorption capacity of the NSWR. This was achieved by systematically investigating the influence of several critical operational parameters, including adsorbent dosage, contact time, initial metal ion concentration, solution pH, temperature, and adsorbent particle size.

3.3.2.1. General Batch Adsorption Procedure

The standard procedure for the batch adsorption experiments involved placing a defined quantity of the NSWR biomass adsorbent into a 250 mL sealed Erlenmeyer flask containing 50 mL of the quaternary metal solution at a specified concentration. These flasks were then agitated at a constant speed of 200 rpm using a GFL 1083 temperature-controlled shaker water bath to ensure a uniform suspension. Unless otherwise specified for thermodynamic studies, the experimental temperature was strictly maintained at (25.6-26.2) °C.

3.3.2.2.Variation of Experimental Parameters

To systematically evaluate the impact of key experimental variables on heavy metal adsorption by NSWR biomass, a series of controlled batch experiments were conducted, varying individual parameters while holding others constant. These parameters and their variation ranges were:
pH Variation: The influence of pH on adsorption was examined over a range from pH 2.0 to 6.0. The pH of the experimental solutions was modulated to the desired values using dilute HNO_3 and NaOH. Post-adsorption, the resulting supernatant was preserved by acidification with 68% HNO_3.

Mixing Time (Contact Time) Variation: The influence of mixing time, representing the duration of contact between the NSWR biomass and the heavy metal solution, was examined across a range of time intervals. 20 hours for coal, and 400 mins.
Particle Size Variation: To evaluate the effect of NSWR biomass particle size on heavy metal adsorption, the adsorbent material was calibrated to different particle size ranges calibrated to ranges including: (<90 μm), (90-250 μm), (250-500 μm), (500-710 μm), and (710-1000 μm).
Temperature Variation: The impact of temperature on heavy metal adsorption was investigated at 5 distinct temperature levels, ranging from 25 °C to 45 °C.
Stirring Speed Variation: The impact of agitation rate was assessed by varying the stirring speed from 40 to 400 rpm utilizing a New Brunswick Scientific Gyrotory shaker (Model G2, US).
Adsorbent Mass Variation: The influence of adsorbent mass was tested by varying the amount of NSWR biomass added to the metal solutions. For MASS Dosage test series list 'MASS 'range of Dosage from 0 - 0.5 g.
Initial Metal-Ion Concentration: The effect of the initial solute concentration was investigated by preparing quaternary heavy metal solutions with concentrations spanning the range of 1 to 100 mg/L.

3.3.3. Batch Adsorption Experiment for Heavy Metals Removal Using Nanocrystals Adsorbent Synthesized from NSWR to Real Laundry Wastewater.

Nanocellulose synthesized from NSWR was used as an adsorbent for the treatment of any potential HMs found in real wastewater effluents resulted from a local laundry shop outlet obtained from Madaba City-Jordan to avoid any potential threats of direct discharge to sewerage system. Several 10 different sets of laundry wastewater samples, each set contains (3 replicates and control) with a volume of 2L, were obtained day by day from the outlet of laundry shop in Madaba, placed in plastic bottles. The pH and temperature were measured onsite to avoid possible misleading or false measurements. The bottled samples were then acidified with a few drops of diluted HNO_3, tightly closed and stored in a laboratory ice container for analysis. The source of feed water was tapping water from municipal origin (was considered as control).
In the experiment of HM 's determination, the measured samples represent the average concentration of the HMs in the 3 replicates minus the concentration of HMs in the feed water.

3.4. Analytical Methods for Pollutant Quantification

To accuramaterials andmine the concentrations of pollutants and evaluate the adsorption efficiency of the prepared materials, HPLC techniques were used. Ciprofloxacin concentrations in aqueous solutions, post-adsorption experiments using coal-based adsorbents, were quantified using High-Performance Liquid Chromatography (HPLC), while heavy metal ion concentrations, in experiments using Picea abies biomass, were determined by (ICP-OES). The detailed methodologies for each analytical technique are described in the following subsections.

3.4.1. High-Performance Liquid Chromatography (HPLC) for Ciprofloxacin Quantification

The concentration of Ciprofloxacin (CFX) in the aqueous samples was quantified using a High-Performance Liquid Chromatography (HPLC) system. The system was equipped with a pump (L-7100), a UV detector (L-7400), and a Rheodyne 7725i injection valve fitted with a 20 μL sample loop. Chromatographic separation was achieved on a Luna column (150 mm × 4.6 mm, Phenomenex, Torrance, USA) featuring a 5 μm PFP (Pentafluorophenyl) stationary phase. The mobile phase

consisted of a 60:40 (v/v) mixture of distilled water and analytical grade methanol, delivered at a constant flow rate of 1.0 mL/min.
Following analysis, the experimental adsorption capacity at equilibrium (Q_e, mg/g) was calculated using the measured initial (C_0) and equilibrium (C_e) CFX concentrations (mg/L), the solution volume (V, mL), and the adsorbent mass (m, mg), as shown in Equation 1,

$$\boldsymbol{Q_e\left(\frac{mg}{g}\right) = \frac{(C_o - C_e)V}{m}} \quad \textbf{(1)}$$

The goodness-of-fit for the kinetic and isotherm models (listed in Supplementary Table S1) was evaluated via nonlinear regression analysis. The degree of correlation was quantitatively assessed using the coefficient of determination (R^2) and the Chi-squared (χ^2) statistic, calculated according to Equations 2 and 3:

$$\boldsymbol{R^2 = 1 - \frac{\Sigma(Q_{e,exp} - Q_{e,cal})^2}{\Sigma(Q_{e,exp} - Q_{e,mean})^2}} \quad \textbf{(2)}$$

$$\chi^2 = \sum \frac{(Q_{e,exp} - Q_{e,cal})^2}{Q_{e,cal}} \quad \textbf{(3)}$$

For the advanced isotherm models derived from statistical physics (**Supplementary Table S1**), the model accuracy was further validated using the root mean square error (RMSE), as defined in Equation 4.

$$RMSE = \sqrt{\frac{\sum_{i=1}^{m}(Q_{cal}^{i} - Q_{exp}^{i})^2}{m' - p}} \quad \textbf{(4)}$$

In this equation, m' represents the number of data points, p is the number of model parameters, and Q_{cali} and Q^{i}_{exp} are the calculated and experimental CFX uptake capacities, respectively.

2.5.2 Determination of Heavy Metal Ion Concentrations via ICP-OES

The quantification of residual heavy metal ion concentrations in the aqueous supernatant following the adsorption experiments was performed using an Inductively Coupled Plasma-Optical Emission Spectrometer (ICP-OES, Horiba Jobin Yvon Activa-M).
From the resulting data, the equilibrium adsorption capacity (q_e, mg/g) and the percentage removal efficiency (R, %) for the NSWR biosorbents were calculated. These calculations were based on Equations 5 and 6 (Rahman & Sathasivam, 2015)

$$\boldsymbol{qe = \frac{(Ci - Cf)}{m} \times V} \quad \textbf{(5)}$$

$$\boldsymbol{R(\%) = \frac{(Ci - Cf)}{Ci} \times 100} \quad \textbf{(6)}$$

In these equations, C_i and C_f represent the initial and final metal ion concentrations (mg/L), respectively; V corresponds to the solution volume (L), and m is the mass of the biosorbent (g).

3.5. Data Analysis and Modeling

To provide a quantitative understanding of the pollutant removal process, the data from the batch adsorption experiments were analysed using a series of established mathematical models. This

analytical approach is essential for interpreting experimental results and elucidating the governing adsorption mechanisms (Pourhakkak et al., 2021). To comprehensively analyse the adsorption process, a suite of mathematical models was applied. Kinetic modelling was utilized to ascertain the rate of solute uptake and to identify the rate-controlling mechanisms of the process. Isotherm models were employed to elucidate the equilibrium characteristics of adsorption and to describe the nature of the interaction between the adsorbate and the adsorbent surface. Furthermore, key thermodynamic parameters were computed to evaluate the spontaneity and energetic profile of the reaction. The applicability of each model was quantitatively assessed by evaluating the goodness-of-fit through rigorous statistical error analysis. The specific models used in this investigation are elaborated upon in the sections that follow.

3.5.1. Kinetic Model Application

To elucidate the rate-controlling mechanisms for the adsorption of both ciprofloxacin and heavy metals, the experimental data were fitted to several kinetic models. This analysis is crucial for understanding mass transfer limitations and for process design (J. Wang & Guo, 2020; Pourhakkak et al., 2021). Both reaction-based models specifically the Pseudo-First Order (PFO), Pseudo-Second Order (PSO), and Elovich equations and diffusion-based models (intraparticle and film diffusion) were applied. The diffusion models were used to determine if the rate-limiting step was governed by mass transfer across the exterior liquid film or by diffusion within the adsorbent's internal pore structure (Hu et al., 2024, Al-Labadi et al., 2025).

The models were fitted to the data via non-linear regression using Origin 2025 software (OriginLab Corporation). The goodness-of-fit for each model was quantitatively evaluated using the coefficient of determination (R^2), as defined in Equation 7.

$$\boldsymbol{R2 = 1 - \left[\frac{\Sigma(qe,exp - qe,cal)2}{\Sigma(qe,exp - qe,mean)}\right]} \qquad \textbf{(7)}$$

In this equation, $q_{e,exp}$ represents the experimental adsorption capacity, and $q_{e,cal}$ is the capacity calculated from the respective kinetic model. An R^2 value approaching 1.0 indicates a superior fit of the model to the experimental data.

3.5.1.1.Adsorption Reaction Models (Empirical kinetic models)

The kinetic data were evaluated using three widely applied empirical models based on reaction kinetics: the Pseudo-First Order (PFO), Pseudo-Second Order (PSO), and Elovich equations. These models, which assume the adsorption rate is controlled by factors like solute concentration or active site availability, were chosen for their proven applicability across diverse adsorption systems. The specific mathematical formulations for both the non-linear and linear forms of these models are presented in **Table 3-1**.

Table 3-1. Mathematical Formulations of Applied Adsorption Kinetic Models.

Kinetic Model	(Linear)	(Non-Linear)	Parameters
PFO	$\log(q_e - q_t) = log\ (q_e) - \left(\frac{k_1}{2.303}\right)t$	$q_t = q_e(1 - e^{-k_1 t})t$	q_e: the amount of metal ion (mg. g^{-1}) at equilibrium. q_t: the amount of metal ion (mg. g^{-1}) k_1: the rate constant in min^{-1}

PSO	$\frac{t}{q_t} = \frac{1}{k_2 q_e^2} - \frac{1}{q_e} t$	$q_t = \frac{q_e^2 k_2 t}{q_e k_2 t + 1}$	k_2: the rate constant in g. mg^{-1}. min^{-1}.
IPD	$q_t = K_{id} t^{\frac{1}{2}} + C$	$q_t = K_{id} t^{\frac{1}{2}}$	K_{id}:the rate constant (mg. g^{-1}. $min^{-0.5}$). $t^{\frac{1}{2}}$: the square root of time ($min^{0.5}$)
ELOVICH	$qt = \frac{ln\ \alpha b}{b} + \frac{1}{b}\ ln\ t$	-	a and b

3.5.1.2.Pseudo-First Order (Lagergren) Model

The Pseudo-First Order (PFO) model, first proposed by Lagergren, is founded on the assumption that the rate of adsorption is directly proportional to the number of available active sites on the adsorbent surface (Mohamed Nasser et al., 2024). Its linear mathematical expression is given by:

$$\boldsymbol{log(q_e - q_t) = log\ (q_e) - \left(\frac{k_1}{2.303}\right) t} \quad \textbf{(8)}$$

Here, q_e (mg/g) and q_t (mg/g) represent the adsorption capacity at equilibrium and at a given time t (min), respectively. The PFO rate constant (k_1, min^{-1}) and the theoretical equilibrium capacity (q_e) are derived from the slope and intercept of a linear plot of log (q_e - q_t) versus t. A noted limitation of this model is its frequent inability to accurately describe the full-time course of adsorption, particularly for systems where the rate-controlling step is diffusion-based (Weber Jr & Morris, 1963).

3.5.1.3. Pseudo-Second-Order Model (Ho and McKay Model)

Conversely, the Pseudo Second Order (PSO) kinetic model is predicated on the assumption that chemisorption is the rate-limiting step, involving direct chemical interactions between the adsorbate and adsorbent (Mohamed Nasser et al., 2024). This premise implies that the adsorption rate is proportional to the square of the unoccupied active sites. The linearized form of the PSO model is expressed as:

$$\boldsymbol{\frac{t}{q_t} = \frac{1}{k_2 q_e^2} - \frac{1}{q_e} t} \quad \textbf{(9)}$$

where The equilibrium adsorption capacity (q_e, mg/g) and the PSO rate constant (k_2, g/mg·min) are determined from the slope ($1/q_e$) and intercept ($1/k_2 q_e^2$) of a linear plot of t/q_t versus t. A significant strength of the PSO model is its frequent and accurate fit to experimental data across the entire adsorption duration, rendering it highly suitable for systems dominated by chemisorption.

.

3.5.1.4. Elovich Model

The Elovich model is an empirical equation used to describe adsorption kinetics, particularly for systems involving chemisorption on energetically heterogeneous surfaces. Its fundamental assumption is that the activation energy of adsorption varies as the extent of surface coverage changes (Yao & Zhu, 2021). The linearized form of this model is expressed as:

:

$$\boldsymbol{qt = \frac{ln\ \alpha b}{b} + \frac{1}{b}\ ln\ t} \quad \textbf{(10)}$$

In this equation, q_t (mg/g) represents the quantity of solute adsorbed at a given time t (min). The model's parameters the initial adsorption rate (a, mg/g·min) and the desorption constant (b, g/mg),

which is related to surface coverage are determined from the slope (1/b) and intercept ((1/b)ln(ab)) of a linear plot of q_t versus ln(t).

3.5.2. Adsorption Diffusion Models (Mass transfer models)

To provide a more mechanistic insight into the adsorption process, diffusion-based models were used to identify potential rate-limiting steps

3.5.2.1.Weber-Morris Intraparticle Diffusion Model

The Weber-Morris intraparticle diffusion model was applied to assess the influence of pore diffusion as a potential rate-controlling step in the adsorption process (Weber Jr & Morris, 1963) The linearized mathematical expression for this model is:

$$\mathbf{qt = Kpt^{0.5} + I} \qquad \mathbf{(11)}$$

In this equation, q_t (mg/g) denotes the adsorption capacity at time t (min), k_p (mg/g·min$^{0.5}$) represents the intraparticle diffusion rate constant, and I is a constant indicative of the boundary layer thickness. The model posits that if a linear plot of q_t against $t^{0.5}$ passes through the origin (i.e., $I \approx 0$), then intraparticle diffusion is the exclusive rate-limiting step. Conversely, a non-zero intercept suggests that the overall adsorption rate is also influenced by external mass transfer, or film diffusion (Mohamed Nasser et al., 2024).

3.5.2.2.The Liquid Film Diffusion Model

To specifically assess the influence of external mass transfer, the liquid film diffusion model was also applied. This model evaluates the resistance to mass transfer across the boundary layer surrounding the adsorbent particle. Its linear form is expressed as:

$$\boldsymbol{ln(1-F) = -Kfdtln(1-F) = -Kfdt} \qquad \mathbf{(12)}$$

where F is the fractional attainment of equilibrium (q_t/q_e) and kpd represents the film diffusion rate constant (min^{-1}). Applicability of this model is indicated when a linear plot of -ln (1 - F) versus t passes through the origin, suggesting that mass transfer across the liquid film is the rate-limiting step.

3.6. Thermodynamics Parameters Calculation

The thermodynamic feasibility and nature of the adsorption process were evaluated by determining the change in Gibbs free energy (ΔG°), enthalpy (ΔH°), and entropy (ΔS°). A negative ΔG° value signifies a spontaneous process. The sign of ΔH° indicates whether the reaction is exothermic (-) or endothermic (+), while ΔS° describes the change in randomness at the solid-liquid interface (Abas et al., 2013) These parameters were calculated from the following thermodynamic relationships:

$$\mathbf{\Delta G^{\circ} = - RT\ lnK_C} \qquad \mathbf{(13)}$$

$$\mathbf{K_c = q_e/C_e} \qquad \mathbf{(14)}$$

$$\mathbf{lnK_C = (\Delta S^{\circ}/R) - (\Delta H^{\circ}/RT)} \qquad \mathbf{(15)}$$

3.7. Adsorption Isotherm Modelling

To describe the equilibrium relationship between the solute concentration and the amount adsorbed at a constant temperature, the data were fitted to several isotherm models. This analysis is crucial for

determining the adsorbent's maximum uptake capacity (q_m) and understanding the surface interaction mechanisms (Abin-Bazaine et al., 2022; Low et al., 2023). Four widely recognized models were Fapplied: Langmuir, Freundlich, Dubinin–Radushkevich (D-R), and Temkin.
The models were fitted using non-linear regression analysis. The coefficient of determination (R^2) was used to assess the goodness-of-fit and identify the most suitable model. The specific equations for these models, including their linear and non-linear forms, key parameters, and general findings, are summarized in **Table A9-3**.

3.8. Thermodynamic Modelling

To elucidate the energetic nature and spontaneity of the metal adsorption onto the NSWR biomass, a thermodynamic analysis was conducted. This was achieved by applying the van't Hoff equation to temperature-dependent equilibrium data:

$$lnKC = (\Delta S^\circ/R) - (\Delta H^\circ/RT) \quad \textbf{(19)}$$

In this equation, R is the universal gas constant (8.314 J/mol·K) and T is the absolute temperature (K). The enthalpy (ΔH°) and entropy (ΔS°) of the process were determined from the slope (-ΔH°/R) and intercept (ΔS°/R) of a linear plot of ln (K_e) versus 1/T. The dimensionless equilibrium constant (K_e) was calculated as the ratio of the solid-phase solute concentration (q_e) to the liquid-phase solute concentration (C_e) at equilibrium. The resulting thermodynamic parameters for the adsorption of the investigated metal ions are presented in Table Apx 2-2.

3.9. Regeneration and Recyclability Studies of CPX on Coal Adsorbent

To evaluate their potential for practical application, the reusability of the N.C, R.C, and S.C adsorbents for CFX removal was investigated. After each adsorption experiment, the spent adsorbents were regenerated through a simple washing and drying procedure. The protocol consisted of washing the materials three times with distilled water, followed by drying at 65°C for 10 hours. This temperature was selected to ensure complete removal of residual moisture while maintaining the integrity of the adsorbent material and the adsorbed CFX molecules, as it is below the reported decomposition temperatures for CFX and is consistent with drying temperatures used in similar studies for coal-based adsorbents (Gao et al., 2013)**.**
The performance of the regenerated adsorbents was then re-tested in subsequent adsorption cycles. These reusability tests were conducted under a fixed set of experimental parameters: an initial CFX concentration of 800 mg/L, an adsorbent dosage of 0.2 g/L, a pH of 8, a contact time of 1,080 minutes, and a temperature of 318.13 K.

3.10. Predictive Model Evaluation and Selection

A comparative analysis of six regression models was performed to identify the most effective approach for predicting the adsorption capacities of Cadmium (Cd), Copper (Cu), Lead (Pb), and Zinc (Zn). The models were evaluated based on key performance metrics, including Mean Absolute Error (MAE) and the coefficient of determination (R^2). The evaluation revealed that ensemble methods, particularly Gradient Boosting and XGBoost, provided the most accurate and reliable predictions, consistently yielding the highest R^2 values. While Decision Tree and Random Forest models performed adequately, they were surpassed by the boosting techniques. In contrast, Linear Regression and Support Vector Regression (SVR) were found to be unsuitable for this application, as indicated by poor performance metrics. Based on this evaluation, the boosting-based ensemble methods were identified as the most robust for simulating the complex process of heavy metal adsorption.

3.11. Computational Workflow for Regression Modeling

The computational workflow for model training and evaluation was executed within a Jupyter Notebook environment and comprised the following key stages:

1. **Data Import and Preprocessing:** The experimental dataset was imported, and standard preprocessing steps were applied. This included handling any missing values and applying feature scaling to normalize the data prior to modeling.
2. **Model Implementation and Training:** The six regression models (Linear Regression, Decision Tree, Random Forest, SVR, Gradient Boosting, and XGBoost) were implemented and subsequently trained on the preprocessed training dataset.
3. **Performance Evaluation:** The predictive performance of each trained model was quantified using standard statistical metrics, including MAE, Root Mean Squared Error (RMSE), and R^2.
4. **Results Visualization:** Graphical representations, such as bar charts, were generated to facilitate a direct visual comparison of model performance across the different metals.
5. **Model Selection:** The final stage involved a comprehensive comparison of the evaluation metrics to identify the optimal predictive model for the adsorption process

4. RESULTS AND DISCUSSION

4.1. Acid-Modified Coal for Ciprofloxacin Removal

4.1.1. Characterization of Acid-Modified Coal

The structural, chemical, and morphological characteristics of the raw coal, alongside its acid-modified counterparts, were examined using a suite of analytical techniques, including X-ray diffraction (XRD), Fourier Transform Infrared Spectroscopy (FTIR), and Scanning Electron Microscopy (SEM). The primary objective of these analyses was to elucidate the transformations in the coal's crystalline structure, surface functional groups, and topography resulting from the acid modification, as these properties fundamentally govern its adsorptive performance. Specifically, XRD analysis was utilized to compare the phase composition and crystalline nature of the raw coal with the modified samples, thereby revealing the structural consequences of the acid treatment.

4.1.1.1. XRD Analysis

The structural modifications induced by acid treatment were investigated by comparing the X-ray diffraction (XRD) patterns of the raw coal (RC) with those of the sulfuric acid-modified (SC) and nitric acid-modified (NC) samples, as depicted in **Figure 4-1**. The diffractogram for the untreated raw coal (**Figure 4-1A**). The broadness of these peaks confirms the amorphous nature of the precursor material prior to modification. Following treatment with H_2SO_4, the resulting SC sample (Figure 3-1B) exhibited a substantial alteration in its diffraction pattern, including a significant shift in the first peak (10°–32°) and a marked decrease in the intensity of the second peak. These changes are indicative of considerable disruption to the C-O-C linkages within the coal structure, a consequence of the oxidation process that enhances the material's amorphous character through dehydration into a polyaromatic carbon structure. A similar, though less pronounced, trend was observed for the NC sample (Figure 3-1C), where the primary peaks showed slight shifts and reductions in intensity relative to the raw coal, but not to the extent seen with the SC sample. Collectively, these XRD findings suggest that sulfuric acid treatment imparts a more profound oxidation and dehydration effect on the coal's structure, leading to a greater degree of amorphization compared to the nitric acid modification.

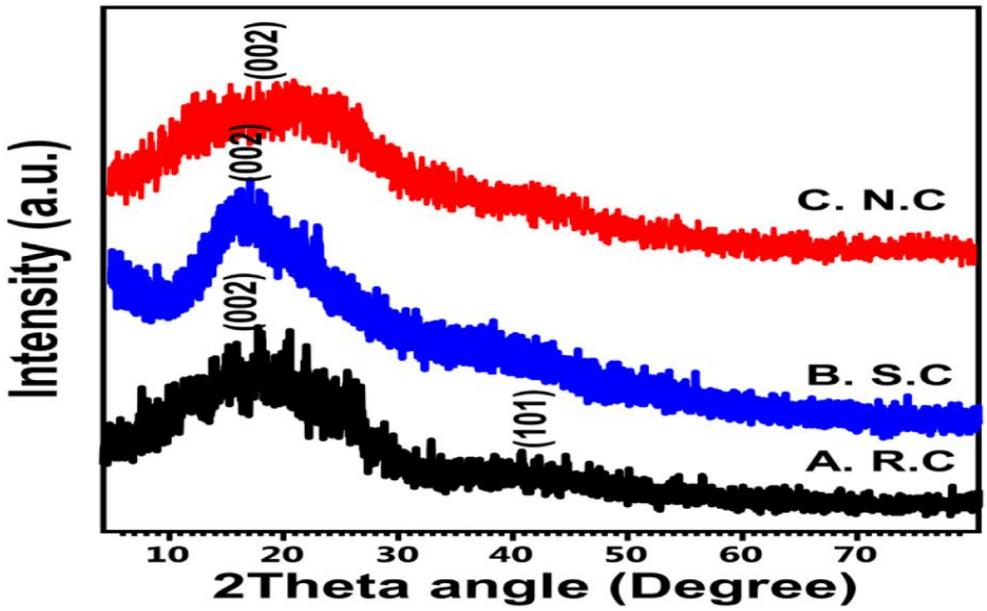

Figure 4-1. Comparative XRD diffractograms of (A) the raw coal (RC) precursor, (B) the sulfuric acid-treated coal (SC), and (C) the nitric acid-treated coal (NC).

4.1.1.2. FTIR Analysis:

Fourier Transform Infrared (FTIR) spectroscopy was employed to identify the changes in surface functional groups resulting from the acid treatments. The FTIR spectrum of the raw coal precursor (**Figure 4-2A**) exhibited characteristic absorption bands, including those for aromatic C-H (500–900 cm^{-1}), aliphatic C-H (2858–2940 cm^{-1}), C-O stretching (1000–1200 cm^{-1}), aromatic C=C (1616 cm^{-1}), carbonyl C=O (1716 cm^{-1}), and a broad -OH band (3000–3600 cm^{-1}) (Boral et al., 2021).

Significant alterations were observed in the spectra of the modified samples. For the sulfuric acid-treated coal (SC), the spectrum (Figure 3-2B) showed a notable intensification of the hydroxyl band (~3398 cm^{-1}) and the C=O band (~1712 cm^{-1}), confirming a strong oxidative effect and the introduction of carboxylic acid groups (–COOH) (Mateo et al., 2021). Furthermore, new bands appeared that are characteristic of sulfur-containing functional groups, including $-SO_3H$ (1133 cm^{-1}), O=S=O (1025 cm^{-1} and 1001 cm^{-1}), and C-S (578 cm^{-1}) (Mateo et al., 2021). Similarly, the nitric acid-treated coal (NC) spectrum (Figure 3-2C) displayed a pronounced shift in the -OH band (~3355 cm^{-1}) and an enhancement of the C=O stretching band (~1716 cm^{-1}). Critically, this sample also showed new absorption bands assigned to nitrogen-containing groups, such as N=O and C-N stretching (~1546 cm^{-1}), which confirms the incorporation of new active sites via nitric acid oxidation (Alvarez et al., 2003).

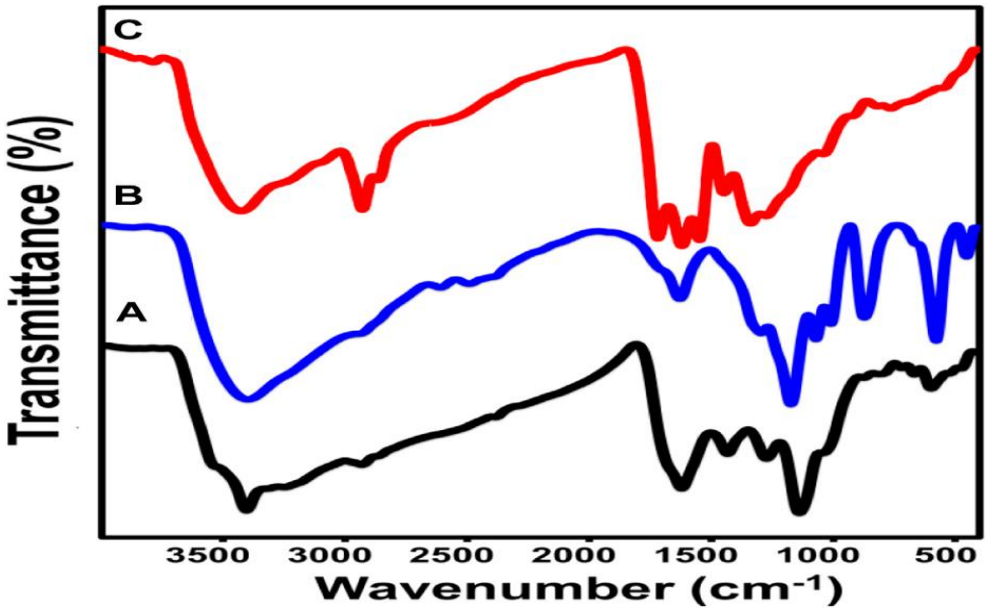

Figure 4-2 Comparative FTIR Spectra Illustrating the Chemical Structure of (A) Raw Coal (RC), (B) Sulfuric Acid-Treated Coal (SC), and (C) Nitric Acid-Treated Coal (NC).

The FTIR analysis was corroborated by elemental analysis, which quantified the changes in the materials' chemical composition (**Table 4-1**). The data reveal a substantial increase in the nitrogen (N) content for the N.C sample and the sulfur (S) content for the S.C sample, confirming the successful incorporation of new, element-specific functional groups during the respective acid modification processes.

Table 4-1. Chemical Composition, Acid Density, and Surface Area Properties of Raw Coal (R.C), Sulfuric Acid-Modified Coal (S.C), and Nitric Acid-Modified Coal (N.C) Adsorbents.

Parameter	**R.C**	**N.C**	**S.C**
C (Wt. %)	68.4	53.2	48.8
S (Wt. %)	2.32	2.12	7.6
N (Wt. %)	2.53	9.3	7.6
H (Wt. %)	6.3	8.72	10.8
O (Wt. %)	10.6	19.7	24.4
Acid density (mmol/g)	0.064	4.62	8.4
Surface area (m^2/g)	5.4	18.3	26.4

The significant increase in sulfur content within the S.C material is attributed to sulfonation reactions. This process is initiated by sulfuric acid's interaction with the coal structure, leading to the cleavage of oxygen-hydrogen bonds and subsequent protonation of oxygen atoms. These interactions facilitate the formation of effective electrophiles, such as protonated sulfur trioxide, from the entrapped sulfur ions (Yu et al., 2018). The subsequent electrophilic assault on the aromatic rings within the coal matrix disrupts the double bonds, enabling the incorporation of new sulfur-containing functional groups. Concurrently, the reaction generates HSO_4^- radicals, which act as effective bases in removing hydrogen protons (S. M. Ibrahim et al., 2021). Similarly, the elevated nitrogen content in the N.C sample is a result of electrophilic nitration of the aromatic structures. In this mechanism, the nitrenium

ion (NO_2^+) acts as the primary electrophile, attacking the aromatic rings to form a σ-complex. This reaction results in the formation of nitrobenzene-type compounds on the coal surface, which accounts for the observed increase in both nitrogen and oxygen content in the treated material (Shi et al., 2012).

4.1.1.3. Morphological and Textural Analysis

Scanning Electron Microscopy (SEM) was used to visualize the morphological changes induced by the acid treatments (**Figure 3-3**). The untreated raw coal (**Figure 3-3A**) presented a relatively smooth and compact surface, characteristic of its natural, layered structure. In stark contrast, the sulfuric acid-treated coal (SC) displayed a markedly more rugged and irregular topography, featuring numerous nanoscale protrusions and the formation of new micropores (**Figures 3-3B, C**). These features are likely a result of the acid leaching mineral impurities from the coal matrix. The nitric acid-treated sample (NC), while also showing evidence of surface modification through the appearance of decorated nanoscale nodules, did not exhibit the same degree of topographical alteration as the SC sample (**Figure 3-3D**). These visual changes corresponded directly with significant alterations in the material's textural properties, as quantified by surface area and porosity analysis (**Table 3-1**). A substantial enhancement in the specific surface area was observed, increasing from 5.4 m^2/g in the raw coal to 18.3 m^2/g for NC and 26.4 m^2/g for SC. This was accompanied by a dramatic increase in the total pore volume, which rose from 0.011 cm^3/g for the raw material to 0.41 cm^3/g and 0.48 cm^3/g for NC and SC, respectively. Concurrently, the treatment led to a reduction in the average pore diameter from 50.2 nm (RC) down to 34.8 nm (NC) and 22.4 nm (SC). The development of this enhanced porosity is primarily attributed to the acid treatments creating new micropores through the dissolution and leaching of mineral impurities originally present in the coal matrix.

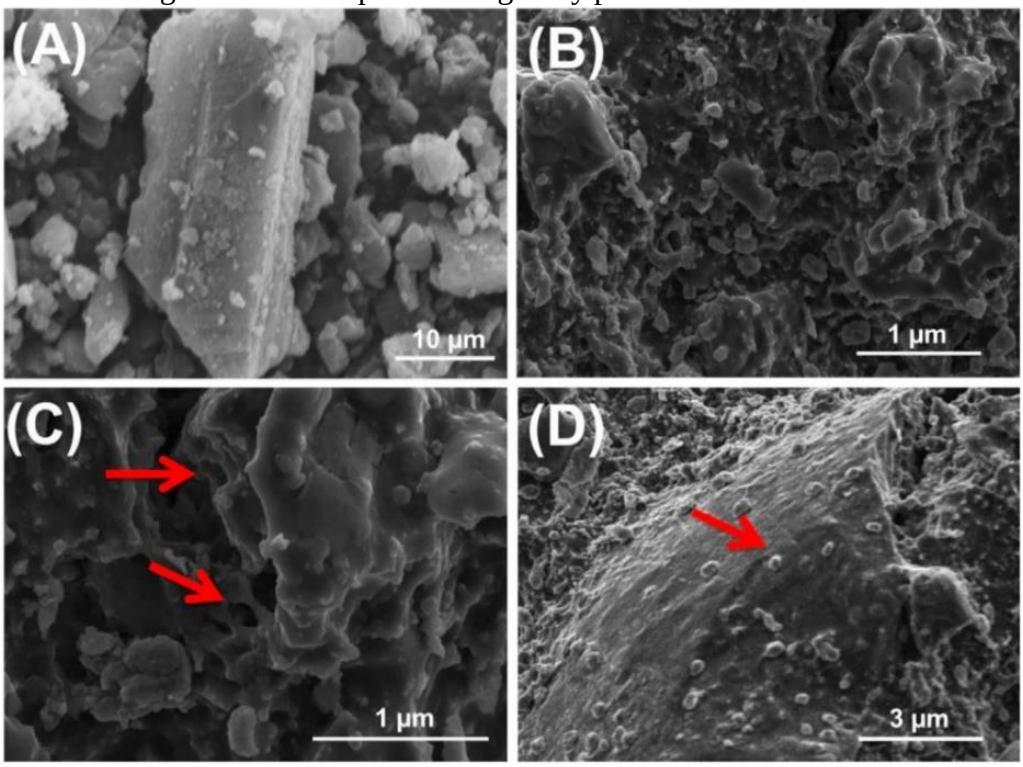

Figure 4-3. SEM micrographs illustrating the surface morphology of: (A) raw coal (RC); (B, C) sulfuric acid-treated coal (SC) at different magnifications; and (D) nitric acid-treated coal (NC).

4.1.2. Adsorption of CFX molecules

4.1.2.1.Effect of Solution pH

The influence of solution pH on the adsorption of Ciprofloxacin (CFX) was investigated over a pH range of 2 to 8, while holding other experimental parameters constant (adsorbent dosage: 0.2 g/L; contact time: 240 min; initial CFX concentration: 200 mg/L; temperature: 298 K). Solution pH is a critical variable as it governs both the surface charge of the adsorbent and the speciation of the CFX molecule in solution. The experimental results show that the CFX uptake capacity for all three adsorbents—raw coal (RC), nitric acid-modified coal (NC), and sulfuric acid-modified coal (SC)—increased progressively with rising pH, reaching maximum values at approximately pH 8 (Figure 3-4A). At this optimal pH, the adsorption capacities were 66.4 mg/g for RC, 82.3 mg/g for NC, and 90.6 mg/g for SC. Beyond this point, at pH 9, a decline in adsorption was observed for all materials.

This behavior can be explained by the interplay between the adsorbent surface charge and the zwitterionic nature of CFX. CFX has two dissociation constants ($pKa_1 = 6.1$ and $pKa_2 = 8.7$), meaning it exists predominantly as a cation (CFX^+) at pH < 6.1, a zwitterion (CFX^{+-}) between pH 6.1 and 8.7, and an anion (CFX^-) at pH > 8.7 (Gor & Dave, 2020). The points of zero charge (pH_{PZC}) for the adsorbents were determined to be 6.6 (RC), 6.2 (NC), and 5.4 (SC). At highly acidic conditions (pH < pH_{PZC}), the adsorbent surfaces are positively charged, leading to electrostatic repulsion with the cationic CFX^+, which limits adsorption. Conversely, at highly alkaline conditions (pH > 9), both the adsorbent surfaces and the CFX molecules are negatively charged, again resulting in electrostatic repulsion. The optimal adsorption observed in the pH 6-8 range is therefore attributed to favorable electrostatic interactions between the negatively charged surfaces of the adsorbents (as the pH is above their respective pH_{PZC} values) and the zwitterionic and cationic forms of the CFX molecules.

4.1.2.2. Kinetic Studies

4.1.2.2.1. Time Interval

To determine the time required to reach equilibrium and to investigate the rate of adsorption, the uptake of CFX onto RC, NC, and SC was monitored over a time course of 1080 minutes. The experiments were performed under fixed conditions: an adsorbent dosage of 0.2 g/L, a solution pH of 8.0, an initial CFX concentration of 200 mg/L, and a temperature of 298 K. The kinetic profiles for all three adsorbents are presented in **Figure 3-4B**. The data reveals a characteristic two-stage adsorption process. An initial, rapid uptake phase was observed, occurring within the first approximately 480 minutes of contact time. This was followed by a much slower secondary phase, where the rate of adsorption gradually diminished until a plateau was reached, indicating that the system had achieved equilibrium. At this point, the equilibrium adsorption capacities (Q_e) were determined to be 88.3 mg/g, 102.5 mg/g, and 127.8 mg/g for RC, NC, and SC, respectively.

This kinetic behavior can be explained by the availability of active sites. The initial rapid adsorption rate is attributed to the abundance of unoccupied, readily accessible active sites on the adsorbent surfaces. As these sites become progressively occupied by CFX molecules over time, the concentration gradient between the solution and the surface decreases, leading to a slower uptake rate. The final plateau in the kinetic curves signifies that the adsorbent surfaces have reached saturation, establishing a dynamic equilibrium where no further net adsorption can occur (El-Sherbeeny et al., 2021).

4.1.2.2.2. Intra-particle Diffusion

The Weber-Morris intra-particle diffusion model was applied to the kinetic data to elucidate the rate-

controlling steps of the CFX adsorption process. The resulting plots of q_t versus $t^{0.5}$ for RC, NC, and SC are presented in Figure 3-4C. The multi-linear nature of these plots, which do not pass through the origin, indicates that the overall adsorption process is not governed by a single mechanism but is instead a multi-stage process influenced by more than one rate-limiting step (El Qada, 2020).
The kinetic data can be interpreted as occurring in three distinct stages:

1. **External Surface Adsorption**: The initial, steepest segment of each plot corresponds to the rapid diffusion of CFX molecules from the bulk solution to the exterior surface of the adsorbent and their subsequent binding to readily available active sites. This stage is primarily controlled by film diffusion (Lin & Lee, 2020).
2. **Intra-particle Diffusion**: The second, less steep segment represents a gradual adsorption phase where the rate is controlled by the diffusion of CFX molecules from the surface into the porous interior of the adsorbent particles. The diminished rate in this stage is due to the increased diffusional resistance within the pores.
3. **Equilibrium:** The final plateau segment signifies the attainment of equilibrium. At this stage, the intra-particle diffusion process slows down significantly as the remaining active sites become saturated, and the system reaches its maximum adsorption capacity (Sayed et al., 2022). The dominant interactions at this point shift from simple binding to weaker interionic and intermolecular attractions within the adsorbed CFX layers (Jiang et al., 2020).

4.1.2.2.3. Kinetic Modeling

The experimental kinetic data for CFX adsorption onto RC, NC, and SC were fitted to the non-linear forms of the Pseudo-First Order (PFO) and Pseudo-Second Order (PSO) models to determine the best-fit model (**Figures 4-4D, E, F**). The goodness-of-fit was quantitatively evaluated by comparing the coefficient of determination (R^2) and Chi-squared (χ^2) values for each model (**Table 4-2**). The results of the non-linear regression analysis indicate that the PFO model provides a superior fit to the experimental data for all three adsorbents. This conclusion is supported by two key observations from **Table 4-2**: first, the PFO model consistently yielded higher R^2 values and lower χ^2 values compared to the PSO model. Second, there is a strong correlation between the experimentally determined equilibrium capacities ($Q_{e,exp}$) and those calculated from the PFO model (Q_{exp}). The strong fit of the PFO model suggests that the adsorption process is predominantly governed by physisorption mechanisms, such as electrostatic attraction (Sherlala et al., 2019). Nevertheless, the data also shows a reasonably strong fit to the PSO model, implying that the overall adsorption mechanism is not exclusively physisorption. It is likely that chemisorption processes—such as surface complexation or electron exchange occur concurrently, albeit to a lesser extent (Sherlala et al., 2019). This suggests a complex interplay of mechanisms, where physically adsorbed CFX molecules may form layers on top of a base layer that is more strongly bound via chemisorption (Jasper et al., 2020).

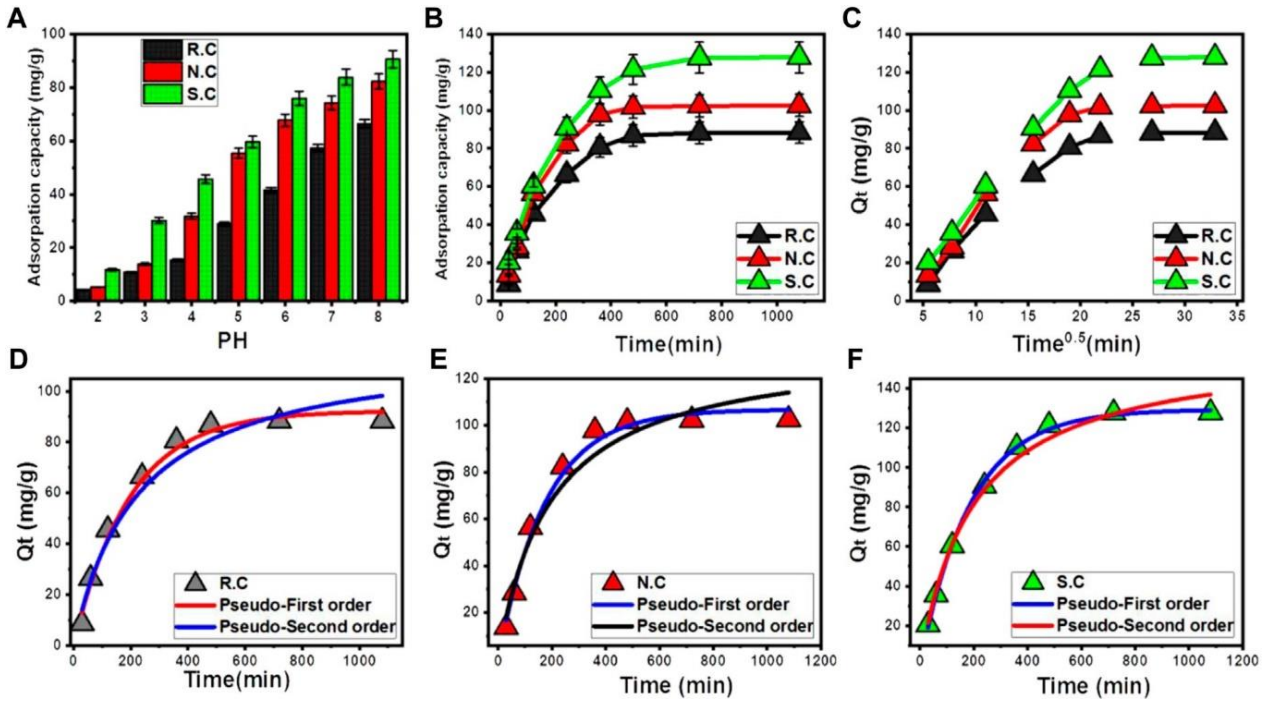

Figure 4-4. Adsorption of CFX onto coal-based adsorbents. (A) Effect of solution pH; (B) Effect of contact time; (C) Intra-particle diffusion model plots. Non-linear kinetic model fitting for (D) RC, (E) NC, and (F) SC.

Table 4-2. Comparison of Parameters Derived from Pseudo-First Order and Pseudo-Second-Order Kinetic Models for CFX Adsorption.

Model	Parameter	Unit	Raw Coal (RC)	Nitric Acid Coal (NC)	Sulfuric Acid Coal (SC)
Pseudo-First Order	k_1	min^{-1}	0.005	0.0056	0.0053
	Q_e,calc	mg/g	92.25	106.70	129.34
	R^2	-	0.98	0.99	0.99
	χ^2	-	0.50	0.28	0.037
Pseudo-Second Order	k_2	g/mg·min	3.77×10^{-5}	3.85×10^{-5}	3.12×10^{-5}
	Q_e,calc	mg/g	118.50	134.37	161.99
	R^2	-	0.96	0.96	0.99
	χ^2	-	1.05	0.97	0.25

4.1.3. Isotherm and Thermodynamic Studies

4.1.3.1. Effect of Initial CFX Concentration and Temperature

To determine the maximum adsorption capacity (Q_{max}) and to investigate the equilibrium behavior, isotherm experiments were conducted by varying the initial CFX concentration from 100 to 800 mg/L. These experiments were performed at three different temperatures (298 K, 308 K, and 318 K) while keeping other parameters constant (adsorbent dosage: 0.2 g/L; pH: 8.0; contact time: 1080 min). As shown in **Figures 4-5A to 4-5C**, the equilibrium adsorption capacity of all three materials increased with higher initial CFX concentrations. This phenomenon is attributed to the enhanced concentration gradient, which provides a greater driving force for mass transfer, thereby increasing the probability of collisions between CFX molecules and the active sites on the adsorbent surfaces (Ashraf et al., 2022). For each adsorbent, the uptake capacity eventually reached a plateau, signifying that the surface had become saturated. This saturation point was reached at approximately 500 mg/L for RC and 600 mg/L for both NC and SC. The experimentally determined maximum adsorption capacities (Q_{max}) highlight two critical findings. First, the acid modification significantly enhanced the adsorption performance of the coal. At 298 K, the Q_{max} increased from 132 mg/g for RC to 316 mg/g for NC and 333.8 mg/g for SC. This improvement is a direct result of the increased surface area and the incorporation of new oxygen-containing functional groups, as demonstrated by the earlier characterization. Second, for all three adsorbents, the Q_{max} values consistently increased with rising temperature. For example, the capacity of the SC adsorbent increased from 333.8 mg/g at 298 K to 453.5 mg/g at 318 K. This positive correlation between adsorption capacity and temperature indicates that the CFX adsorption process is endothermic in nature.

4.1.3.2. Application of Isotherm Models

To describe the equilibrium behavior of the CFX adsorption systems, the experimental data were fitted to the non-linear forms of three widely recognized isotherm models: Langmuir, Freundlich, and Dubinin–Radushkevich (D-R). The graphical fits for each model are presented in Figures 3-5D through 3-5L. The best-fit model was identified by comparing the coefficient of determination (R^2) and Chi-squared (χ^2) values obtained from the non-linear regression analysis (**Table 4-3**). The results clearly indicate that the Langmuir model provides a superior fit to the equilibrium data for all three adsorbents across all tested temperatures, as evidenced by its consistently higher R^2 and lower χ^2 values compared to the other models. The strong applicability of the Langmuir model suggests that the adsorption of CFX primarily occurs as a monolayer onto a finite number of energetically homogeneous active sites on the adsorbent surfaces (Abukhadra et al., 2022; Sayed et al., 2022). Furthermore, the calculated Langmuir separation factor (R_L) values were all between 0 and 1, confirming the favorable nature of the adsorption process. The maximum adsorption capacities (Q_{max}) calculated from the Langmuir model at 318 K were 230.7 mg/g for RC, 685.4 mg/g for NC, and 854.2 mg/g for SC. To further investigate the energetic nature of the adsorption, the D-R model was applied. The mean free energy of adsorption (E) calculated from this model can distinguish between physisorption (E < 8 kJ/mol) and chemisorption (E > 8 kJ/mol) (Dawodu et al., 2012).

For all adsorbents and temperatures, the calculated E values were consistently below 8 kJ/mol, ranging from 3.02 kJ/mol for RC to 4.66 kJ/mol for SC (Table 3-3). This result strongly supports the conclusion that the dominant mechanism governing the adsorption of CFX onto these coal-based materials is physisorption.

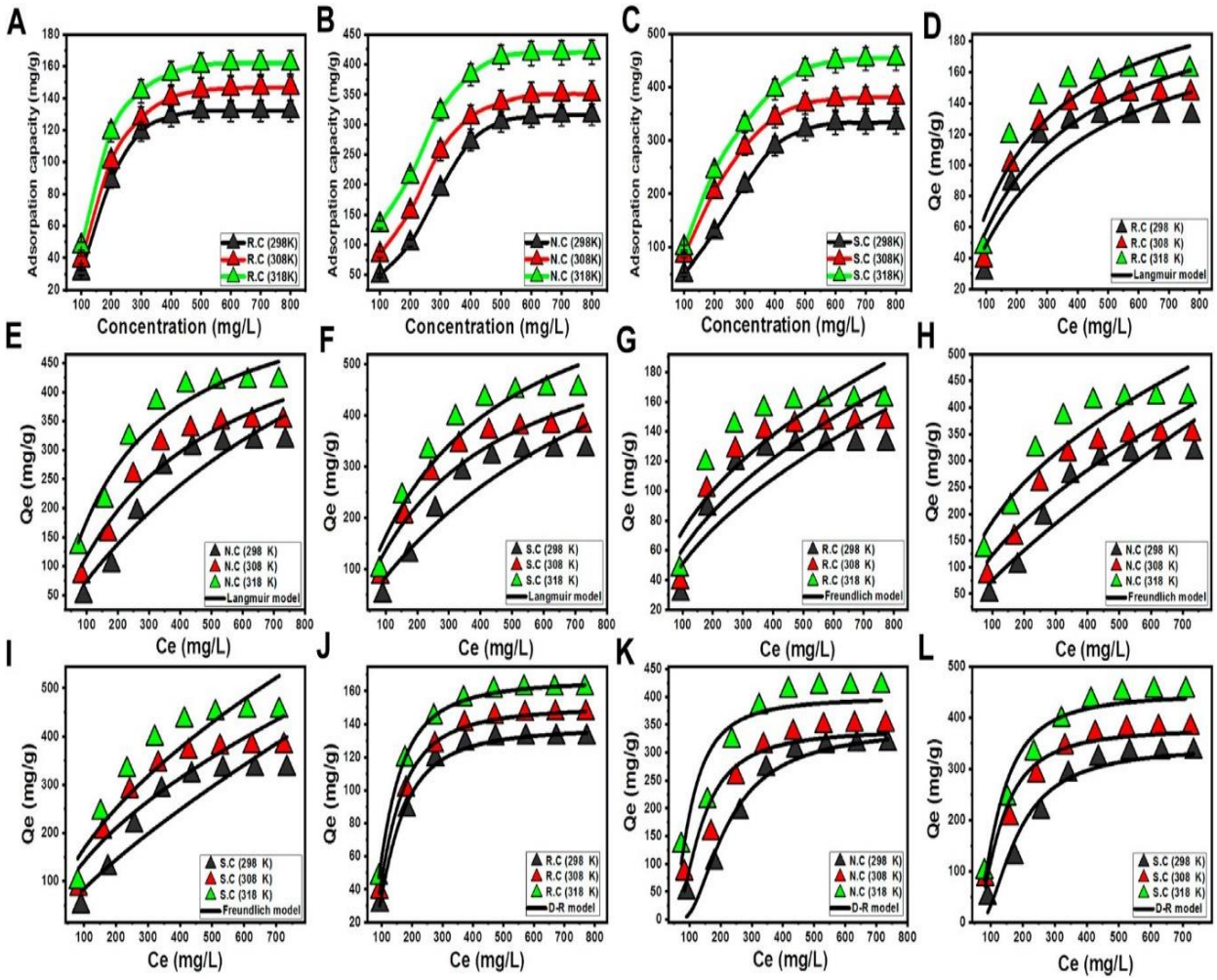

Figure 4-5. Isotherm analysis of CFX adsorption. (A-C) Effect of initial concentration at different temperatures. Non-linear isotherm model fits for (D-F) Langmuir, (G-I) Freundlich, and (J-L) Dubinin-Radushkevich models.

Table 4-3. Calculated Parameters and Goodness-of-Fit Metrics for Isotherm Models Applied to CFX Adsorption.

Isotherm Model	Parameter	Adsorbent	298 K	308 K	318 K
Langmuir	Q_{max}	RC	210.3	220.3	230.7
		NC	605.0	608.3	685.4
		SC	628.8	751.2	854.2
	R^2	RC	0.89	0.91	0.90
		NC	0.96	0.95	0.93
		SC	0.94	0.94	0.93
Freundlich	n	RC	1.84	2.00	2.17
		NC	1.25	1.67	2.13
		SC	1.28	1.75	1.72
	R^2	RC	0.82	0.83	0.81
		NC	0.90	0.90	0.91
		SC	0.90	0.89	0.89
Dubinin–Radushkevich	E	RC	3.02	3.22	3.45
		NC	3.04	3.49	4.05
		SC	3.83	4.01	4.66
	R^2	RC	0.99	0.99	0.99
		NC	0.91	0.93	0.89
		SC	0.95	0.97	0.97

4.1.4. Energetic Properties

4.1.4.1. Adsorption Energy Analysis

The dominant mechanism of adsorption (i.e., physical vs. chemical) was further investigated by calculating the adsorption energy (ΔE). Generally, ΔE values ≤ 40 kJ/mol are indicative of physisorption processes—such as hydrogen bonding (<30 kJ/mol), van der Waals forces (4–10 kJ/mol), and dipole forces (2–29 kJ/mol)—whereas values > 80 kJ/mol suggest chemisorption (Ashraf et al., 2022). The adsorption energy was calculated theoretically using the following equation

(Dhaouadi et al., 2020).

$$\Delta E = RT\, ln\left(\frac{S}{C}\right) \qquad \textbf{(3-1)}$$

where R is the universal gas constant (0.008314 kJ/mol K), T is the absolute temperature (K), S is the solubility of the adsorbate, and C is the adsorbate concentration at half-saturation.

The calculated ΔE values for the adsorption of CFX are presented in **Table 4-5**. For all three adsorbents (RC, NC, and SC) across the entire temperature range studied, the ΔE values were found to be less than 5 kJ/mol. Specifically, for the sulfuric acid-treated coal (SC), the values were 4.51 kJ/mol (298 K), 3.81 kJ/mol (308 K), and 3.89 kJ/mol (318 K). These low energy values strongly indicate that the uptake of CFX onto the raw and acid-modified coal surfaces is predominantly controlled by physical adsorption processes, such as van der Waals forces, dipole-dipole interactions, and hydrogen bonding.

4.1.4.2. Advanced Thermodynamic and Energetic Properties

To gain deeper insight into the adsorbent-adsorbate interactions at a molecular level, advanced thermodynamic parameters were calculated based on a statistical physics framework. The configurational entropy (S_a), internal energy (E_{int}), and free enthalpy (G) were determined as a function of CFX concentration. These parameters are calculated using complex models that incorporate variables such as the number of molecules per site (n), the density of occupied sites (N_m), the concentration at half-saturation ($C_{1/2}$), and the translational partition function (Z_v) (Sellaoui et al., 2016). The calculated configurational entropy (S_a) provides a measure of the disorder at the solid-liquid interface **(Figures 4-6 A-C**). For all adsorbents, the entropy was observed to decrease significantly as the concentration of CFX increased. This trend indicates that as more CFX molecules adsorb, they become more ordered and arranged on the adsorbent surface, which reduces the degrees of freedom of the system. The maximum entropy value for each system was found at a concentration close to the half-saturation concentration ($C_{1/2}$), which corresponds to the point of greatest randomness before the surface becomes crowded. The values of Sa can be calculated according to **Eq.3-2** using the previously obtained values of n, Nm (CFX), and C1/2 (concentration at half saturation) (Sellaoui et al., 2016).

$$\frac{E_{int}}{K_B T} = nN_m \left[\left(\frac{\left(\frac{C}{C_{1/2}}\right)^n ln\left(\frac{C}{Z_v}\right)}{1+\left(\frac{C}{C_{1/2}}\right)^n} \right) - \left(\frac{n\, ln\left(\frac{C}{C_{1/2}}\right)\left(\frac{C}{C_{1/2}}\right)^n}{1+\left(\frac{C}{C_{1/2}}\right)^n} \right) \right] \qquad \textbf{(3-2)}$$

The calculated configurational entropy (S_a) provides a measure of the disorder at the solid-liquid interface (Figures 3-6A-C). For all adsorbents, the entropy was observed to decrease significantly as the concentration of CFX increased. This trend indicates that as more CFX molecules adsorb, they become more ordered and arranged on the adsorbent surface, which reduces the degrees of freedom of the system. The maximum entropy value for each system was found at a concentration close to the half-saturation concentration ($C_{1/2}$), which corresponds to the point of greatest randomness before the surface becomes crowded. The values of S_a can be calculated according to the following equation:

$$\frac{S_a}{k_B} = N_m \left\{ \ln\left(1 + \left(\frac{C}{C_{1/2}}\right)^n\right) - n\left(\frac{C}{C_{1/2}}\right)^n \frac{\ln\left(\frac{C}{C_{1/2}}\right)}{1 + \left(\frac{C}{C_{1/2}}\right)^n} \right\} \quad (3\text{-}3)$$

Where S_a represents the adsorption entropy, k_B is the Boltzmann constant, Nm is the density of occupied adsorption sites, C is the concentration of CFX, and $C_{1/2}$ is the concentration at half saturation. The calculation of these parameters provides further insight into the adsorption mechanism.

4.1.4.3. Classical Thermodynamic Analysis

The spontaneity and energetic nature of the overall adsorption process were also evaluated using classical thermodynamics. The key parameters—Gibbs free energy (ΔG°), enthalpy (ΔH°), and entropy (ΔS°) were determined from the temperature dependence of the equilibrium constant.
The Gibbs free energy (ΔG°) values were found to be negative across the entire temperature range (298 K - 318 K) for all three adsorbents. This result confirms that the adsorption of CFX onto RC, NC, and SC is a spontaneous process. Furthermore, the ΔG° values became more negative as the temperature increased, indicating that the process becomes more favorable at higher temperatures.

$$\frac{E_{int}}{K_B T} = nN_m \left[\left(\frac{\left(\frac{c}{c_{1/2}}\right)^n \ln\left(\frac{c}{z_n}\right)}{1+\left(\frac{c}{c_{1/2}}\right)^n} \right) - \left(\frac{n \ln\left(\frac{c}{c_{1/2}}\right)\left(\frac{c}{c_{1/2}}\right)^n}{1+\left(\frac{c}{c_{1/2}}\right)^n} \right) \right] \quad \textbf{(3-3)}$$

$$\frac{G}{K_B T} = nN_m \frac{\ln\left(\frac{c}{z_n}\right)}{1+\left(\frac{c_{1/2}}{c}\right)^n} \quad \textbf{(3-4)}$$

The negative values of ΔG° confirm the spontaneity of the adsorption process across the studied temperature range. The positive ΔH° values indicate the endothermic nature of the process. The trend of increasing spontaneity (i.e., ΔG° becoming more negative) with temperature is consistent with an endothermic adsorption process where the positive entropy term ($T\Delta S_\circ$) becomes increasingly significant." (Figures 3-7G-I would support the ΔG° trend).

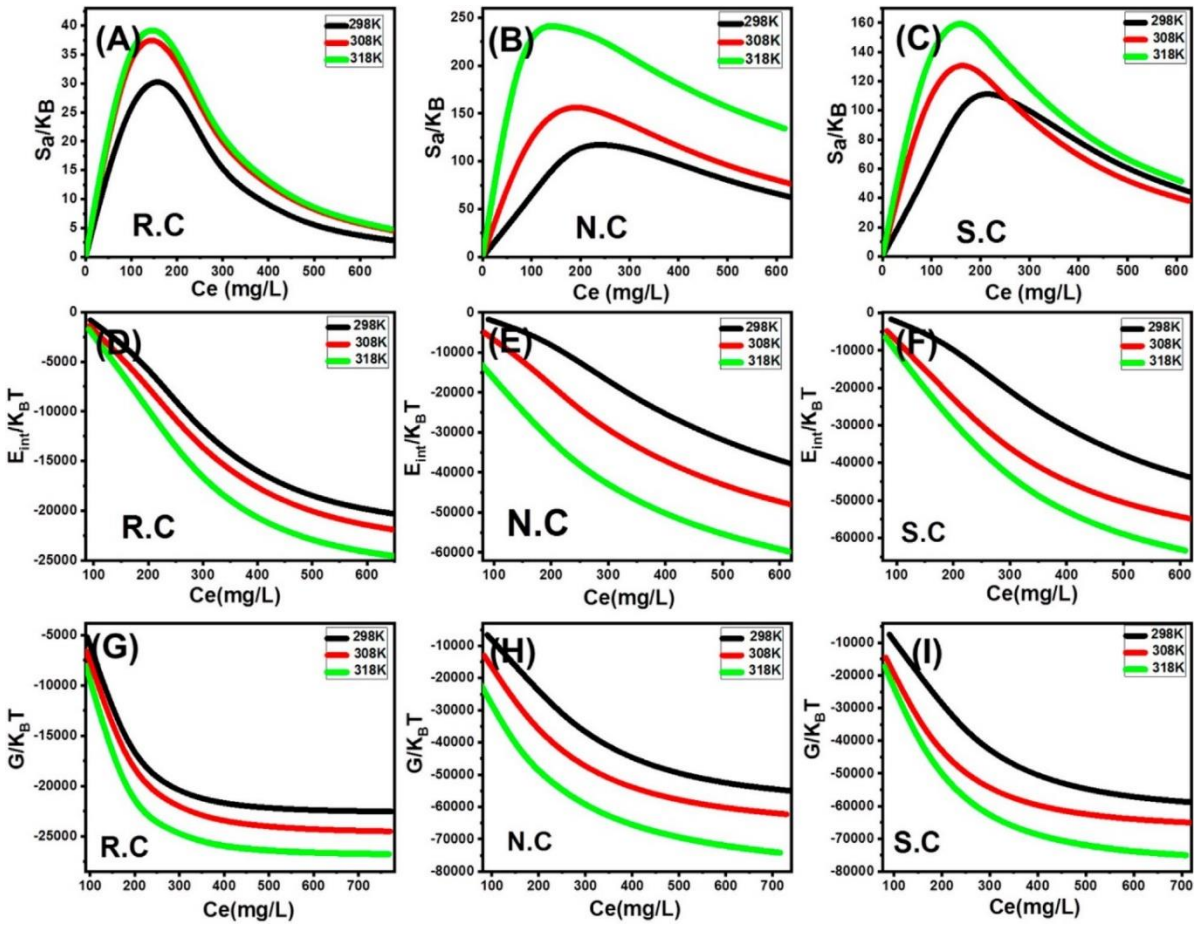

Figure 4-6. Advanced thermodynamic modeling of CFX adsorption at different temperatures. Variation of (A-C) configurational entropy (S_a), (D-F) internal energy (E_{int}), and (G-I) free enthalpy (G) as a function of CFX concentration.

4.1.5. Adsorbent Recyclability

The potential for practical application of the coal-based adsorbents was evaluated by conducting five consecutive adsorption-desorption cycles. After each adsorption cycle, the spent adsorbent was regenerated by washing it three times with distilled water for 10 minutes per wash, followed by drying at 65°C for 10 hours. The regenerated material was then reused in the next cycle under the previously determined optimal adsorption conditions.

The results of the reusability study are presented in **Figure 4-7**. All three materials demonstrated significant stability and retained a high percentage of their initial adsorption capacity over the five cycles. For the sulfuric acid-modified coal (SC), the most effective adsorbent, the CFX uptake capacity decreased only slightly, from an initial 453.5 mg/g in the first run to 415.2 mg/g in the fifth run. Similarly, the capacities for NC decreased from 420 to 367.2 mg/g, and for RC, from 161.8 to 122.8 mg/g over the same number of cycles. The gradual decline in adsorption performance observed with each successive cycle can be attributed to two main factors. First, a minor loss of adsorbent mass likely occurs during the physical washing and recovery steps. Second, some active sites may become irreversibly blocked by strongly bound CFX molecules or surface complexes that are not removed by the simple water-washing regeneration method.

.

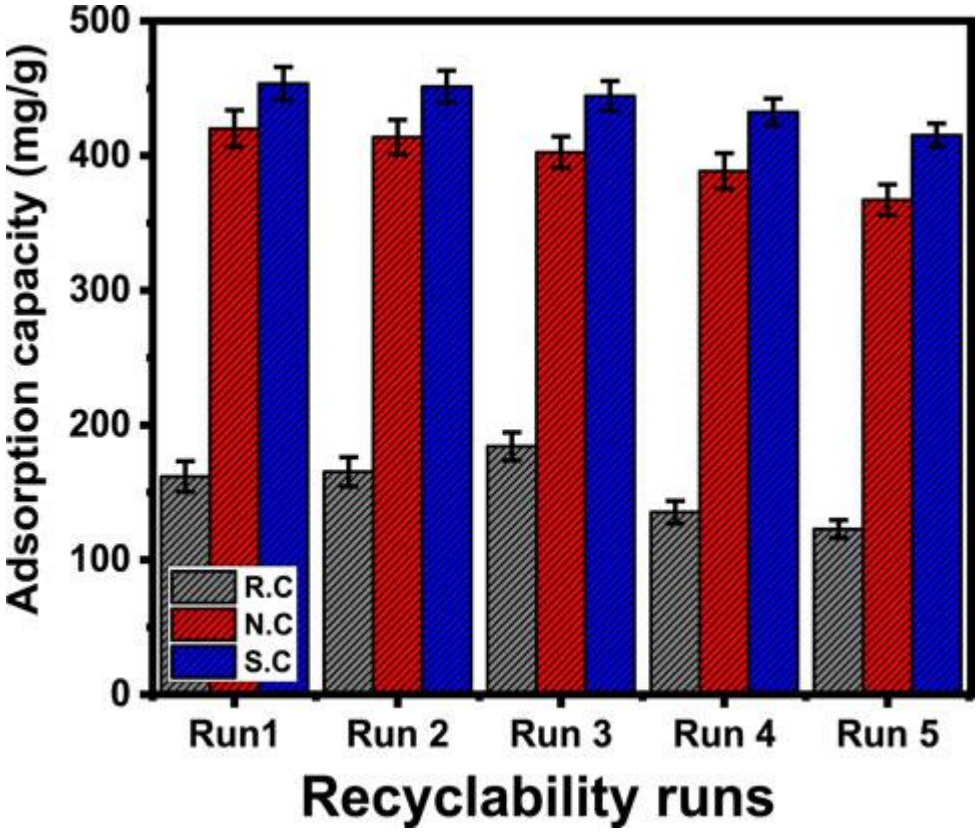

Figure 4-7. Performance of Raw Coal (RC), Nitric Acid-Modified Coal (NC), and Sulfuric Acid-Modified Coal (SC) over five consecutive cycles of CFX adsorption and regeneration.

4.1.6. Proposed Adsorption Mechanism

Based on the comprehensive material characterization and the results of the equilibrium studies, a multi-faceted adsorption mechanism is proposed to explain the uptake of Ciprofloxacin (CFX) onto the surfaces of the acid-modified coal adsorbents (NC and SC). The successful incorporation of numerous oxygen-, sulfur-, and nitrogen-containing functional groups creates a chemically active surface capable of binding CFX molecules through several simultaneous interaction pathways, as illustrated in **Figure 4-8**. The primary mechanisms are identified as:

- **Electrostatic Attraction:** The deprotonated acidic functional groups on the adsorbent surface (e.g., carboxyl $–COO^-$ and sulfonate $–SO_3^-$) are negatively charged at the optimal pH. These sites can therefore exert a strong electrostatic attraction on the positively charged moieties of the CFX molecule, acting as a primary driving force for adsorption.
- **Hydrogen Bonding:** The surfaces of the modified coals are rich in hydrogen-bond donor groups (e.g., –OH, –COOH). These can form strong hydrogen bonds with the numerous hydrogen-bond acceptor atoms (specifically nitrogen and oxygen) present in the chemical structure of the CFX molecule.
- **π–π Stacking Interactions:** The extensive network of aromatic rings within the coal's graphitic structure provides an electron-rich surface. This can interact with the aromatic rings of the CFX molecule through non-covalent π–π stacking, a mechanism that involves dispersion and dipole-induced dipole forces.

.

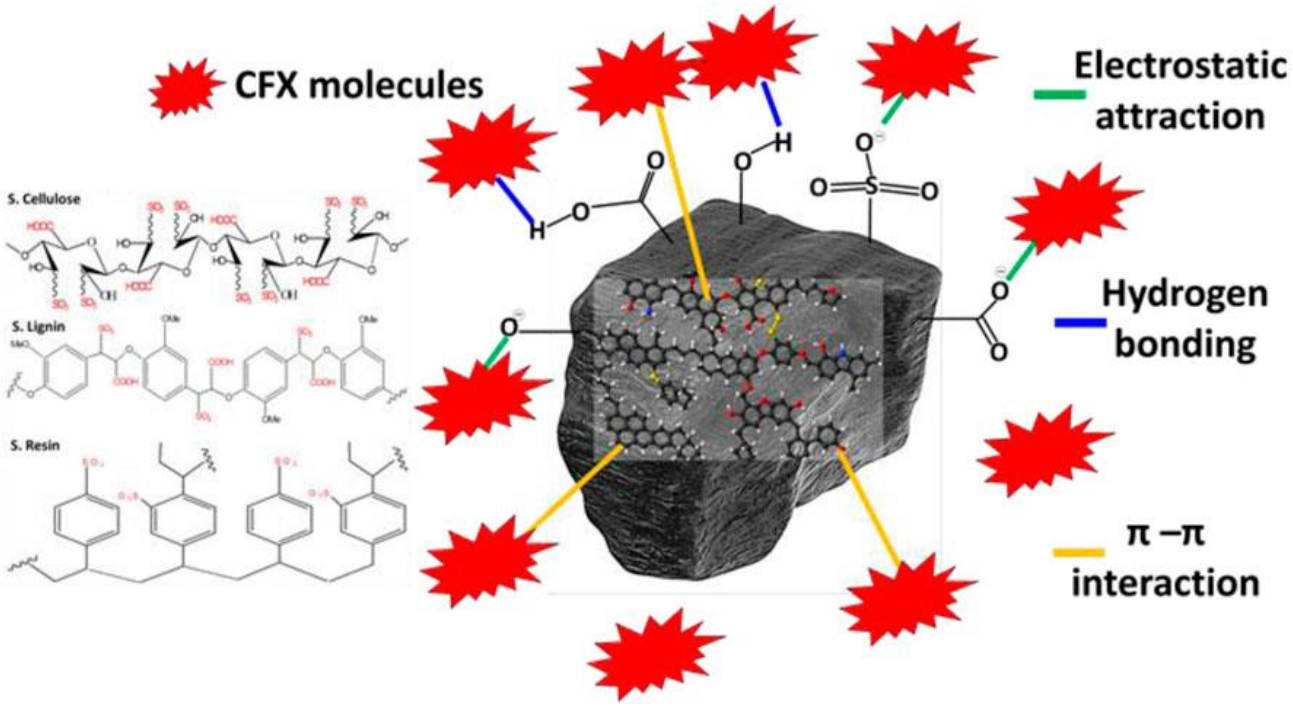

Figure 4-8. Proposed multi-modal mechanism for the adsorption of Ciprofloxacin (CFX) onto the surface of modified coal, illustrating the key roles of electrostatic attraction, hydrogen bonding, and π–π interactions.

4.2. Picea abies Biomass for Heavy Metal Removal

4.2.1. Biosorbent Characterization

4.2.1.1. Bulk Composition and Inherent Properties

The physicochemical characteristics of the Norway Spruce Wood Residue (NSWR) were analysed to establish its baseline properties as a biosorbent. The composition of the NSWR is typical of a lignocellulosic material, which is primarily composed of cellulose, hemicellulose, and lignin (Bhardwaj et al., 2025) (Meshitsuka & Isogai, 2017). This was substantiated by elemental analysis, which determined the material to be comprised predominantly of carbon (43.46%), oxygen (50.86%), and hydrogen (5.52%). Furthermore, proximate analysis of the <0.180 mm particle fraction quantified a volatile content of 71.7±0.3% and a fixed carbon content of 22.5±0.6%. To ensure that pre-existing metals in the biomass would not interfere with the adsorption experiments, the background concentrations of the target heavy metals were quantified. The inherent levels were found to be negligible, with measured values of 0.00028 mg/g for Cd^{2+}, 0.0096 mg/g for Cu^{2+}, 0.0047 mg/g for Pb^{2+}, and 0.022 mg/g for Zn^{2+}.

4.2.1.2. Crystalline Structure Analysis

The X-ray diffraction (XRD) pattern of the unmodified NSWR biomass is presented in **Figure 4-9**. The diffractogram is dominated by a single, broad halo centred in the 2θ range of 15-22°, which is a characteristic feature confirming the predominantly amorphous or poorly crystalline nature of lignocellulosic materials. In addition to this broad amorphous peak, two minor, sharper peaks are discernible at approximately 2θ = 26.6° and 36.5°. The presence of these weak, sharp peaks may be attributed to trace amounts of crystalline inorganic minerals, such as silica (quartz) or calcite, which have been previously reported as minor components in wood-based materials (Ivanovska et al., 2021).

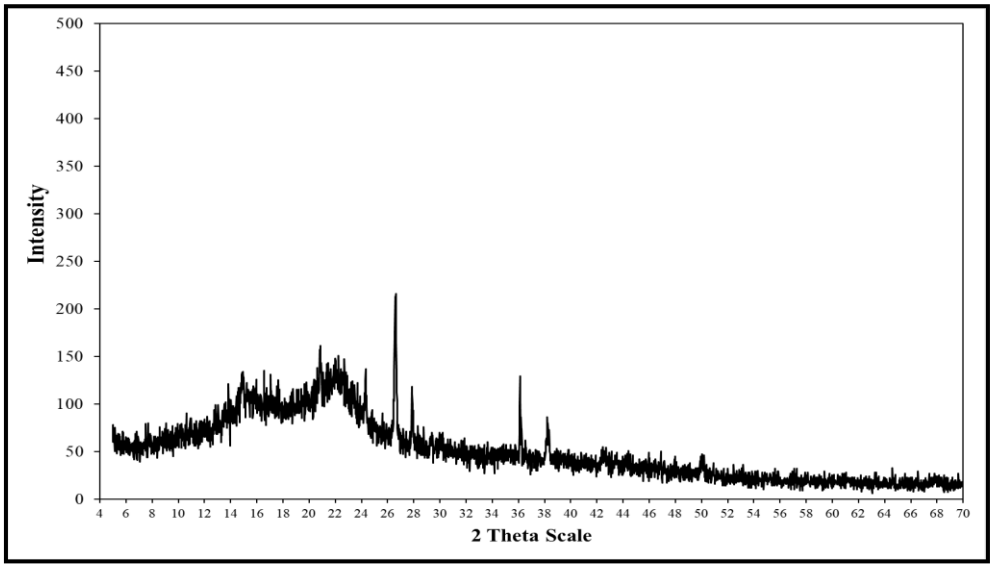

Figure 4-9. X-ray diffractogram of the NSWR biomass, illustrating its predominantly amorphous structure.

4.2.1.3. Surface Functional Groups (FTIR)

To identify the functional groups on the NSWR surface available for metal binding, Fourier Transform Infrared (FTIR) spectroscopy was performed (**Figure 4-10**). The resulting spectrum displays several key absorption bands that confirm the material's lignocellulosic nature. A prominent, broad absorption band centered at approximately 3330 cm^{-1} is attributed to the O-H stretching vibrations of hydroxyl groups present in cellulose, lignin, and adsorbed water. The peaks observed at ~2920 cm^{-1} and ~2854 cm^{-1} correspond to the C-H stretching of aliphatic groups. The aromatic structure of lignin is confirmed by the presence of characteristic C=C skeletal vibration peaks at 1605 cm^{-1} and 1513 cm^{-1}. The most intense feature in the spectrum is the broad band centered near 1025 cm^{-1}, which is characteristic of C-O stretching and C-O-C ether linkages within the cellulose and hemicellulose polymer backbones. Collectively, the presence of this diverse array of oxygen-containing functional groups—particularly hydroxyl, ether, and potential carboxyl/carbonyl groups—indicates that the NSWR surface possesses numerous potential active sites for the complexation and sequestration of heavy metal cations.

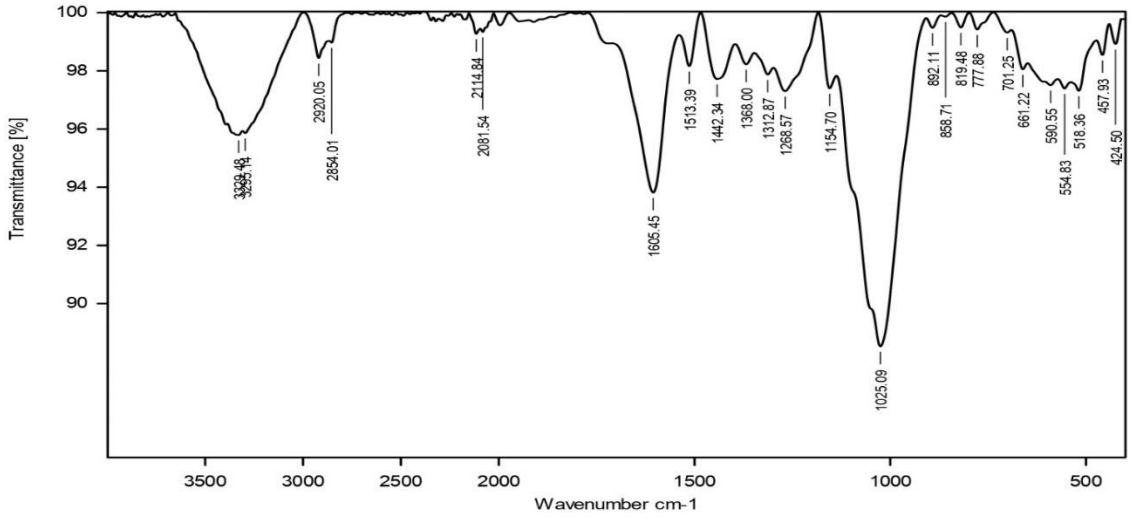

Figure 4-10. FTIR spectrum of the NSWR biomass, identifying key surface functional groups.

4.2.1.4. Surface Morphology Analysis

The surface topography of the NSWR biosorbent was visualized using Scanning Electron Microscopy (SEM) both before and after the adsorption of heavy metals (**Figure 4-11**). The micrograph of the pristine, pre-adsorption material reveals a highly heterogeneous and irregular surface, characterized by significant roughness and a porous architecture (**Figure 4-11, A**). After the adsorption process, the fundamental morphology of the NSWR appeared largely unaltered, retaining its complex and uneven surface features (**Figure 4-11, B**). While no major structural changes were observed, this inherent topographical complexity is indicative of a large surface area, which is a crucial characteristic for facilitating effective adsorbent-adsorbate interactions.

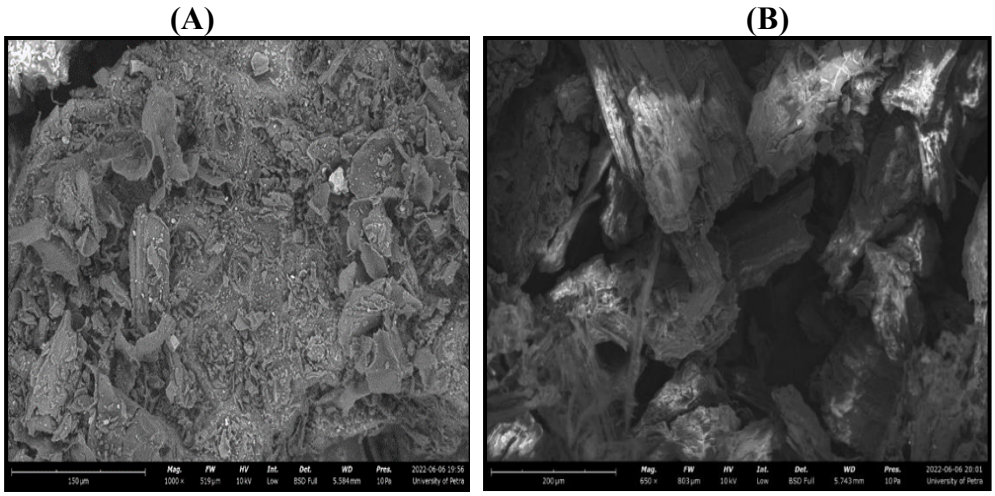

Figure 4-11. Scanning Electron Micrographs showing the surface topography of the NSWR biosorbent (A) before and (B) after the heavy metal adsorption process.

4.2.1.5. Surface Elemental Composition Analysis (EDS)

Energy-Dispersive X-ray Spectroscopy (EDS) was employed to determine the elemental composition of the NSWR surface following the adsorption process. A representative EDS spectrum (**Figure 4-12**) confirmed the successful uptake of all four target heavy metals, as evidenced by the distinct characteristic peaks for Lead (Pb), Copper (Cu), Cadmium (Cd), and Zinc (Zn). In addition to the primary matrix elements (Carbon and Oxygen), the analysis also detected several inherent elements, with semi-quantitative results presented in **Table 4-4**. Most notably, a high abundance of Calcium (approx. 16 wt%) was detected, along with smaller amounts of Silicon, Phosphorus, and Sulfur. The significant presence of these inherent cations, particularly Ca^{2+}, strongly suggests that ion exchange is a key contributing mechanism to the overall heavy metal adsorption process (Marin & Ayele, 2002)

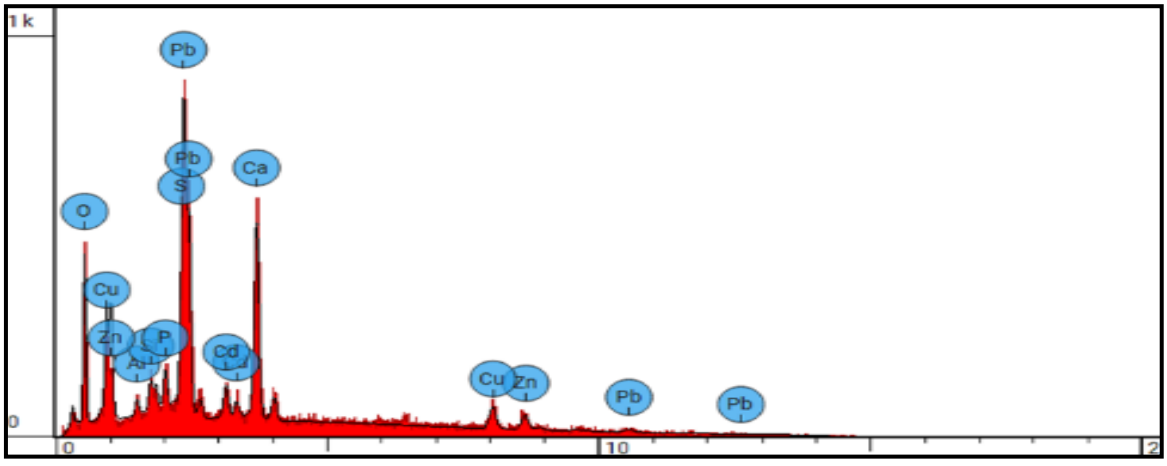

Figure 4-12 Energy-Dispersive X-ray Spectrum of the NSWR biomass following the adsorption of the quaternary heavy metal solution.

Table 4-4. Semi-Quantitative Elemental Composition of the NSWR Surface Post-Adsorption.

Atomic Number (Z)	Element Name	Atomic %.	Weight %.
8	Oxygen	46.47	14.49
13	Aluminium	1.33	0.70
14	Silicon	1.46	0.80
15	Phosphorus	2.65	1.60
16	Sulfur	1.92	1.20
20	Calcium	20.47	15.98
29	Copper	7.91	9.79
30	Zinc	3.92	5.00
48	Cadmium	3.01	6.59
82	Lead	10.86	43.86

4.2.1.6. Surface Area and Porosity (BET)

The textural properties of the NSWR biosorbent were quantified using N_2 adsorption-desorption analysis. The material was found to possess a Brunauer-Emmett-Teller (BET) specific surface area of 4.56 m^2/g and a total pore volume of 0.0053 cm^3/g. Furthermore, the analysis yielded a Langmuir surface area of 7.19 m^2/g and an average pore width of 46.66 Å. The value for the average pore width suggests a predominantly mesoporous structure, which can provide accessible pathways for metal ions to reach internal binding sites within the biosorbent matrix.

4.2.1.7. Point of Zero Charge (pHpzc) Determination

The point of zero charge (pH_{PZC}) of the NSWR biosorbents was determined to be 5.7, as illustrated in **Figure 4-13**. The pH_{PZC} represents the pH at which the net charge on the adsorbent's surface is neutral. Consequently, at pH values greater than 5.7, the NSWR surface will carry a net negative charge, creating favorable conditions for the electrostatic attraction of positively charged heavy metal cations (Al-Labadi et al., 2025).

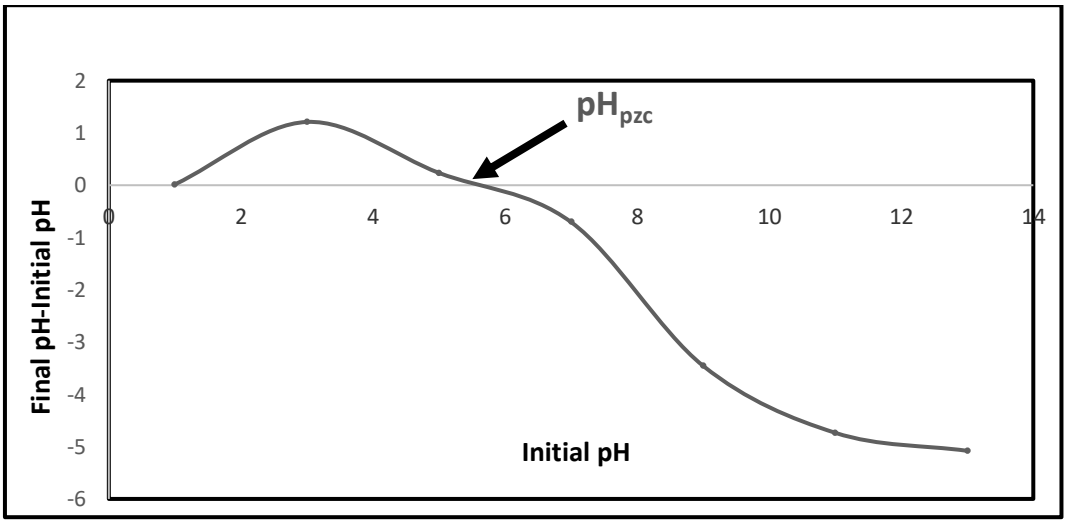

Figure 4-13. Determination of the point of zero charge (pH $_{PZC}$) for the NSWR biosorbent using the pH drift method.

4.2.2. Proposed Adsorption Mechanism

The collective results from the physicochemical characterization and equilibrium studies suggest that the adsorption of heavy metals onto the NSWR biosorbent is not governed by a single mechanism but rather by a combination of synergistic processes. The primary mechanisms identified are surface complexation and ion exchange, which are driven by the material's unique structural and chemical properties. The physical structure of NSWR, as visualized by SEM, is highly heterogeneous and irregular, with a rough topography that provides a large, accessible surface area for interaction with metal ions. While the BET surface area (4.56 m^2/g) is modest, the material's effectiveness is more significantly influenced by its chemical composition. The predominantly amorphous nature of the lignocellulosic matrix, confirmed by XRD, allows for hydration and accessibility to internal binding sites.

The most critical factor is the abundance of surface functional groups identified by FTIR spectroscopy. The prevalence of hydroxyl (-OH), ether (C-O-C), and likely carboxyl groups creates numerous active sites for metal sequestration. These oxygen-containing groups can directly bind metal cations through surface complexation and electrostatic interactions. Furthermore, the EDS analysis provides compelling evidence for the crucial role of ion exchange. The detection of significant quantities of inherent cations, particularly Calcium (Ca^{2+}), on the biomass surface strongly supports a mechanism where these native ions are released into the solution and replaced by the target heavy metal ions. (Singh et al., 2022) (Orozco et al., 2023). This ion exchange pathway, combined with direct surface complexation, constitutes the primary mechanism for the effective removal of heavy metals by the NSWR biosorbent.

4.2.3. Parametric Studies

4.2.3.1. Influence of Biosorbent Dosage

The effect of the NSWR biosorbent dosage on the removal efficiency (R%) of the four heavy metals was investigated to determine the optimal adsorbent mass. The dosage was varied from 0.005 g to 0.1 g in a 10 mL solution, while other experimental conditions were held constant (as detailed in the **Figure 4-14**). The experimental results, depicted in Figure 3-14, demonstrate a direct positive correlation between the adsorbent dosage and the removal efficiency for all four metal ions. Specifically, as the dosage was increased from 0.005 g to 0.1 g, the removal of Pb^{2+} increased most significantly, from 64.6% to 99.1%, while Cu^{2+} removal rose from 60.3% to 94.9%. Similar enhancements were observed for Cd^{2+} (42.7% to 88.5%) and Zn^{2+} (45.9% to 86.5%). This trend is attributed to the increased availability of total active binding sites as more biosorbent mass is introduced into the fixed volume of solution. With a greater number of unsaturated surface functional groups available, a higher fraction of the metal ions can be sequestered. The removal efficiency for all metals approached a maximum at a dosage of 0.1 g. Beyond this point, further increases in dosage yielded negligible improvement. Therefore, a dosage of 0.1 g in 10 mL (equivalent to 10 g/L) was selected as the optimal condition for subsequent experiments.

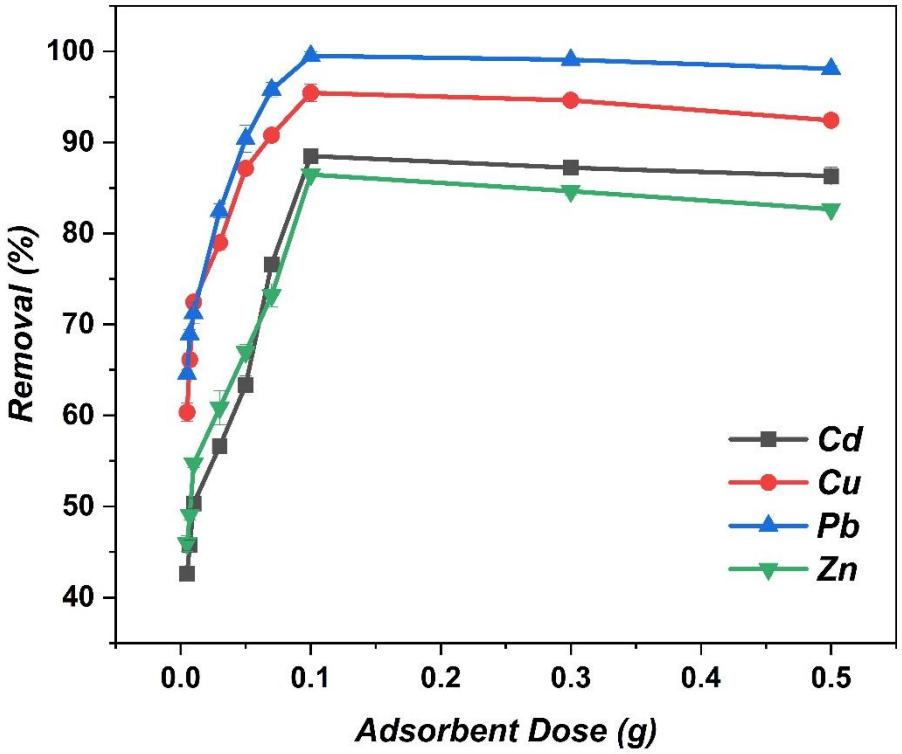

Figure 4-14. Influence of NSWR dosage on the removal efficiency (%) of Cd (II), Cu (II), Pb (II), and Zn (II). (Conditions: initial metal conc. = 50 mg/L; pH = 5-6; particle size = 90-250 μm; stirring speed = 200 rpm).

4.2.3.2. Influence of Contact Time

The effect of contact time on the adsorption of Cd(II), Cu(II), Pb(II), and Zn(II) was investigated to determine the equilibrium time for the system. As illustrated in **Figure 4-15**, the adsorption process was characterized by an initial, rapid uptake phase. Within the first 20 minutes, a substantial portion of the total removal was achieved, with efficiencies reaching 97.6% for Pb^{2+}, 94.9% for Cu^{2+}, 65.5% for Cd^{2+}, and 64.4% for Zn^{2+}.

Following this initial phase, the adsorption kinetics varied among the metals. For Pb^{2+} and Cu^{2+}, the removal efficiency remained largely constant after 20 minutes, indicating that equilibrium was reached very quickly. In contrast, the adsorption of Cd^{2+} and Zn^{2+} continued at a much slower rate until approximately 200 minutes, at which point a plateau was observed for all four metals. This slower, secondary phase is likely controlled by the gradual diffusion of the metal ions into the porous interior of the biosorbent.

The initial rapid uptake is attributed to the immediate availability of numerous active sites on the exterior surface of the biosorbent. As these external sites become saturated, the rate of adsorption decreases, and the process becomes limited by the slower diffusion of ions into the biomass structure. The final plateau signifies that a dynamic equilibrium has been established between the adsorption and desorption processes. Since no significant increase in removal was observed for any metal ion after 200 minutes, this was determined to be the equilibrium time and was used for subsequent batch experiments.

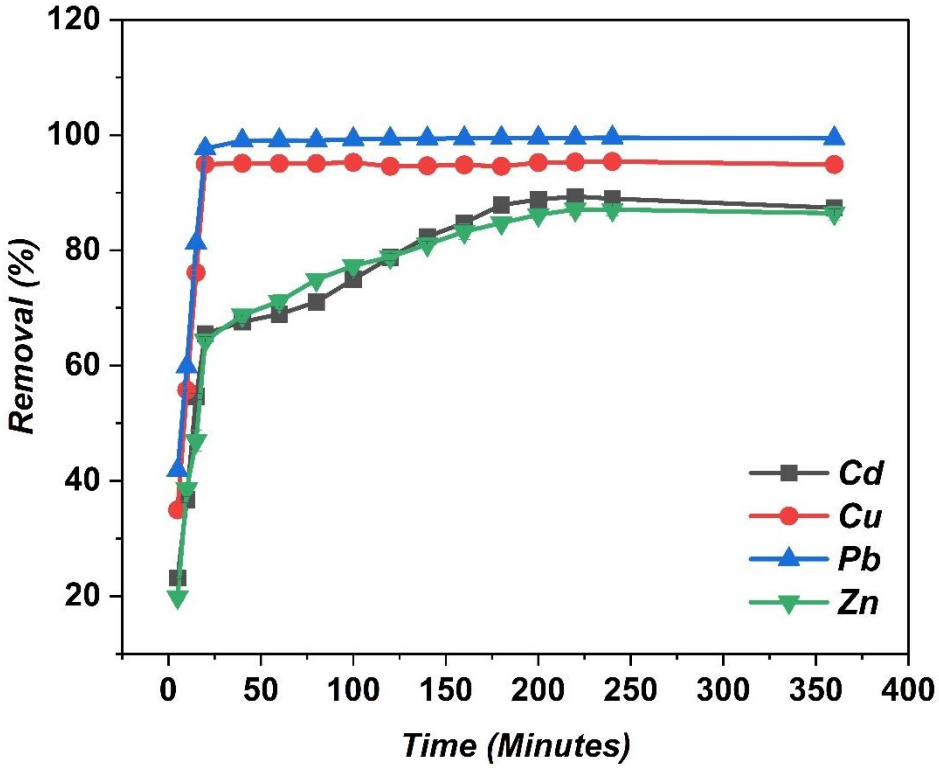

Figure 4-15. Effect of contact time on the removal efficiency (%) of Pb(II), Cu(II), Zn(II), and Cd(II) by the NSWR biosorbent. (Conditions: initial metal conc. = 50 mg/L; dosage = 10 g/L; pH = 5-6).

4.2.3.3. Impact of Solution pH

The solution pH is a critical parameter in heavy metal biosorption, as it simultaneously controls the speciation of the metal ions in solution and the surface charge of the biosorbent's functional groups (Cruz-Lopes et al., 2021). The effect of pH on the removal of Pb(II), Cu(II), Zn(II), and Cd(II) by NSWR was therefore investigated over a range from pH 2 to 6. The optimal pH range for adsorption was identified as 5 to 6 (**Figure 4-16)**. In this range, the removal of Cu^{2+} and Pb^{2+} was nearly complete and plateaued, while the uptake of Cd^{2+} and Zn^{2+} continued to increase. Based on these findings, and to avoid the potential precipitation of metal hydroxides at pH values above 6 (Kariuki et al., 2017), a pH of 5-6 was selected for subsequent experiments. This optimal range aligns with previous studies that have identified pH 5-6 as ideal for heavy metal biosorption onto various cellulosic materials (Bhattacharjee et al., 2020).

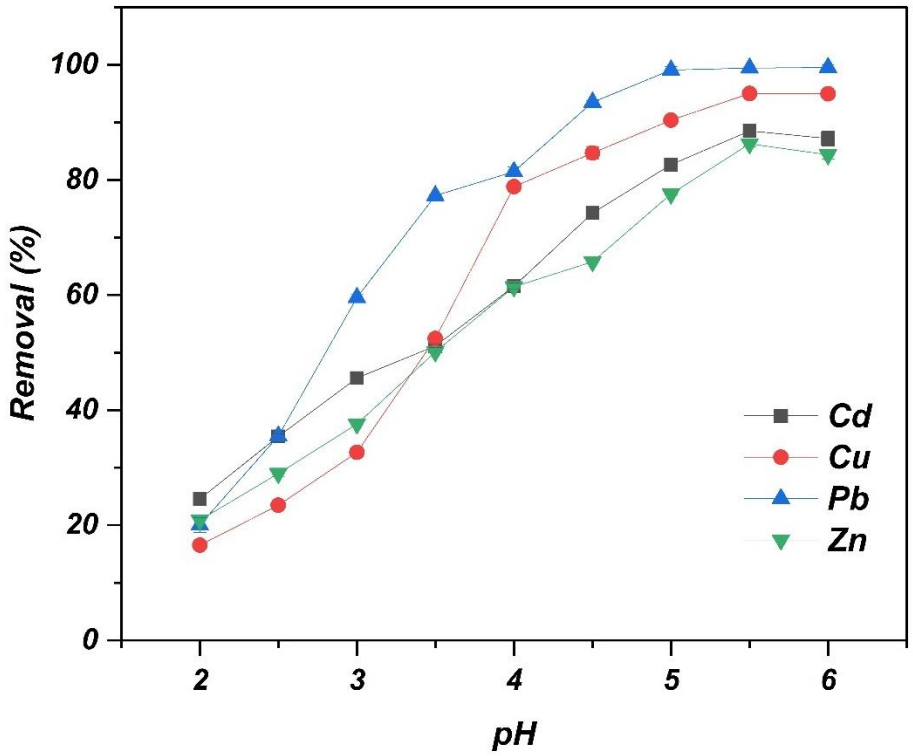

Figure. 4-16: The effect of solution pH on the removal efficiency (%) of Pb(II), Cu(II), Zn(II), and Cd(II) by the NSWR biosorbent.

4.2.3.4. Influence of Temperature

The effect of temperature on the biosorption process was investigated over a range of 25°C to 45°C to determine the thermodynamic nature of the reaction. As shown in **Figure 4-17**, the removal efficiency for all four heavy metal ions exhibited a positive correlation with temperature. Specifically, as the temperature was increased from 25°C to 45°C, the uptake of all metals increased, indicating that the adsorption process is endothermic. This behavior is likely due to two primary factors. First, an increase in temperature enhances the kinetic energy and mobility of the metal ions in the solution, which increases the frequency of collisions with the biosorbent's active sites. Second, higher temperatures can promote the swelling of the internal structure of the lignocellulosic biomass, potentially increasing the accessibility of internal binding sites.

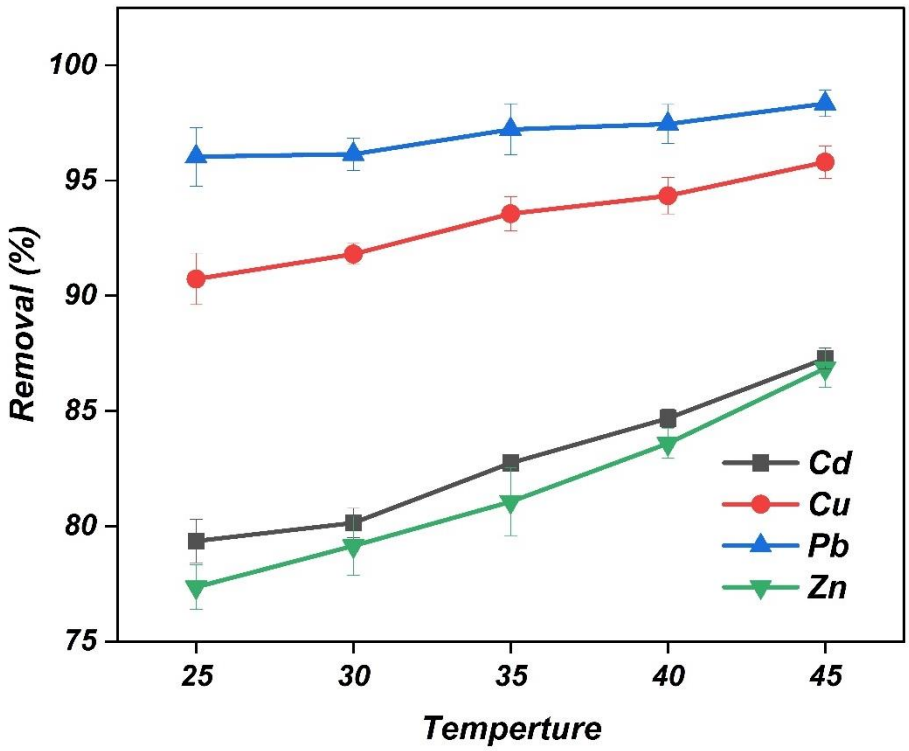

Figure 4-17. The effect of temperature on the removal efficiency (%) of Cd(II), Cu(II), Pb(II), and Zn(II) by the NSWR biosorbent.

4.2.3.5. Influence of Particle Size

The effect of biosorbent particle size on the removal of the four heavy metals was investigated across five different particle size fractions, as detailed in **Figure 4-18**. Since biosorption is a surface-dependent phenomenon, a general inverse relationship between particle size and adsorption efficiency is expected, as smaller particles provide a larger specific surface area and shorter intraparticle diffusion paths (Kumar et al., 2019)The experimental results largely align with this expectation. A discernible, albeit slight, increase in the removal efficiency for all four metal ions was observed as the particle size was reduced from the largest fraction (1000-250 μm) to the smaller fractions. This confirms that decreasing the particle size enhances the availability of active binding sites, thereby improving overall removal performance.

However, an interesting deviation from this trend was noted for the finest particle size fraction (<90 μm). In this range, the removal efficiencies for Cd^{2+} and Cu^{2+} showed no further improvement, while the uptake of Pb^{2+} and Zn^{2+} exhibited a slight decrease. This counterintuitive result may be attributed to particle agglomeration effects. When the particles are extremely fine, they may tend to aggregate in the aqueous solution, which can reduce the effective surface area that is accessible to the metal ions and hinder mass transfer, thereby slightly diminishing the overall removal efficiency.

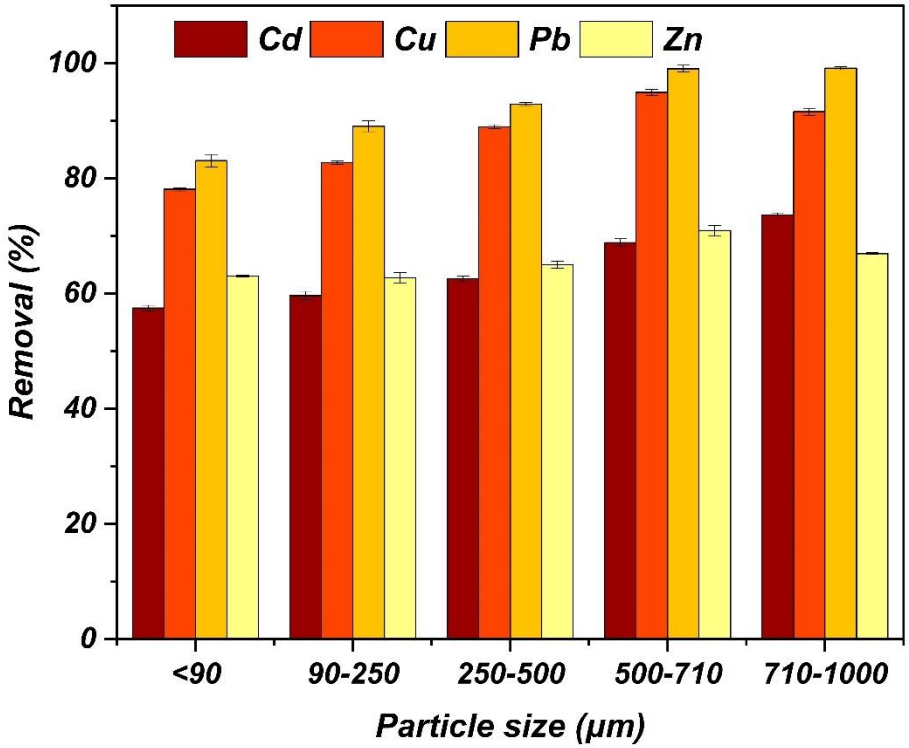

Figure. 4-18: The effect of NSWR particle size fraction on the removal efficiency (%) of Cd(II), Cu(II), Pb(II), and Zn(II).

4.2.3.6. Competitive Adsorption and Selectivity

To evaluate the performance of NSWR in a multi-component system, competitive adsorption experiments were conducted using a quaternary solution containing Cd(II), Cu(II), Pb(II), and Zn(II). The results demonstrate a clear selectivity sequence for the NSWR biosorbent, which was determined to be: **Pb(II) > Cu(II) > Cd(II) > Zn(II)**. As shown in **Figure 4-19**, Pb(II) was preferentially adsorbed with the highest uptake capacity, a finding that is highly consistent with the literature for various biosorbents, which often report the efficient removal of lead even in the presence of competing ions (Amar et al., 2021). The competitive nature of the system meant that the presence of multiple metals, particularly the highly preferred Pb(II), suppressed the uptake of the other ions compared to single-solute systems. This observed selectivity can be correlated with the intrinsic physicochemical properties of the metal ions (**Table 4-5**). A strong positive correlation was observed between the adsorption capacity and both the electronegativity and the covalent index of the metal ions. Lead (Pb) has the highest electronegativity (2.33) and covalent index (6.41), followed by Copper (1.90 and 2.98), Cadmium (1.69 and 2.71), and Zinc (1.65 and 2.04). The covalent index, in particular, reflects a metal ion's propensity to form stronger, more covalent-like bonds with the functional groups on the biosorbent surface (Batool et al., 2022).

The preferential uptake of metals with a higher covalent index suggests that the adsorption mechanism involves more than simple electrostatic attraction and includes contributions from softer, more covalent interactions, which aligns with the principles of the Hard-Soft Acid-Base (HSAB) theory.

When compared to other biosorbents reported in the literature, the NSWR demonstrates competitive performance for a low-cost, unmodified material. A summary of kinetic and thermodynamic data for

various lignocellulosic biomasses is provided in **Table A9-1**, while **Table A9-2** offers a comparative list of maximum adsorption capacities (Qmax) from several relevant studies.. The maximum adsorption capacities in the quaternary system—10.3 mg/g for Pb(II), 7.9 mg/g for Cu(II), 6.3 mg/g for Cd(II), and 6.0 mg/g for Zn(II) position NSWR as a viable candidate for the treatment of multi-metal wastewater streams.

.

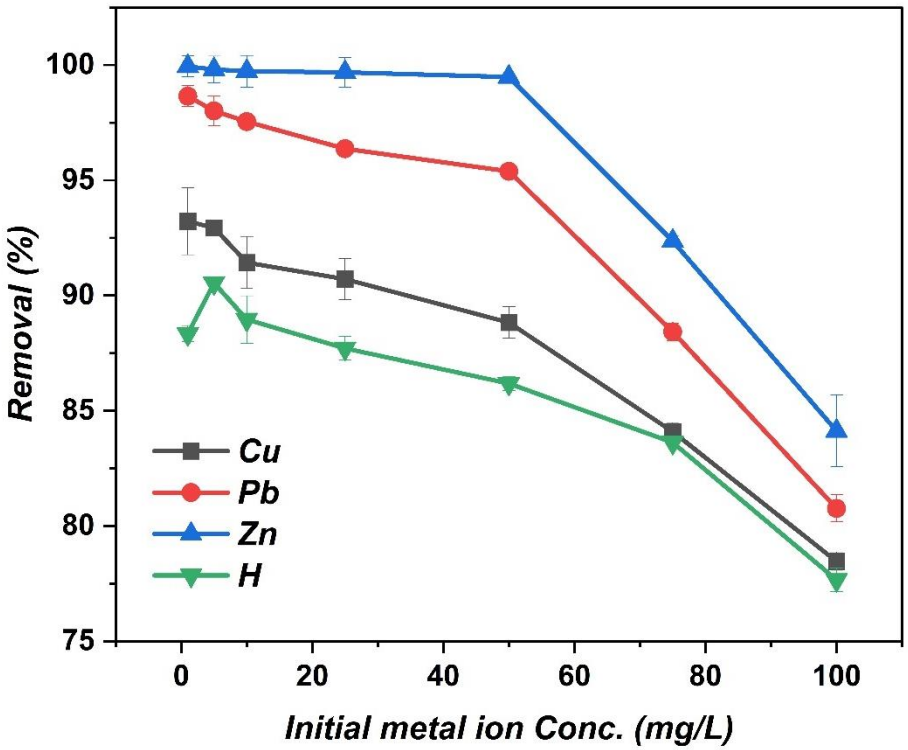

Figure 4-19. Competitive adsorption of Cd(II), Cu(II), Pb(II), and Zn(II) onto the NSWR biosorbent from a quaternary solution as a function of initial metal concentration..

Table 4-5 Selected Physicochemical Properties of the Investigated Heavy Metal Ions**.**

Property	Symbol / Abbr.	Cd	Cu	Pb	Zn
Ionic Radius (Å)	I.R.	0.97	0.72	1.33	0.74
Electronegativity	E	1.69	1.90	2.33	1.65
Hydrated Radius (Å)	H.R.	4.26	4.19	4.01	4.30
Covalent Index	C.I.	2.71	2.98	6.41	2.04

Sources: (Kong et al., 2020),

**AR: E: Electronegativity, H.R: Hydrated Radius (Å), M.M: Mole Mass (g/mol), C I: Covalent Index.

4.2.3.7. Influence of Agitation Speed

The effect of agitation speed on the heavy metal removal efficiency was investigated over a range of 40 to 400 rpm to determine the optimal conditions for mass transfer. Agitation speed is a critical parameter as it influences the thickness of the external boundary layer surrounding the adsorbent particles and ensures the uniform suspension of the biosorbent in the solution.
The experimental results, shown in **Figure 4-20**, indicate that the removal efficiency for all four metal ions was low at agitation speeds below 150 rpm. This is likely due to insufficient mixing, which leads to the settling of biosorbent particles and the formation of a thick, stagnant boundary layer that increases mass transfer resistance. As the agitation speed was increased from 150 to 200 rpm, a significant improvement in removal efficiency was observed. This is attributed to increased turbulence, which reduces the thickness of the boundary layer and enhances the diffusion of metal ions from the bulk solution to the adsorbent surface. However, no further significant improvement in adsorption was observed at speeds above 200 rpm. This suggests that at 200 rpm, the external mass transfer resistance has been minimized, and the adsorption rate becomes controlled by other factors, such as intraparticle diffusion. Therefore, an agitation speed of 200 rpm was identified as optimal and was used for all other experiments. This finding is consistent with similar studies on other biomass-based adsorbents (Kebede et al., 2018).

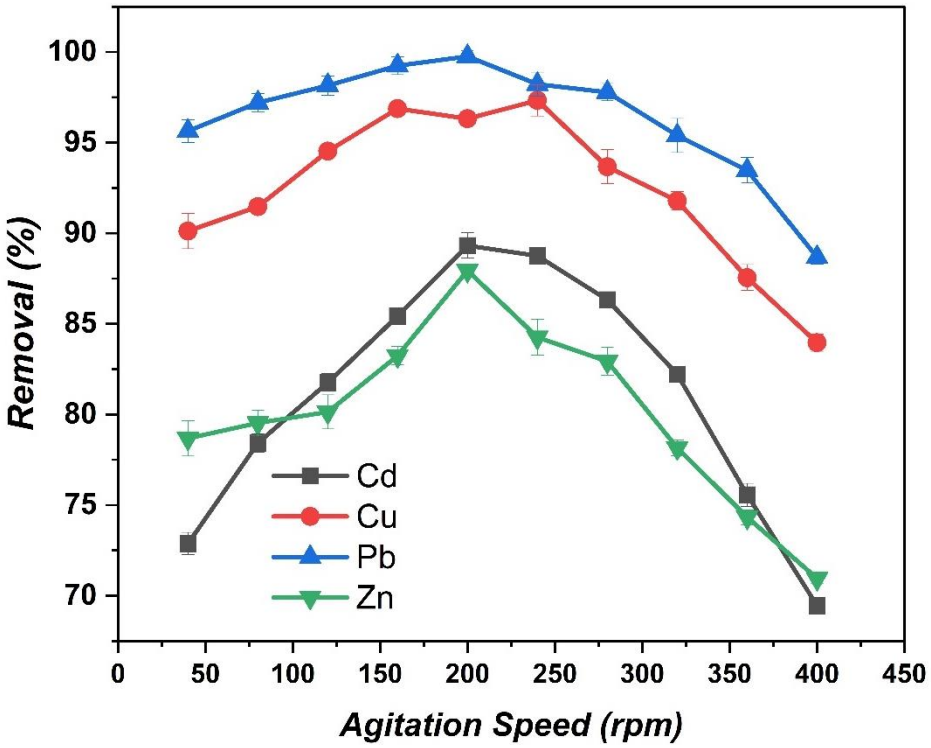

Figure. 4-20: Effect of agitation speed (rpm) on the removal efficiency (%) of Cd(II), Cu(II), Pb(II), and Zn(II) by the NSWR biosorbent..

4.2.4. Adsorption Isotherm Analysis

To characterize the equilibrium behavior of heavy metal adsorption onto NSWR, the experimental data were fitted to the Langmuir and Freundlich isotherm models. The best-fit model for describing

the relationship between the metal ion concentration in solution and the amount adsorbed at the surface was determined by comparing the correlation coefficients (R^2) from non-linear regression analysis (**Figure 4-21, Table 4-6**).

A comparative analysis of the goodness-of-fit metrics clearly indicates that the Langmuir model provides a superior description of the equilibrium data for all four metals ($R^2 > 0.99$) compared to the Freundlich model ($R^2 \approx 0.90–0.96$). The strong adherence to the Langmuir isotherm suggests that adsorption occurs predominantly as a monolayer onto a finite number of energetically uniform active sites on the biosorbent surface. This type of fit is often indicative of a chemisorption-controlled process (Akpomie et al., 2023; Mo et al., 2023). The maximum monolayer adsorption capacities (q_m) derived from the Langmuir model confirmed the selectivity sequence of Pb^{2+} (10.3 mg/g) > Cu^{2+} (7.9 mg/g) > Cd^{2+} (6.3 mg/g) > Zn^{2+} (6.0 mg/g).

Although the Freundlich model provided a less accurate fit, its parameters offer additional insight. The Freundlich intensity factor, 1/n, was found to be less than 1 for all metals (ranging from 0.55 to 0.68). Values of 1/n in this range confirm the favorable nature of the adsorption process and can suggest a degree of surface heterogeneity, even if the system is best approximated by the homogeneous Langmuir model.

Table 4-6. Langmuir and Freundlich isotherm parameters for the biosorption of heavy metals onto NSWR.

Element	Model
Langmuir	
Cd^{2+}	q_m(mgg^{-1}) =6.277, K_L (Lmg^{-1}) =0.2298, $R_L = R^2 \approx$%99
Pb^{2+}	q_m(mgg^{-1}) =*10.325*, K_L (Lmg^{-1}) =3.211, $R_L = R^2 \approx$*0.99*
Cu^{2+}	q_m(mgg^{-1}) = *7.853*, K_L (Lmg^{-1})=0.5785, $R_L = R^2 \approx$ *0.99*
Zn^{2+}	q_m(mgg^{-1}) =*6.029*, K_L (Lmg^{-1}) =0.1712, $R_L = R^2 \approx$*0.99*
Freundlich	
Cd^{2+}	K_f (mgg^{-1}) =0.9312, 1/n (gL^{-1}) =0.635, $R^2 \approx$*0.91*
Pb^{2+}	K_f (mgg^{-1})=2.3577, 1/n (gL^{-1})=0.55, $R^2 \approx$*0.96*
Cu^{2+}	K_f (mgg^{-1})=1.2915, 1/n =0.576, $R^2 \approx$*0.94*
Zn^{2+}	K_f (mgg^{-1})=0.8383, 1/n (gL^{-1})=0.675, $R^2 \approx$*0.9*

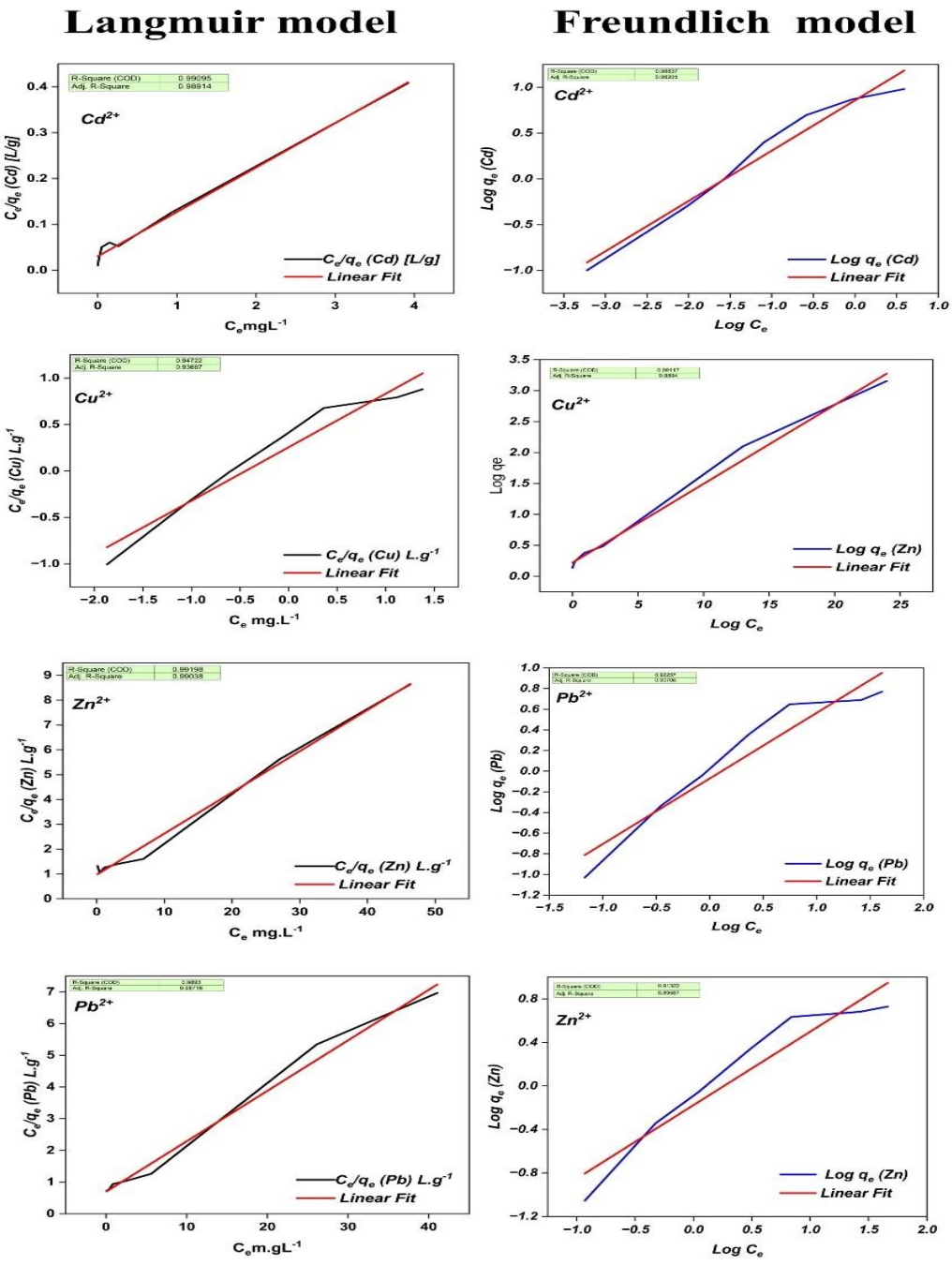

Figure 4-21. Non-linear fits of the Langmuir and Freundlich isotherm models to the equilibrium adsorption data for Cd(II), Cu(II), Pb(II), and Zn(II) onto NSWR..

4.3. Kinetic Modelling

4.3.1. Analysis of Adsorption Kinetics and Mechanisms

An analysis of the kinetic data revealed that the adsorption process was best described by the Pseudo-Second-Order (PSO) model, which consistently yielded the highest coefficient of determination (R^2) values. The strong fit to the PSO model suggests that the rate-limiting step is likely chemisorption, involving valence forces and the sharing or exchange of electrons between the metal ions and the adsorbent's active functional groups (Vishan et al., 2019)(Weyrich et al., 2023). To further elucidate the mass transfer mechanisms, the data were also analyzed using the intraparticle diffusion model. As shown in **Figures 4-22 and 4-23**, the plots for each metal ion displayed linear regions but did not pass through the origin. This finding indicates that while intraparticle diffusion is a significant rate-controlling step, it is not the sole mechanism governing the process. The presence of a non-zero intercept implicates the concomitant influence of external mass transfer resistance across the boundary layer (Malima et al., 2021). Therefore, it can be concluded that the overall adsorption of heavy metals onto the biomass is a complex process, with the rate being co-limited by both film diffusion and intraparticle diffusion.

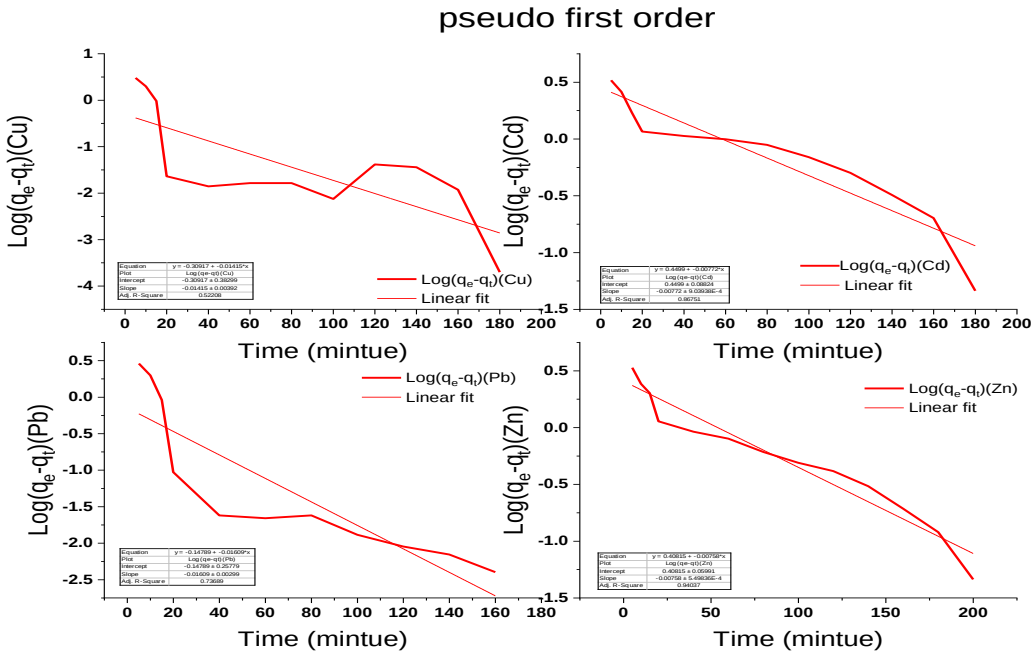

Figure 4-22. Pseudo first order model of Cd^{2+}, Cu^{2+}, Pb^{2+} and Zn^{2+} onto NSWR biomass

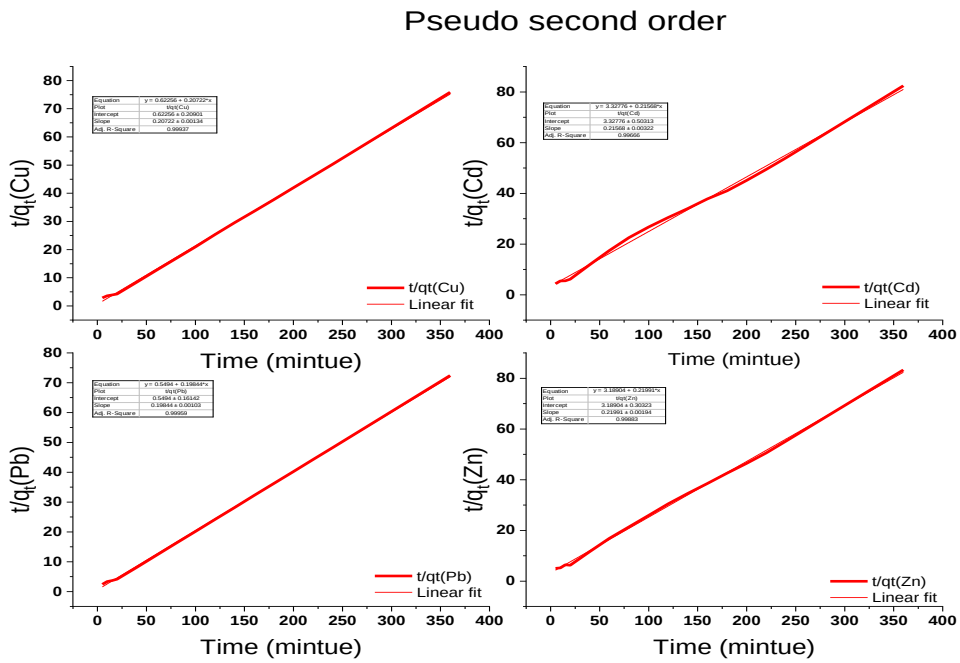

Figure 4-23. Pseudo second order model of Cd^{2+}, Cu^{2+}, Pb^{2+} and Zn^{2+} onto NSWR biomass

4.3.2. Adsorption Diffusion Models (Mass Transfer Models)

To complement the empirical kinetic analysis, diffusion-based models were employed to provide a more mechanistic understanding of the mass transfer phenomena. This approach is essential for distinguishing between the potential rate-limiting steps of the adsorption process: (1) external mass transfer, which involves the transport of ions across the liquid boundary layer surrounding the adsorbent (film diffusion), and (2) internal mass transfer, which involves the transport of ions within the porous structure of the adsorbent (intraparticle diffusion). This section evaluates the experimental data using the Weber-Morris and liquid film diffusion models to further elucidate these mass transfer steps for the adsorption of heavy metals onto NSWR.

4.3.2.1. Weber-Morris Intraparticle Diffusion Model (IDP)

The Weber-Morris model was specifically applied to assess the influence of intraparticle diffusion on the overall rate of adsorption. According to this model, a plot of the adsorption capacity at time t (q_t) versus the square root of time ($t^{0.5}$) that yields a straight line passing through the origin indicates that intraparticle diffusion is the sole rate-limiting step. Conversely, a multi-linear plot or a non-zero intercept suggests that other mechanisms, such as film diffusion, are also involved.

Figure 4-25 presents the Weber-Morris plots for the adsorption of Cd^{2+}, Cu^{2+}, Pb^{2+}, and Zn^{2+} onto the NSWR biomass. An analysis of these plots, in conjunction with the film diffusion analysis presented in **Figure 4-26**, allows for the identification of the dominant mass transfer resistances governing the adsorption process.

.

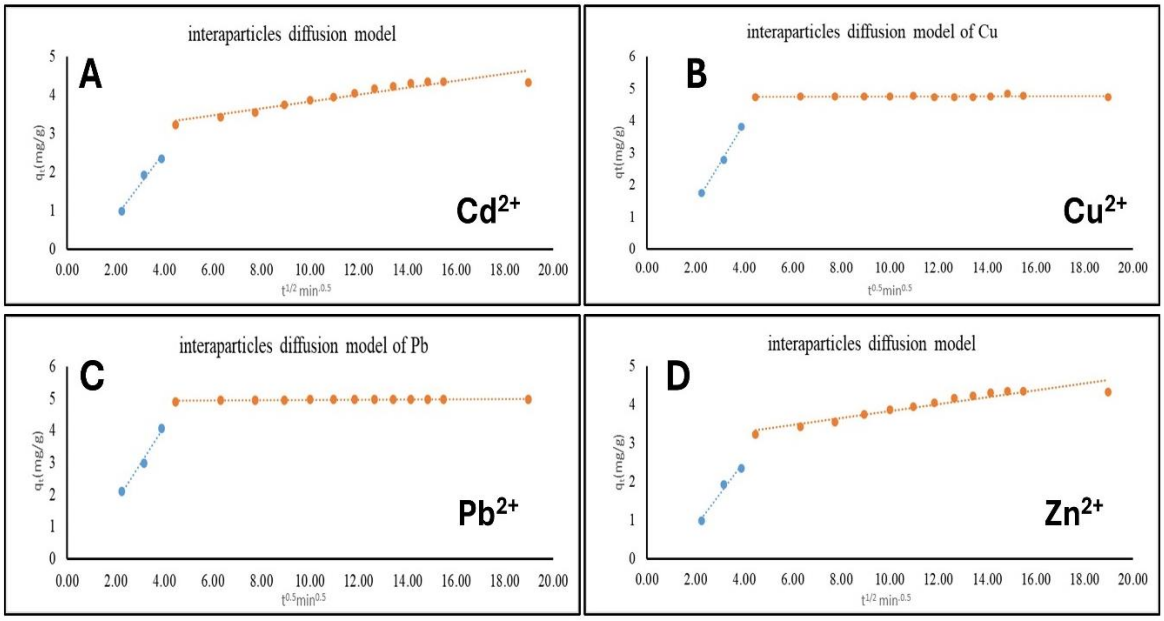

Figure 4-24. Weber-Morris intraparticle diffusion plots (q_t vs. $t^{0.5}$) for the adsorption of (A) Cd^{2+}, (B) Cu^{2+}, (C) Pb^{2+}, and (D) Zn^{2+} onto NSWR biomass. The presence of distinct linear regions for each metal ion indicates that the adsorption process involves multiple diffusion stages rather than a single rate-limiting step.

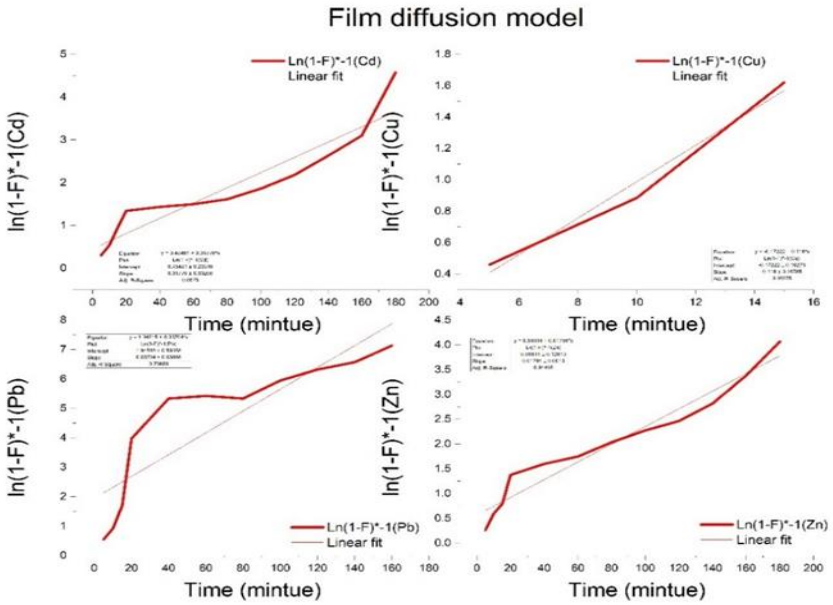

Figure 4-25. Application of the Liquid Film Diffusion model (ln(1-F) vs. time) for the adsorption kinetics of Cd^{2+}, Cu^{2+}, Pb^{2+}, and Zn^{2+} onto NSWR biomass. The plots evaluate the contribution of external mass transfer resistance.

4.3.2.2. The pseudo-second-order kinetic model

The kinetic parameters derived from fitting the Pseudo-First Order (PFO) and Pseudo-Second Order (PSO) models to the experimental data are presented in **Table 4-7**. This summary includes the calculated equilibrium capacities (q_e), the respective rate constants (k_1 and k_2), and the coefficients of determination (R^2) for each model, which facilitates a direct comparison of their goodness-of-fit.

Table 4-7. Kinetic parameters of PFO and PSO kinetic models of the 4 HMs on NSWR

Metal ion	Pseudo-first order (PFO)			Pseudo-second order (PSO)		
	K_1 ($_{minute}^{-1}$)	q_e (calculated) (mg/g)	R^2	K_2 [g/(mg·min)]	q_e (calculated) (mg/g)	R^2
Cd	0.003343	2.817	0.8796	0.0140	4.6364	0.9969
Cu	0.006165	0.49	0.5655	0.0687	4.8314	0.9993
Pb	0.00699	0.711	0.7632	0.0717	5.0392	0.9996
Zn	0.002996	2.376	0.9478	0.0152	4.5473	0.9989

As previously described in the methods, the parameters for the PSO model were determined from the slope and intercept of the linearized plot of t/q_t versus t.

4.3.2.3.Weber-Morris Intraparticle Diffusion Model

The kinetic parameters derived from the application of the Weber-Morris Intraparticle Diffusion (IDP) model are summarized in **Table 4-8**. This table presents the calculated values for the intraparticle diffusion rate constant (K_p), the intercept (I), and the coefficient of determination (R^2) for the adsorption of heavy metals onto NSWR biomass. Consistent with the multi-linear nature of the IDP plots, the parameters in the table are categorized into distinct stages. This approach is necessary to reflect the complexity of the diffusion process, where different mass transfer mechanisms may be rate-limiting step at different phases of the adsorption process (Al-Kahtani et al., 2024).

Table 4-8. Intra-particle diffusion model of Cd, Cu, Pb & Zn onto NSWR biomass.

Metal	The Intraparticle Diffusion (Stage 1)			The Intraparticle Diffusion (Stage 2)			The Intraparticle Diffusion (Without Separation)		
	K_p (1)	**I (1)**	**R^2 (1)**	**K_p (2)**	**I (2)**	**R^2 (2)**	**Kp**	**I**	**R^2**
Cd	0.952	-1.035	0.977	0.104	2.786	0.862	0.174	1.866	0.786
Cu	1.251	-1.086	0.995	0.001	4.745	0.033	0.115	3.241	0.421
Pb	1.194	-0.641	0.984	0.005	4.906	0.562	0.113	3.476	0.436
Zn	0.836	-0.825	0.980	0.090	2.932	0.905	0.173	1.829	0.760

4.3.3. Comparison of Predictive Model Performance

Future work could involve systematic parameter tuning of these AI models, such as exploring different feature selections and hyperparameter optimization techniques (e.g., grid search, cross-validation), to further enhance their predictive accuracy and uncover deeper insights into the adsorption mechanisms.

Such detailed optimization would better leverage the capabilities of AI for more robust modelling and potentially identify novel relationships between input parameters and adsorption outcomes.

An evaluation of six different regression models for predicting the adsorption capacities of Cd, Cu, Pb, and Zn revealed significant differences in their predictive accuracy, as detailed in **Table A9-4**, which presents the Mean Absolute Error (MAE), Root Mean Squared Error (RMSE), and R^2 scores for each model. The ensemble methods, particularly Gradient Boosting and XGBoost, demonstrated superior performance, consistently yielding the lowest Mean Absolute Error (MAE) and Root Mean Squared Error (RMSE) values, along with the highest R^2 scores. For several metals, the R^2 values for these boosting models exceeded 0.92, indicating exceptional reliability. While the Decision Tree and Random Forest models also performed well, they were slightly less accurate than the boosting-based techniques. In stark contrast, both Linear Regression and Support Vector Regression (SVR) proved to be unsuitable for this application. These models failed to capture the complex, non-linear patterns of the adsorption process, as evidenced by their poor performance metrics, including negative R^2 values for Cu and Pb. These results underscore the robust capability of advanced ensemble methods like XGBoost and Gradient Boosting for accurately simulating complex environmental processes such as heavy metal adsorption, handling complex interactions between multiple variables, and potentially accelerating the discovery of optimal experimental conditions, thereby reducing the need for extensive experimental trials. These results illustrate the efficacy of ensemble learning tools, including boosting techniques, in simulating complex adsorption processes. However these regression models provide us with good forecasting potentials regarding kinetic models' performances compared to classical kinetic models, the overall evaluation must consider the optimization of various affecting parameters, and thus the benefit of applying machine learning and AI will be maximized. The following bar charts show the performance of different regression models for each metal **Figure 4-26.**

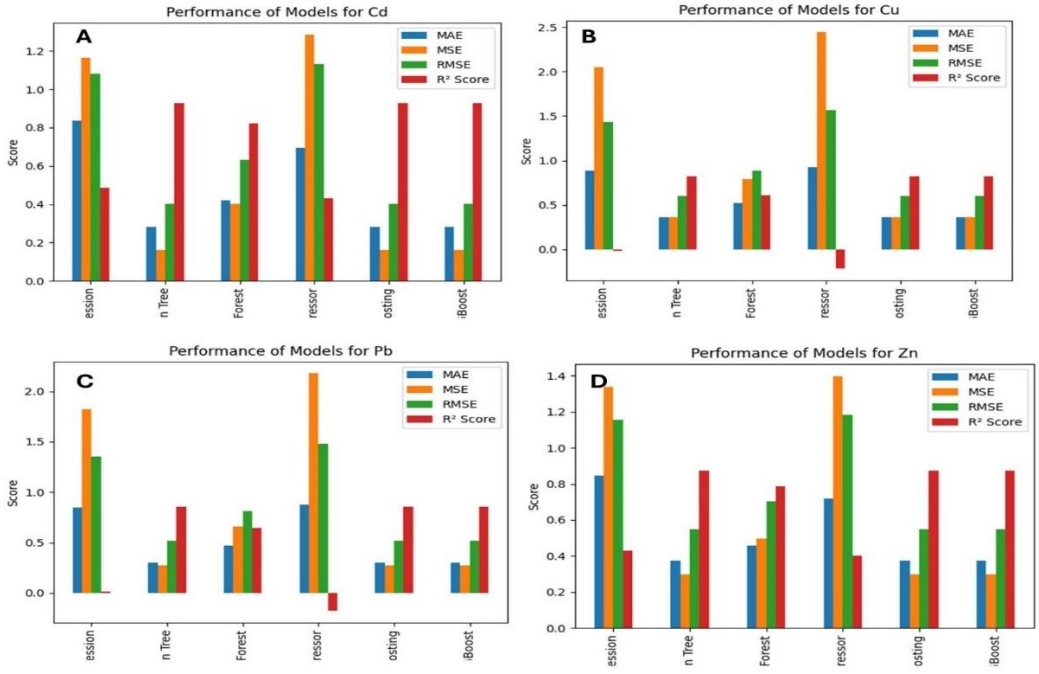

Figure 4-26. Performance of models for A; Cd, (B); Cu, (C) Pb and (D) Zn.

4.3.4. Isothermal Modelling

The equilibrium data were analyzed using four isotherm models: Langmuir, Freundlich, Temkin, and Dubinin-Radushkevich (D-R). The linearized plots for each of these models, applied to the adsorption data for Cd^{2+}, Cu^{2+}, Pb^{2+}, and Zn^{2+} onto NSWR, are shown in **Figure 4-27, Table 4-9**. A summary of the key parameters derived from these models is provided in Table 3-13. An evaluation of the coefficient of determination (R^2) values indicates that the goodness-of-fit for the models followed the order: Langmuir > Freundlich > Dubinin-Radushkevich > Temkin. Notably, the Langmuir model provided an excellent correlation with the experimental data, yielding R^2 values greater than 0.99 for all four metal ions. This strong fit suggests that the adsorption process occurs as a monolayer on a homogeneous surface, where all active sites have an equal affinity for the adsorbate and there are no interactions between adjacent adsorbed molecules (Akpomie et al., 2023; Mo et al., 2023).

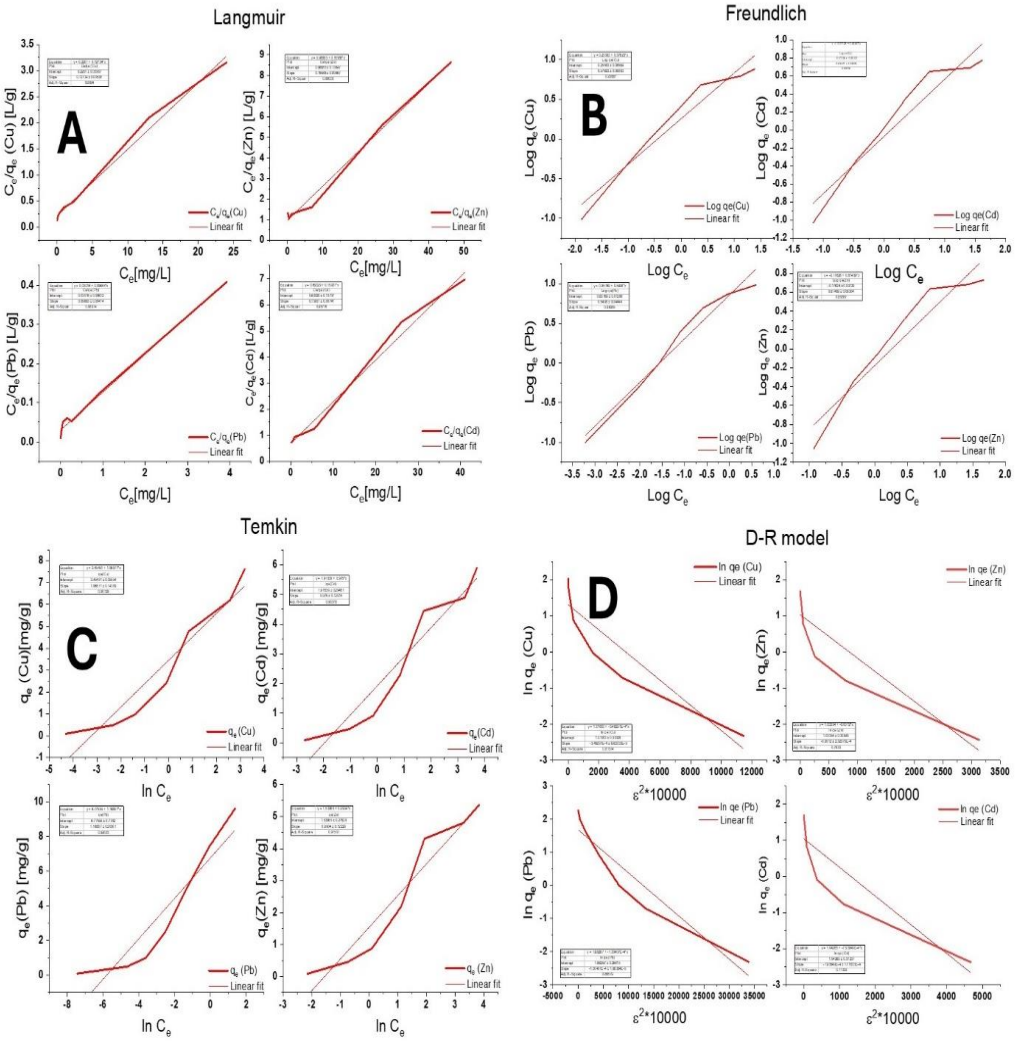

Figure 4-27. Linearized isotherm plots for the adsorption of Cd^{2+}, Cu^{2+}, Pb^{2+}, and Zn^{2+} onto NSWR biomass, showing the application of the: (A) Langmuir (C_e/q_e vs. C_e), (B) Freundlich (log q_e vs. log C_e), (C) Temkin (q_e vs. ln C_e), and (D) Dubinin-Radushkevich (ln q_e vs. ε^2) models.

Table 4-9. Summary of Calculated Isotherm Parameters for the Adsorption of Pb^{2+}, Cd^{2+}, Cu^{2+}, and Zn^{2+} onto the NSWR Biosorbent.

Element	Model
	Langmuir
Cd^{2+}	$q_m(mgg^{-1})$ =6.277, K_L (Lmg^{-1}) =0.2298, R^2 ≈%99
Pb^{2+}	$q_m(mgg^{-1})$ =*10.325,* K_L (Lmg^{-1}) =3.211, R^2 ≈*0.99*
Cu^{2+}	$q_m(mgg^{-1})$ = *7.853,* K_L (Lmg^{-1})=0.5785, R^2 ≈ *0.99*
Zn^{2+}	$q_m(mgg^{-1})$ =*6.029,* K_L (Lmg^{-1}) =0.1712, R^2 ≈*0.99*
	Freundlich
Cd^{2+}	K_f (mgg^{-1}) =0.9312, 1/n (gL^{-1}) =0.635, R^2≈*0.91*
Pb^{2+}	K_f (mgg^{-1})=2.3577, 1/n (gL^{-1})=0.55, R^2≈*0.96*
Cu^{2+}	K_f (mgg^{-1})=1.2915, 1/n =0.576, R^2≈*0.94*
Zn^{2+}	K_f (mgg^{-1})=0.8383, 1/n (gL^{-1})=0.675, R^2≈*0.9*
	Dubinin–Radushkevich (D-R)
Cd^{2+}	q_m (mgg^{-1}), E=(KJ/Mole), R^2≈*0.77,* β (K_{DR})= ($Mole^2$/ KJ^2)
Pb^{2+}	q_m (mgg^{-1}), E=(KJ/Mole), R^2≈*0.89,* β (K_{DR})= ($Mole^2$/ KJ^2)
Cu^{2+}	q_m (mgg^{-1}), E=(KJ/Mole), R^2≈*0.82,* β (K_{DR}) = ($Mole^2$/KJ^2)
Zn^{2+}	q_m (mgg^{-1}), E=(KJ/Mole), β (K_{DR})= ($Mole^2$/ KJ^2), R^2≈*0.78*
	Temkin
Cd^{2+}	B_T=, K_T ($LmgL^{-1}$) =, R^2≈*0.90*
Pb^{2+}	B_T=, K_T ($LmgL^{-1}$) =, R^2≈*0.84*
Cu^{2+}	B_T=, K_T ($LmgL^{-1}$) =, R^2≈*0.90*
Zn^{2+}	B_T=, K_T ($LmgL^{-1}$) =, R^2≈*0.92*

4.3.5. Advanced Isotherm Modelling (Thermodynamic Modelling)

To gain a more profound understanding of the adsorption mechanism at a molecular level, the equilibrium data were analysed using advanced isotherm models derived from statistical physics. These models interpret the adsorption process through key steric and energetic parameters, including the number of molecules adsorbed per site (n), the density of active sites (N_m), and the theoretical saturation capacity (Q_{sat}). Model fitting was performed via non-linear regression using the Levenberg–Marquardt algorithm. Based on a comprehensive evaluation of R^2 and RMSE values, the "monolayer model with a single energy site" was identified as the most suitable advanced model for describing CFX adsorption onto RC, NC, and SC (**Table 4-10, Figures 4-28**). The key parameters derived from this model are discussed below.

The thermodynamic parameters calculated for the adsorption of heavy metals onto the NSWR biomass are summarized in Table 3-14 and illustrated in Figure 3-39. The analysis provides key insights into the nature of the adsorption process. The consistently positive values for the change in enthalpy (ΔH°) across all investigated metals confirm that the adsorption process is endothermic, indicating that it is

more favorable at higher temperatures. This is further supported by the trend of the Gibbs free energy (ΔG°), which became more negative as the temperature increased, signifying greater spontaneity under warmer conditions (Khoshraftar et al., 2023). Furthermore, the positive values for the change in entropy (ΔS°) suggest an increase in randomness at the solid-liquid interface during the adsorption process. This is characteristic of a structurally favourable and stable biosorption mechanism (Haggag et al., 2021). The spontaneity of the reaction, however, was found to be metal-specific at the tested temperatures. The negative ΔG° values observed for Cu^{2+} and Pb^{2+} indicate that their adsorption is a spontaneous and highly favorable process. In contrast, the positive ΔG° values for Cd^{2+} and Zn^{2+} suggest that their adsorption is less spontaneous under the same conditions.

These findings—specifically an endothermic, entropy-driven process that is best described by a pseudo-second-order kinetic model—are in strong agreement with previous studies on heavy metal adsorption onto similar lignocellulosic materials, such as sawdust (Meez et al., 2021).

Table 4-10. Thermodynamic parameters of NSWR

Metal	ΔH° (KJ.mol^{-1})	ΔS° (KJ.mol^{-1}. K^{-1})	R^2	ΔG° (KJ.mol^{-1})				
				298 K	303 K	308 K	313 K	318 K
Cd	23.35	0.07	0.9558	2.37	2.29	1.88	1.54	0.98
Cu	32.56	0.11	0.9754	0.03	-0.29	-0.96	-1.33	-2.18
Pb	34.80	0.12	0.9134	-2.19	-2.30	-3.21	-3.50	-4.70
Zn	25.33	0.08	0.9558	2.66	2.44	2.17	1.75	1.09

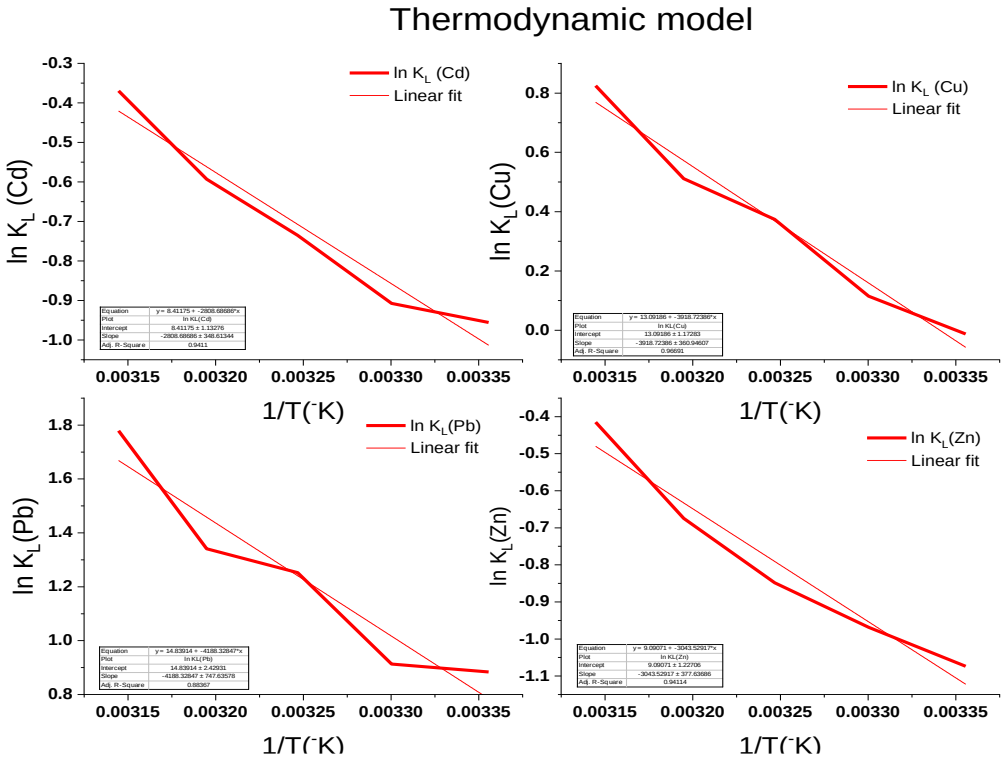

Figure 4-28. Thermodynamic graph of Cd^{2+}, Cu^{2+}, Pb^{2+} and Zn^{2+} onto NSWR biomass.

4.3.6. Comparison between the Performance of NSWR and Nano Particles from NSWR on Synthesized Wastewater and on Real Wastewater Obtained from "Laundry shop"

Several wastewater samples were collected from commercial laundry shop in Madaba-Jordan, the sample represents the average content of several obtained samples. The removal percentages of the four heavy metals (Pb, Cu, Pb, Zn) have been measured using Batch-mode experiments according to previous mentioned method. The results of applying Nano NSWR on laundry water samples, including their maximum adsorption capacities, are shown in **Table 4-11 and Table 4-12** in the appendices. It is noteworthy to mention that some important parameters such as BOD5, COD, Turbidity, Phosphate, Nitrate, Chloride, Sulphate and Total Kjeldahl Nitrogen (TKN), organic matters and microbial content have not been determined. Knowing that laundry wastewater is a complicated mixture of different ions and various components and can be characterized by its highly fluctuated nature. Consequently, to design a proper wastewater treatment regime it is highly recommended to determine the overall constituents and to have a full physical, chemical and biological analysis side by side with other interesting influencing parameters. More samples should be regularly and frequently analysed to correctly and precisely judge the overall situation. On the other hand, it is recommended to apply the continues fluid regime (fixed bed column) method on large scale rather than batch mode. **Figure 4-29** in the appendixes explains the difference in the performance between NSWR and Nano NSWR. From this figure, it can be noticed that using Nano NSWR for the treatment of synthesized sample contains the 4 PTEs provided better results than NSWR.

Table 4-11. Average concentrations of PTEs obtained from laundry wastewater

TDS	pH	Temp.	Cd	Pb	Cu	Zn
1870	10.3	27 °C	0.031 mg/L	0.32 mg/L	1.2 mg/L	2.1 mg/L

Table 4-12. Average concentrations of PTEs obtained after treatment with nanocrystals from NSWR

	Cd	Pb	Cu	Zn
Treated water with nanocrystals (mg/L)	Not Detected	Not Detected	0.108	0.231
Removal efficiency %	100%	100%	91%	89%

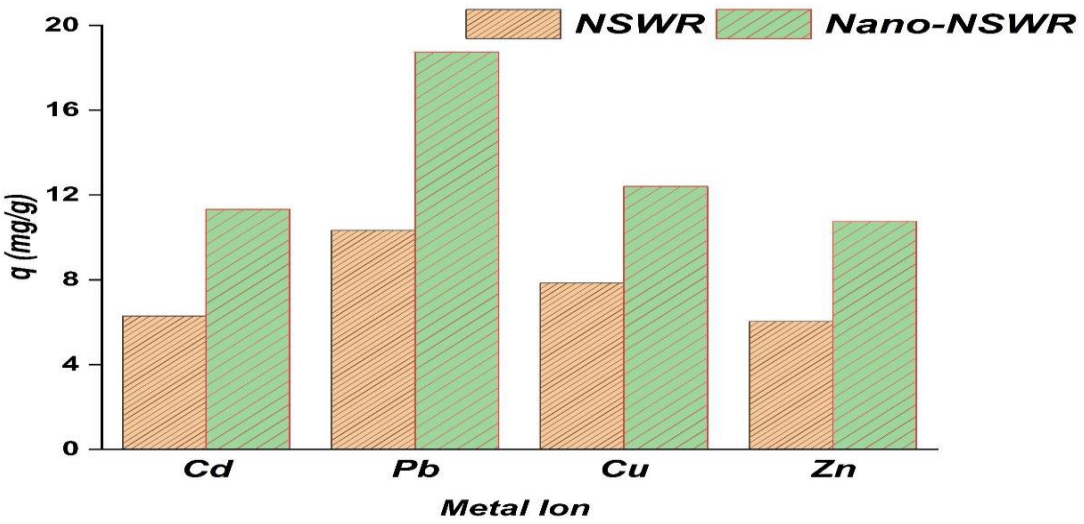

Figure 4-29. Comparison between NSWR and Nano-NSWR performance on (Cd, Pb, Cu, Zn) removal.

Analysing the means of the two groups: NSWR and Nano-NSWR values explores that the value of probability between 0.01 and 0.05 indicates the difference between the two groups is significant at 0.05 level of significance. These statistical analyses were carried out by Statistical Package for the Social Sciences **(SPSS)**.

4.3.7. Isotherm Modelling and Enhanced Adsorption Capacity of Nano-NSWR.

To quantitatively validate the superior performance of the nano-formulated biosorbent, equilibrium adsorption data for Nano-NSWR were analyzed using the Langmuir isotherm model. As presented in **Figure 4-30**, the linearized plots for all four metal ions (Cd^{2+}, Cu^{2+}, Pb^{2+}, and Zn^{2+}) exhibit strong linearity, which is confirmed by consistently high coefficients of determination ($R^2 > 0.97$). This excellent fit to the model is a strong indicator that the adsorption process onto the Nano-NSWR surface proceeds as a monolayer, where metal ions bind to a finite number of discrete and energetically uniform active sites. This mechanistic conclusion is in excellent agreement with the kinetic analysis (**Section 4.4.1**), which identified chemisorption via the Pseudo-Second-Order model as the rate-limiting step, a process inherently based on specific site interactions.

The theoretical maximum monolayer adsorption capacities (q_{max}) derived from the Langmuir model are summarized in **Table 4-13**. These values provide the most critical insight of this analysis, revealing a dramatic enhancement in adsorption performance compared to the original NSWR biosorbent (**Table 4-9**). Specifically, the q_{max} for Nano-NSWR was substantially higher across all tested metals:

- For **Lead (Pb^{2+})**, capacity increased by **76%**, from 10.33 mg/g to **18.18 mg/g**.
- For **Copper (Cu^{2+})**, capacity increased by **63%**, from 7.85 mg/g to **12.82 mg/g**.
- For **Cadmium (Cd^{2+})**, capacity increased by **89%**, from 6.28 mg/g to **11.87 mg/g**.
- For **Zinc (Zn^{2+})**, capacity increased by **84%**, from 6.03 mg/g to **11.11 mg/g**.

This profound improvement in uptake capacity is primarily attributed to the increased surface area-to-volume ratio inherent in nanomaterials. The nano-synthesis process effectively increased the density of available surface functional groups, which act as the primary binding sites for metal ions. Furthermore, the nano-structuring may have enhanced the accessibility of the adsorbent's internal pore network, further contributing to the increased capacity.

It is noteworthy that while the *quantity* of adsorption sites was significantly increased, the intrinsic affinity of these sites for the metals remained consistent. The selectivity order for Nano-NSWR was $\mathbf{Pb^{2+} > Cu^{2+} > Cd^{2+} > Zn^{2+}}$, the same order observed for the original NSWR material. This suggests that the fundamental surface chemistry of the biosorbent was preserved during nano-synthesis. The continued preference for Pb^{2+} can be linked to its favorable physicochemical properties, such as high electronegativity and an optimal ionic radius, which facilitate strong chelation with the biomass's active sites.

Table 4-13. Langmuir Isotherm Parameters for Heavy Metal Adsorption onto Nano-NSWR.

Metal Ion	Maximum Adsorption Capacity (q_{max}) (mg/g)	Coefficient of Determination (R^2)
$\mathbf{Pb^{2+}}$	18.18	0.9782
$\mathbf{Cu^{2+}}$	12.82	0.9998
$\mathbf{Cd^{2+}}$	11.87	0.9891
$\mathbf{Zn^{2+}}$	11.11	0.9934

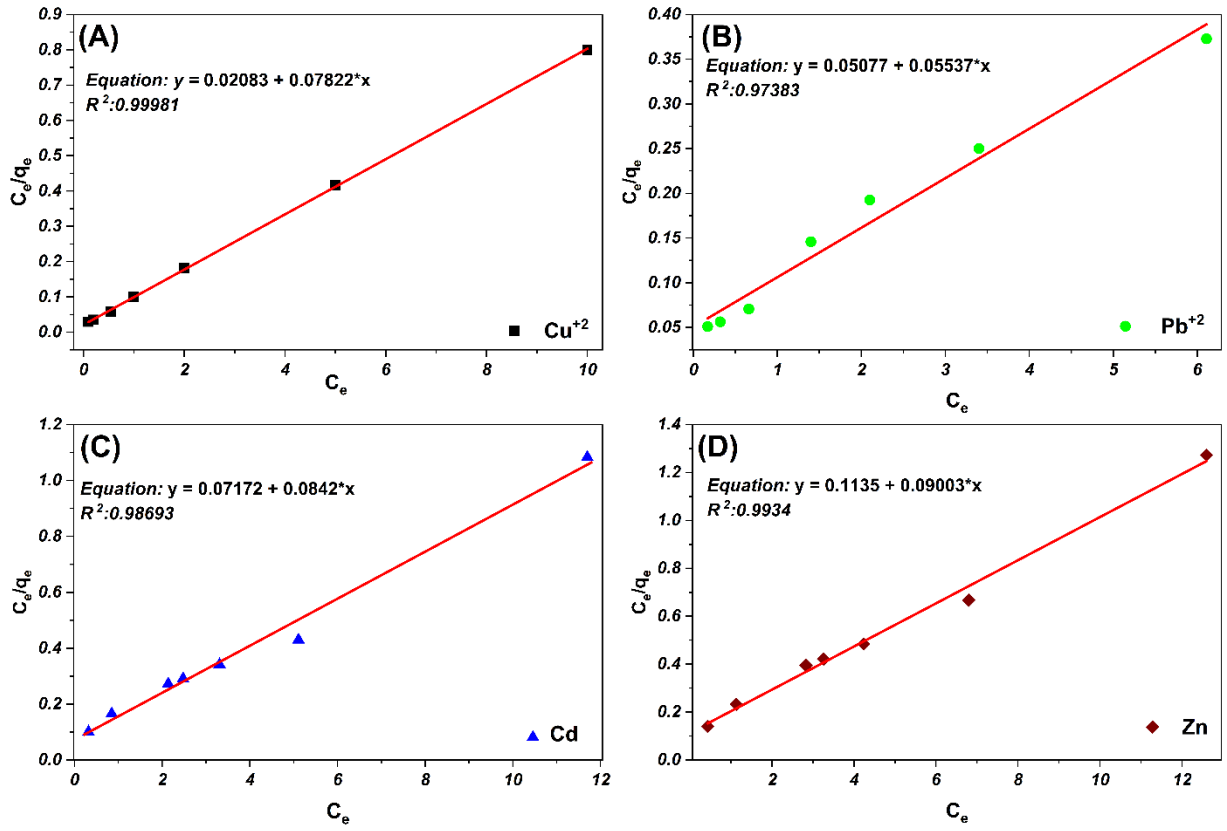

Figure 4-30. Linearized Langmuir isotherm plots (C_e/q_e vs. C_e) for the adsorption of Cu^{2+} (A), Pb^{2+} (B), Cd^{2+} (C), and Zn^{2+} (D) ions onto Nano-NSWR biomass.

4.4. Economic Feasibility of Sulfuric Acid Modification

The practical viability of an adsorbent is critically dependent on its economic feasibility. Therefore, a preliminary cost analysis was conducted to evaluate the preparation cost of the sulfuric acid-modified coal (S.C) and compare it to a commercial benchmark. The overall cost of adsorbent synthesis is influenced by several factors, including the price of raw materials, the cost of chemical reagents, energy consumption, and the adsorbent's performance metrics like capacity and reusability.

The primary chemical reagent for the modification is sulfuric acid (H_2SO_4). The cost estimation was based on the following calculations and assumptions:

1. **Reagent Preparation:** Commercially available 98% H_2SO_4 (density ≈ 1.84 g/mL) has a molarity of approximately 18.4 M. The experimental protocol requires a 1 M solution. Based on the dilution equation ($M_1V_1 = M_2V_2$), preparing 1 liter of 1 M H_2SO_4 requires approximately 54.3 mL of the concentrated acid.

2. **Treatment Ratio:** The modification procedure utilizes 10 liters of 1 M H_2SO_4 per kilogram of raw coal.

The total preparation cost for 1 kg of the S.C adsorbent was estimated by summing the primary cost components based on approximate Jordanian market prices:

- **Cost of Precursor:** The market price of 1 kg of raw sub-bituminous coal is estimated at **0.20 JOD**.
- **Cost of Reagent:** The price of 10 L of the prepared 1 M H_2SO_4 solution is estimated at **1.40 JOD**.
- **Energy Cost:** The electricity expenditure required for grinding 1 kg of coal is estimated at **0.25 JOD**.
- **Ancillary Costs:** The cost of 10 L of deionized water for washing is estimated at **0.10 JOD**.

The total estimated cost for producing 1 kg of the S.C adsorbent is the sum of these components: (0.20 + 1.40 + 0.25 + 0.10) = **1.95 Jordanian Dinars (JOD)**, which is equivalent to approximately ≈ **2.75 US Dollars**.

To contextualize this expense, the preparation cost was compared against the price of a standard commercial adsorbent. The average market price for 1 kg of commercial granular activated carbon in Jordan is approximately **4.00 JOD ≈ 5.6 US Dollars $ (*Cost varies** by country and is correlated with **market fluctuations**).

This economic analysis confirms that modifying local coal with sulfuric acid is a highly cost-efficient approach. At an estimated preparation cost of 1.95 JOD/kg, the S.C adsorbent is less than half the price of commercial activated carbon (**4.00 JOD/kg ≈ 5.6 $).** This significant cost advantage, coupled with its high ciprofloxacin uptake and proven renderability, establishes the developed adsorbent as a practical and economically sustainable solution for real-world water treatment applications.

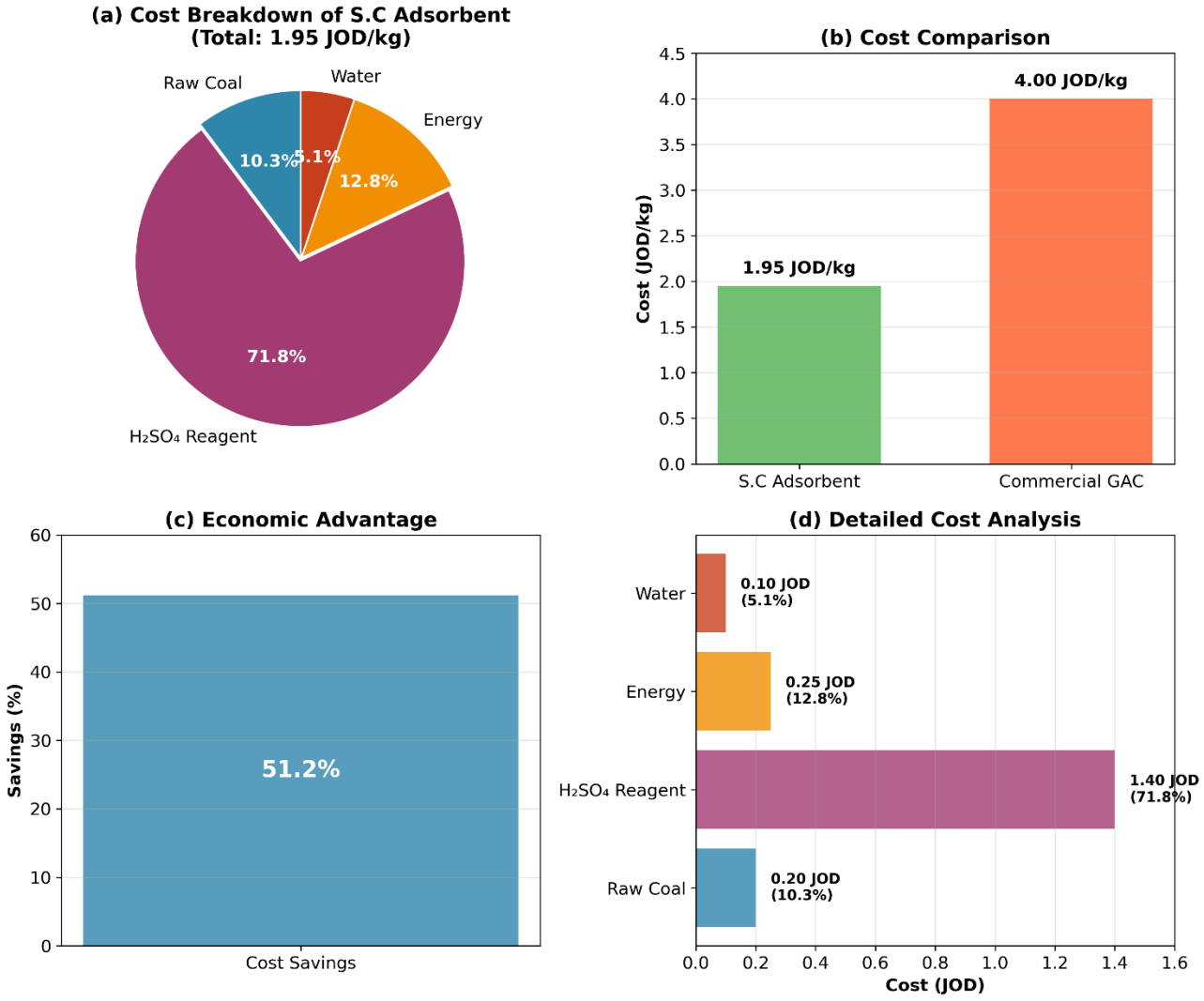

Figure 4-31. Economic Feasibility Analysis: Sulfuric Acid-Modified Coal (S.C) Adsorbent

4.5. Case Study: Cadmium Contamination at the Madaba Landfill and the need for Sustainable Environmental Management

To establish the practical context for this research, an evaluation of Cadmium (Cd) contamination was conducted at the Madaba landfill site. This case study serves to bridge the gap between the laboratory-scale development of low-cost adsorbents and their real-world application in mitigating pollution from hazardous waste sites. The reliance on uncontrolled landfills is a significant environmental issue in Jordan, where a substantial portion of solid waste is disposed of in such sites, often with inadequate containment measures. This practice poses severe risks of soil and groundwater contamination, highlighting the urgent need for effective and sustainable waste management solutions.

The generation of leachate a highly contaminated liquid that percolates through waste is a primary concern for all landfills. In arid regions like Jordan, it was once assumed that the lack of significant rainfall would minimize leachate formation. However, research has shown that other factors, such as the initial moisture content of the waste, ambient temperature, and capillary action in subsurface soils,

can contribute to leachate generation even in dry climates. Once formed, this leachate can migrate downwards, contaminating the underlying soil and, critically, the aquifer system. This is particularly concerning because groundwater contamination is often irreversible, and restoring a polluted aquifer to its original quality is exceedingly difficult and costly.
In Jordan, the deterioration of groundwater quality due to various point and non-point pollution sources is a well-documented and growing problem. For instance, long-term monitoring of groundwater wells near the Akaider landfill in northern Jordan has shown a gradual increase in contaminant concentrations over several decades (Igboama et al., 2022). Even in modern engineered landfills with liner systems, the risk of leachate leakage persists, posing a considerable threat to ecosystems and public health (Saha et al., 2021).

Cadmium (Cd) was selected as the target contaminant for this investigation due to its high toxicity, environmental mobility, and common presence in municipal solid waste. It is recognized as one of the most problematic heavy metals in landfill environments because of its propensity to leach from waste materials (Zheng et al., 2022). Common sources of Cd in landfills include discarded nickel-cadmium batteries, electronic waste, pigments, metal alloys, and tire rubber.
The concentration and subsequent retention of cadmium (Cd) in soil are governed by a complex interplay of factors. These include the inherent composition of the soil, such as its clay and organic matter content, alongside physicochemical conditions like pH. Furthermore, operational practices at landfill sites can significantly influence Cd levels. (Kubier et al., 2019).

In parallel with direct soil analysis, a comprehensive assessment of groundwater vulnerability was undertaken utilizing the Simplified Groundwater Vulnerability Index (SGVI) method. The SGVI is a specialized, GIS-based model developed for the specific hydrogeological context of Jordan. It provides a systematic framework for evaluating an aquifer's susceptibility to contamination by integrating seven critical parameters:

- Depth to Groundwater (DG)
- Soil Texture (ST)
- Lineament Density (LD)
- Rainfall (RF)
- Topographic Slope (TS)
- Drainage Density (DD)
- Land Use/Land Cover (LC)

The methodological workflow for the Simplified Groundwater Vulnerability Index (SGVI), which involved rating, reclassifying, and applying a weighted overlay to these parameters, is illustrated in the flowchart presented in **Figure A9-1**. The analysis was performed using GIS and PCI Geomatica software, with input data sourced from various platforms and organizations; the details of these sources and their respective resolutions are provided in **Table A9-5**. The analysis of soil samples collected from the site revealed Cd concentrations ranging from 3 to 24 µg/g. These values significantly exceed the maximum permissible limits of 0.8 µg/g and 3 µg/g set by Dutch and FAO/WHO standards, respectively. This level of soil contamination indicates a significant risk to the underlying groundwater aquifer. It must be noted, however, that this investigation represents a preliminary assessment. A full evaluation of the environmental risk would necessitate long-term, seasonal monitoring to account for temporal variations in contaminant mobility(Xu et al., 2011).

Based on these findings, several sustainable management practices are proposed. The most direct application of this research involves the engineering of enhanced landfill liner systems. Utilizing low-cost, locally sourced adsorbent materials—such as the Jordanian zeolite noted for its high affinity for heavy metals (Igwegbe et al., 2024) could create a reactive barrier to capture Cd and prevent its migration into the subsurface. It was suggested that lateritic clay stabilized with less than 10% sawdust be used as landfill liners since it satisfies the standard hydraulic conductivity criterion and exhibits good Pb and Cd absorption. While the ideal moisture content and hydraulic conductivity rose as the sawdust content increased, the soil's specific gravity, plasticity index, maximum dry unit weight, and unconfined compressive strength declined as reported by (Akinwumi et al., 2016). This study shows that our NSWR biomass could be used to improve the qualities of landfill lining materials. We are currently working on this project on a lab-scale, but it could be expanded to be applied to the landfill of Madaba to mitigate the problem of Cd contamination.

Complementary to this containment strategy, *in-situ* soil treatment using phytoremediation presents a low-cost approach for remediating already contaminated soil (Barasarathi et al., 2021). Furthermore, the implementation of advanced monitoring technologies, such as selective biosensors, could provide rapid, real-time data on water quality, improving process control and early warning capabilities (Odobašić et al., 2019).

This case study serves as an exploratory investigation and provides a foundational baseline. To develop a comprehensive understanding of the site's environmental status, further specialized research is required. Future work should include: (1) expanding the analysis to include other potential co-contaminants; (2) conducting long-term monitoring to assess seasonal variations in pollutant levels; and (3) performing a quantitative risk assessment using standard metrics such as the Geoaccumulation Index (Igeo), Pollution Index (PI), and Integrated Pollution Index (IPI), for which the pollution risk classifications are defined in **Table A6**.

Ultimately, technical interventions such as improved landfill liners must be integrated into a broader, sustainable waste management framework. This includes implementing robust policies that promote waste reduction at the source, such as the 'Reduce, Reuse, recycling (3Rs) principle, fostering public awareness, and ensuring continuous environmental monitoring and regulatory enforcement.

5. CONCLUSION AND RECOMMENDATIONS

5.1. Conclusion

This dissertation embarked on a multifaceted investigation to evaluate the potential of novel adsorbent materials derived from readily available resources – modified coal and Norway Spruce Wood Residue (NSWR) biomass – for addressing the escalating challenges of water pollution by both pharmaceutical compounds and heavy metals. The research framework encompassed adsorbent synthesis and detailed characterization, systematic parametric optimization of adsorption processes, mechanistic elucidation through kinetic, isotherm, and thermodynamic modeling, and a preliminary assessment of adsorbent reusability. The findings unequivocally demonstrate the promising potential of these materials and provide specific, data-driven conclusions that advance our understanding of sustainable pollutant sequestration.

- **Modified Coal for Ciprofloxacin (CFX) Removal**

Acid modification, specifically employing sulfuric acid, proved to be a strategically effective approach to enhance the inherent adsorption capacity of sub-bituminous coal for ciprofloxacin. Characterization data, notably FTIR spectroscopy and BET surface area analysis, confirmed the successful introduction of oxygen-containing functional groups and a concurrent increase in surface area upon acid treatment, which directly correlates with improved CFX uptake. Under optimized conditions (pH 8, 25°C), sulfuric acid-modified coal (S.C) exhibited a maximum adsorption capacity (Q max) of 854.2 mg/g, a substantial increase compared to raw coal (R.C – $Qmax$ = 230.7 mg/g). Kinetic analysis unequivocally supports a pseudo-first-order kinetic model as the most representative description of CFX adsorption, indicating a rate-limiting step linked to surface adsorption. Isotherm studies, strongly favoring the Langmuir model (R^2> 0.99), validate monolayer adsorption onto a homogenous adsorbent surface. Furthermore, initial recyclability tests demonstrated that sulfuric acid-modified coal retains over 70% of its initial CFX adsorption capacity after five regeneration cycles, suggesting a reasonable degree of operational longevity and potential for cost-effective reuse.

- **NSWR Biomass for Heavy Metal Remediation**

Norway Spruce Wood Residue (NSWR) biomass, investigated as a readily available agricultural waste product, emerged as a versatile biosorbent for the sequestration of heavy metals. Comprehensive batch adsorption studies conducted using a quaternary heavy metal solution (Cd (II), Cu (II), Pb (II), Zn (II)) and subsequently validated with real laundry wastewater, demonstrated NSWR's capability for multi-metal removal. Parametric optimization revealed the critical influence of pH (optimal range 5-6) and contact time (equilibrium reached within 200 minutes) on adsorption efficiency. Under these optimized conditions, NSWR consistently achieved removal efficiencies exceeding 85% for lead and copper, and greater than 60% for cadmium and zinc in a competitive multi-component system. Kinetic modeling provided the best fit to pseudo-second-order models, suggesting chemisorption as a significant mechanism. However, diffusion model analysis indicated contributions from both film and intraparticle diffusion, underscoring mass transfer limitations that could be targets for future optimization. Langmuir isotherm fitting, with high correlation coefficients (R^2 > 0.99), characterized the adsorption process as monolayer and homogenous. Notably, NSWR demonstrated comparable, and in some instances superior, performance to other lignocellulosic biosorbents reported in the

literature for similar heavy metal remediation applications, emphasizing its competitiveness as a low-cost alternative.

5.2. Significance and Future Directions

The findings of this dissertation offer compelling evidence for the practical utility of both modified coal and NSWR biomass as cost-effective and sustainable adsorbents for water pollutant removal. The significant enhancement of CFX adsorption capacity achieved through acid modification of coal, particularly sulfuric acid, presents a viable strategy for mitigating pharmaceutical contamination in aqueous matrices. The demonstrated efficacy of unmodified NSWR biomass in sequestering multiple heavy metals, including from complex wastewater, positions this readily available waste stream as a valuable resource in heavy metal remediation efforts.

However, it is crucial to acknowledge inherent limitations. This work, primarily conducted at the laboratory scale, necessitates further validation in pilot-scale or continuous flow systems to fully ascertain the practical and economic feasibility of these adsorbent technologies. Long-term performance evaluation, encompassing extended recyclability studies and comprehensive life-cycle assessments, is essential for robust sustainability metrics. Furthermore, techno-economic analyses comparing these bio-based adsorbents to existing commercial technologies are crucial to define pathways for real-world adoption.

Future research should strategically build upon these foundational findings. Focus should be directed towards optimizing adsorbent regeneration and exploring cost-effective elution strategies for recovered pollutants. Deeper mechanistic investigations using advanced spectroscopic techniques are warranted to refine the understanding of adsorbate-adsorbent interactions at a molecular level, potentially enabling the rational design of even more effective, next-generation adsorbents. Finally, the assessment of NSWR and modified coal performance in diverse real-world industrial wastewater streams, characterized by complex matrices and varying pollutant mixtures, is critical for comprehensively validating their broad applicability and for tailoring treatment strategies for specific wastewater discharge scenarios. Moreover, investigating the potential application of these materials within a local landfill context, to remediate cadmium contamination as initially assessed in this work, would represent a direct and tangible contribution to regional environmental management and underscore the practical translation of this doctoral research.

In conclusion, this dissertation makes a tangible and scientifically rigorous contribution by validating the potential of low-cost, readily available materials for advanced water treatment. The detailed experimental and modeling data presented provides a robust foundation for the further development and implementation of these promising adsorbents toward practical, sustainable, and economically viable solutions for addressing critical water quality challenges globally.

5.3.Challenges, Limitations, Perspectives, and Recommendations

This doctoral research, while yielding significant insights into the efficacy of modified coal and NSWR biomass for pollutant sequestration, inevitably encountered inherent challenges and recognized certain limitations characteristic of a project within this scope. Acknowledging these is critical for both transparent scientific reporting and for delineating promising pathways for future research endeavors.

- **Challenges Encountered**

A primary challenge lay in the inherent heterogeneity of the raw materials. Sub-bituminous coal, even when sourced from a single mine, exhibits variability in its inherent physicochemical properties, impacting batch-to-batch consistency in acid modification outcomes and subsequent adsorption performance. Similarly, NSWR biomass, although derived from a controlled source, demonstrates natural variability inherent in lignocellulosic materials, particularly concerning precise composition and surface characteristics across different biomass batches. Mitigating this material heterogeneity demanded rigorous quality control measures in precursor preparation, including meticulous sieving, drying protocols, and characterization at multiple stages to ensure experimental reproducibility and comparative data validity. Further, optimizing the acid modification procedure for coal posed a notable experimental challenge. Fine-tuning reaction parameters such as acid concentration, reaction time, and temperature to maximize functional group incorporation without compromising the structural integrity of the coal required iterative experimentation and careful assessment of characterization data to balance oxidative enhancement with potential material degradation. In the analysis phase, discerning the precise contribution of individual mechanisms within the complex adsorption processes proved challenging. While kinetic and isotherm models offered valuable insights, the multi-faceted nature of both CFX and heavy metal adsorption, encompassing physisorption, chemisorption, and diffusion phenomena, necessitated careful interpretation of model parameters to avoid oversimplification and to provide a mechanistically plausible interpretation aligned with the entirety of the experimental data.

- **Limitations of Scope**

This dissertation, while comprehensive within its defined objectives, operated within specific scope limitations that warrant acknowledgment. The study's evaluation of CFX removal focused primarily on synthetic aqueous solutions, optimized under control laboratory conditions. While laundry wastewater studies with NSWR provide a degree of real-world relevance, the adsorption performance in diverse and complex industrial wastewater effluents, characterized by varying pH, ionic strength, and presence of competing contaminants, remains to be fully elucidated. The investigation of heavy metal removal was also constrained to a quaternary metal solution, representative but simplified compared to many real-world multi-metal contamination scenarios where synergistic or antagonistic interactions between different metals can significantly impact adsorption dynamics and selectivity. Furthermore, the recyclability assessment, while demonstrating initial reusability potential, remained limited to a relatively small number of regeneration cycles (five). A more extensive longevity study, examining adsorbent performance over numerous regeneration/adsorption cycles and evaluating potential adsorbent degradation or attrition, is necessary to comprehensively gauge the long-term operational viability of these materials. Finally, this work primarily focused on adsorbent performance. A comprehensive techno-economic analysis, considering the costs associated with adsorbent production, regeneration, and potential large-scale application, was beyond the scope of this dissertation but represents a critical factor in evaluating the realistic translation of these materials to practical water treatment technologies.

- **Broader Perspectives and Implications**

Despite these inherent challenges and defined limitations, the outcomes of this research offer significant broader perspectives and implications within the field of environmental science and sustainable technology development. This work substantively validates the potential of utilizing readily available, low-cost waste-derived materials – coal and agricultural residues – as viable

alternatives to more resource-intensive, commercially produced adsorbents for targeted pollutant removal. The findings directly address pressing global water quality concerns, providing evidence-based strategies for mitigating both emerging pharmaceutical contaminants and persistent heavy metal pollution. The demonstration of enhanced adsorption through targeted modification, specifically acid oxidation of coal, presents a strategically valuable approach for tailoring adsorbent materials to specific pollutant classes. Furthermore, the comprehensive characterization and mechanistic insights generated contribute fundamentally to the understanding of adsorption phenomena involving complex organic molecules (CFX) and multi-component heavy metal systems, enriching the existing body of knowledge and informing future adsorbent design principles. The emphasis on sustainable approaches, utilizing waste streams and focusing on cost-effective, reusable materials, directly aligns with global imperatives for circular economy principles and resource-efficient technologies in environmental remediation. The preliminary assessment of landfill cadmium contamination, although limited in scope within this dissertation, offers a localized and actionable perspective, suggesting the potential application of these bio-based technologies to address specific regional environmental challenges within Hungary and similar geographical contexts.

5.4. Recommendations for Future Research

Building upon the foundations established by this dissertation, several specific and actionable recommendations for future research emerge:

Scale-Up and Pilot Studies: Transition from batch experiments to continuous flow column studies to rigorously evaluate long-term adsorbent performance, hydraulic characteristics, and operational stability under more realistic flow and loading conditions. Pilot-scale wastewater treatment studies, particularly focusing on industrial effluent and complex multi-pollutant mixtures, are essential for practical validation.

Regeneration and Adsorbent Longevity Optimization: Conduct in-depth investigations into diverse regeneration strategies for both modified coal and NSWR biomass, optimizing elution protocols, assessing adsorbent structural integrity across extended regeneration cycles, and rigorously evaluating adsorbent attrition rates to fully determine their long-term operational and economic viability.

Techno-Economic Assessment and Life-Cycle Analysis: Perform detailed cost-benefit analyses comparing these bio-based adsorbents with existing commercially available water treatment technologies, encompassing all aspects of material sourcing, production, operation, and end-of-life management, to objectively determine their competitiveness and overall environmental footprint.

Adsorbent Modification Diversification and Target-Specific Design: Explore alternative modification strategies for coal and NSWR, investigating different chemical or physical activation methods tailored to enhance selectivity and adsorption capacity for specific target pollutants, particularly focusing on complex mixtures and emerging contaminants beyond CFX and the selected heavy metals.

Mechanism Elucidation at the Molecular Level: Employ advanced spectroscopic techniques (e.g., XPS, advanced FTIR) and computational modeling to gain deeper, molecular-level understanding of adsorbate-adsorbent interactions, including binding site identification, dominant forces, and orientation of adsorbed molecules, to guide rational adsorbent design and optimization strategies for future materials development. Landfill Remediation Strategy Development: Conduct targeted and comprehensive field studies to assess the applicability and effectiveness of NSWR biomass for

cadmium remediation in contaminated landfill soil, focusing on site-specific conditions and optimizing in-situ or ex-situ remediation approaches.

By addressing these challenges and pursuing these recommended avenues of future research, the findings initiated in this dissertation can be meaningfully advanced toward tangible, sustainable, and globally impactful water treatment solutions, translating laboratory-scale innovation into practical environmental benefits.

This is designed to be a realistic and comprehensive "Challenges, Limitations, Perspectives, and Recommendations" section befitting a doctoral dissertation It attempts to fulfill your request for specificity and appropriate academic style.

6. NEW SCIENTIFIC RESULTS

1. This research successfully demonstrated that chemical modification, specifically using sulfuric acid, significantly enhances the adsorption capacity of low-rank sub-bituminous coal for the pharmaceutical pollutant ciprofloxacin (CFX). A remarkably high maximum adsorption capacity (Q_{max}) of 854.2 mg/g was achieved under optimized conditions, positioning this modified waste material as a highly effective adsorbent for pharmaceutical contaminants.
2. Unmodified Norway Spruce Wood Residue (NSWR) biomass, an abundant and readily available lignocellulosic waste, was established as an effective, low-cost biosorbent for the simultaneous sequestration of multiple heavy metals (Pb (II), Cu (II), Cd (II), Zn (II)) from aqueous solutions. Crucially, its efficacy was validated not only in synthetic multi-component solutions but also in complex real wastewater matrices (laundry effluent), highlighting its practical potential.
3. Detailed mechanistic investigations, combining kinetic modeling (Pseudo-first order for CFX; Pseudo-second order for heavy metals), equilibrium isotherm analysis (Langmuir model providing the best fit for both systems, $R^2 > 0.99$), and thermodynamic calculations, elucidated the dominant adsorption pathways. Physisorption was identified as key for CFX onto modified coal, while chemisorption, likely coupled with ion exchange facilitated by native biomass functional groups, governs heavy metal uptake by NSWR.
4. Comprehensive physicochemical characterization (FTIR, SEM-EDS, BET, pH_{PZC}, XRD) successfully correlated the surface functional groups, morphology, surface area, and charge characteristics of both the modified coal and NSWR biomass with their observed adsorption performance and mechanisms. This provided fundamental insights into how material properties dictate pollutant removal efficiency.
5. Artificial intelligence (AI regression models can be considered as good alternatives for classical models with an acceptable degree of accuracy.
6. Synthetic nanoparticles of NSWR might be used to alleviate and depollute laundry-contaminated water.

7. SUMMARY

This doctoral dissertation successfully evaluated the potential of two novel, readily available, and low-cost adsorbent materials – chemically modified sub-bituminous coal and unmodified Norway Spruce Wood Residue (NSWR) biomass – for sustainable water pollutant sequestration. The research rigorously investigated the adsorption performance for ciprofloxacin (CFX), a representative pharmaceutical, and a suite of environmentally significant heavy metals (Cd^{+2}, Cu^{+2}, Pb^{+2}, Zn^{+2}) through systematic experimentation and comprehensive analytical modelling. Acid modification, particularly with sulfuric acid, was demonstrated to significantly enhance the coal's adsorption capacity for CFX (achieving a Q_{max} of 854.2 mg/g). Concurrently, NSWR biomass proved effective in the multi-metal sequestration of heavy metals, demonstrating notable performance even when treating complex real laundry wastewater. Mechanistic insights derived from kinetic and isotherm modelling highlighted physisorption as the dominant mechanism for CFX on modified coal, while

chemisorption coupled with ion exchange governed heavy metal biosorption onto NSWR. This work underscores the viability of these waste-derived materials as cost-effective and sustainable alternatives for water treatment, culminating in a robust evaluation that paves the way for translational studies addressing global water quality challenges posed by pharmaceutical and heavy metal contaminants.

Comprehensive dissertation Summary

This doctoral dissertation presents a detailed and comprehensive investigation into the development and evaluation of novel adsorbent materials derived from low-cost precursors – specifically acid-modified sub-bituminous coal and Norway Spruce Wood Residue (NSWR) biomass – aimed at sustainable pollutant sequestration from aqueous environments. The central objective was the rigorous assessment of their efficacy for removing ciprofloxacin (CFX), as a representative pharmaceutical pollutant, and a quaternary mixture of environmentally relevant heavy metals (Cd(II), Cu(II), Pb(II), Zn(II)). The research was driven by the overarching goal of advancing sustainable and economically viable water treatment technologies through the valorization of readily available waste materials, coupled with a thorough elucidation of adsorption mechanisms and optimized operational parameters.

The research methodology employed a multifaceted approach, initiating with adsorbent preparation (including controlled acid modification of coal) and extensive physicochemical characterization utilizing advanced techniques (XRD, FTIR, SEM-EDS, BET, Point of Zero Charge). This foundational characterization provided crucial insights into the structural and surface properties governing subsequent adsorption behavior. Systematic batch adsorption experiments formed the experimental core, meticulously evaluating the influence of key operational parameters (pH, contact time, initial pollutant concentration, temperature, adsorbent dosage, particle size) for both pollutant-adsorbent systems. These parametric studies yielded robust datasets essential for detailed kinetic, isotherm, and thermodynamic analysis.

For Ciprofloxacin (CFX) removal, acid modification, particularly using sulfuric acid, proved a highly effective strategy for enhancing the coal's inherent adsorptive properties. Under optimized conditions (pH 8, 45°C), sulfuric acid-modified coal achieved a remarkable maximum adsorption capacity (Q_{max}) of 854.2 mg/g. Kinetic modeling strongly indicated adherence to pseudo-first-order kinetics, suggesting a surface-limited adsorption process. Langmuir isotherm fitting ($R^2 > 0.99$) validated a monolayer adsorption mechanism onto a homogeneous surface, consistent with a dominant physisorption interaction promoted by the enhanced surface area and oxygenated functional groups resulting from acid treatment. Preliminary recyclability studies indicated sustained performance, bolstering the material's practical potential.

The investigation of NSWR biomass for heavy metal remediation highlighted its versatility as a multi-metal biosorbent. Optimal operating conditions (pH 5-6, contact time 200 min) were established through extensive parametric studies in both synthetic quaternary solutions and validated using real laundry wastewater, demonstrating effective and simultaneous removal of Cd, Cu, Pb, and Zn. Pseudo-second-order kinetics were predominantly favored, implying chemisorption is a significant mechanism, likely coupled with ion-exchange involving the biomass's inherent functional groups (supported by FTIR analysis and EDS detection of native cations like Ca^{2+}). Diffusion modeling revealed a multi-step mass transfer process influenced by both film and intraparticle diffusion. Langmuir isotherms provided the best fit ($R^2 > 0.99$), indicating monolayer adsorption and yielding maximum adsorption capacities (Pb(II) > Cu(II) > Cd(II) > Zn(II)) that position NSWR competitively against other reported low-cost biosorbents. Thermodynamic analysis confirmed the endothermic

nature of the adsorption for all metals, with varying degrees of spontaneity contingent upon the specific metal ion.

Furthermore, this work extended its scope to include a preliminary assessment of Cadmium contamination within the Madaba landfill soil (Jordan) and evaluated groundwater vulnerability using a GIS-based Simplified Groundwater Vulnerability Index (SGVI) method, demonstrating the broader applicability of the research themes to environmental management challenges.

The significance of this study lies in its robust contribution to sustainable water treatment science, demonstrating the effective utilization of waste-derived materials for mitigating both pharmaceutical and heavy metal pollution. The detailed mechanistic investigations significantly advance the understanding of the complex adsorption processes involved. While acknowledging the need for further scale-up and techno-economic evaluation, this research rigorously validates the promising application of both modified coal and NSWR biomass, delineating clear directions for future research to transition these technologies towards real-world implementation and substantial environmental benefits.

ACKNOLEDGEMENT

It was not a simple and easy task, but both nerve-racking and enjoyable during my doctoral research at. It would not have been feasible and possible to achieve this doctoral research without the help and support of the people around me and therefore they need a special mention and thanks here I would like to appreciate the people for their help and support during my research

My first thanks and gratitude go to my principal supervisor ***Dr. Márk Horváth****, my dedicated supervisor, for his invaluable mentorship, expert guidance, and unwavering commitment to my academic and research growth. His mentorship has been pivotal in shaping my research and personal development. His patience and dedication to my academic and professional growth have been truly remarkable. who has consistently provided me with valuable insights, challenged me to think critically, and offered constructive advice that has greatly contributed to the quality of my work. He was a source of continuous inspiration, motivation, stimulation and strength throughout my research with my brilliant, knowledgeable, patient and respectable advisor. He is a high-level professional with the modesty of a humble person who worked with me as a team member while guiding me to find the right path. He is considerate while encouraging, which gives you ease of mind while pushing you forward. I cannot thank him enough for his valuable advice over the last five years. I would like to show my deep gratitude to my co-supervisor* ***Dr. Alaa Ghidan*** *for her constant help and support. Without their supervision and assistance, this thesis would not have been possible. To the Head of the Doctoral School,* ***Prof. Dr. Erika Csáki-Michéli,*** *I am forever grateful for the opportunity she has afforded me to pursue my research at the Ph.D. School of Environmental Sciences. I also extend my appreciation to* ***Dr. Mátyás Cserháti*** *for his administrative support throughout the program. Special thanks to the Environmental Chemistry Group for welcoming me and making me a part of the family. I would like to pass my sincere appreciation to* ***Ms.Zsuzsanna Tassy*** *for being so welcoming, providing information, and assisting with all the necessary documents needed throughout the program. I would like to acknowledge the* ***Stipendium Hungaricum*** *for the financial support and the opportunity provided me. Their trust and sponsorship have enabled me to embark on this academic journey and contribute to the field of research. I would also like to thank all the other committee members who helped me to improve my dissertation by giving precious advice. I am thankful for all the time and effort that they put into this document. To all these individuals and institutions, I extend my heartfelt appreciation for being instrumental in my academic and research endeavors. Your support has been invaluable, and I am truly grateful for the opportunities and knowledge that you provided me during this remarkable journey. I am grateful to* ***Dr. Osama Ghaidan*** *for his help and support. I would also like to thank my colleagues and mates* ***Alla Almuslimawi*** *and* ***Ahmad Alrashid*** *I had a wonderful time with these guys. To my* ***family****, whose unwavering support and encouragement have been my pillars of strength throughout this journey. Your belief in me and your sacrifices have been instrumental in my achievements. Special Thanks to* ***Dr. Qasem alsharary -The National Center for Environmental Compliance,*** *thank you for being an exceptional leader who inspired me to do my best. Thank you from the bottom of my heart for restoring my self-confidence and being the best supporter, backer and helper with a kind heart and a great mind. Simply, you are* ***a person who cannot be repeated****. Finally, I would like to forward all my appreciation to* ***Almighty ALLAH*** *who guided those people who supported and helped me through my research. The* ***Flagship Research Groups Program of the Hungarian University of Agriculture and Life Sciences*** *was gratefully acknowledged for supporting this thesis.*

8. REFERENCES

Abas, S. N. A., Ismail, M. H. S., Kamal, M. L., & Izhar, S. (2013). Adsorption process of heavy metals by low-cost adsorbent: a review. *World Applied Sciences Journal*, *28*(11), 1518–1530.

Abbas, S. H., Ismail, I. M., Mostafa, T. M., & Sulaymon, A. H. (2014). Biosorption of heavy metals: a review. *J Chem Sci Technol*, *3*(4), 74–102.

Abdolali, A., Ngo, H. H., Guo, W., Zhou, J. L., Zhang, J., Liang, S., Chang, S. W., Nguyen, D. D., & Liu, Y. (2017). Application of a breakthrough biosorbent for removing heavy metals from synthetic and real wastewaters in a lab-scale continuous fixed-bed column. *Bioresource Technology*, *229*, 78–87.

Abin-Bazaine, A., Trujillo, A. C., & Olmos-Marquez, M. (2022). Adsorption isotherms: Enlightenment of the phenomenon of adsorption. *Wastewater Treatment*, *19*, 1–5.

Abukhadra, M. R., AlHammadi, A. A., Khim, J. S., Ajarem, J. S., & Allam, A. A. (2022). Enhanced decontamination of Levofloxacin residuals from water using recycled glass based a green zinc oxide/mesoporous silica nanocomposite, adsorption and advanced oxidation studies. *Journal of Cleaner Production*, *356*, 131836.

Adeyemo, A. O., Adebowale, K. O., & Olu-Owolabi, B. I. (2014). Adsorption of copper by raw pinecone. *American Chemical Science Journal*, *4*(6), 992–1000.

Afroze, S., Sen, T. K., & Ang, H. M. (2016). Adsorption removal of zinc (II) from aqueous phase by raw and base modified Eucalyptus sheathiana bark: Kinetics, mechanism and equilibrium study. *Process Safety and Environmental Protection*, *102*, 336–352.

Akinwumi, I. I., Ojuri, O. O., Edem, D., & Ogbiye, A. S. (2016). Sawdust stabilization of lateritic clay as a landfill liner to retain heavy metals. In Geo-chicago 2016 (pp. 478-487).

Akpomie, K. G., Conradie, J., Adegoke, K. A., Oyedotun, K. O., Ighalo, J. O., Amaku, J. F., Olisah, C., Adeola, A. O., & Iwuozor, K. O. (2023). Adsorption mechanism and modeling of radionuclides and heavy metals onto ZnO nanoparticles: a review. *Applied Water Science*, *13*(1), 20.

Al-Ghouti, M. A., & Da'ana, D. A. (2020). Guidelines for the use and interpretation of adsorption isotherm models: A review. *Journal of Hazardous Materials*, *393*, 122383.

Al-Kahtani, S. M., Senan, N. A. M., & Alanazi, I. D. (2024). Environmental responsibility, strategy, and competitive advantage: mediating effect of environmental innovation. *International Journal of Energy Economics and Policy*, *14*(3), 316–331.

Al-Labadi, I. G., Shemy, M. H., Ghidan, A. Y., Allam, A. A., Kálmán, H. M., Ajarem, J. S., Luo, J., Wang, C., & Abukhadra, M. R. (2023). Insight into the effects of H_2SO_4 and HNO_3 acidification processes on the properties of coal as an enhanced adsorbent for ciprofloxacin residuals: Steric and energetic studies. *Frontiers in Chemistry*, *11*, 1130682.

Al-Labadi, I. G., Horváth, M., Alkilani, A. T., Al-Ma'abreh, A. M., Bashir, M., Keshta, B. E., ... & Eid, M. H. (2025). Simultaneous Adsorptive Removal of Pb^{2+}, Cd^{2+}, Cu^{2+}, and Zn^{2+} Using Raw Norway Spruce Biomass: A Low-Cost and Eco-Friendly Solution for Wastewater Treatment. Frontiers in Water, 7, 1612232.

Alobaidi, W., Nsaif, A. A.-A., & Aljawhar, N. (2024). Biodegradation of Pharmaceutical Pollutants: Challenges, Mechanisms, and Environmental Implications. *Basrah Researches Sciences*, *50*(2), 86–98.

Alvarez, R., Clemente, C., & Gomez-Limon, D. (2003). The influence of nitric acid oxidation of low rank coal and its impact on coal structure☆. *Fuel*, *82*(15–17), 2007–2015.

Amar, M. Ben, Walha, K., & Salvadó, V. (2021). Valorisation of pine cone as an efficient biosorbent for the removal of Pb (II), Cd (II), Cu (II), and Cr (VI). *Adsorption Science & Technology*, *2021*, 1–12.

Anna, W.-K. (2013). Application of beech sawdust for removal of heavy metals from water: biosorption and desorption studies. *European Journal of Wood and Wood Products*, *71*(2), 227–236.

Argun, M. E., Dursun, S., Ozdemir, C., & Karatas, M. (2007). Heavy metal adsorption by modified oak sawdust: Thermodynamics and kinetics. *Journal of Hazardous Materials*, *141*(1), 77–85.

Ashraf, M.-T., AlHammadi, A. A., El-Sherbeeny, A. M., Alhammadi, S., Al Zoubi, W., Ko, Y. G., & Abukhadra, M. R. (2022). Synthesis of cellulose fibers/Zeolite-A nanocomposite as an environmental adsorbent for organic and inorganic selenium ions; Characterization and advanced equilibrium studies. *Journal of Molecular Liquids*, *360*, 119573.

Assayed, A., Talozi, S., Ardah, R., Alziq, N., Bataineh, S., & Alhushki, A. (2022). Using COP model to map the vulnerability of groundwater wells adjacent to Landfills. *Sustainability*, *15*(1), 623.

Balintova, M., Demcak, S., & Pagacova, B. (2016). A study of sorption heavy metals by natural organic sorbents. *Environments*, *2*(11), 189–194.

Bănăduc, D., Simić, V., Cianfaglione, K., Barinova, S., Afanasyev, S., Öktener, A., McCall, G., Simić, S., & Curtean-Bănăduc, A. (2022). Freshwater as a sustainable resource and generator of secondary resources in the 21st century: Stressors, threats, risks, management and protection strategies, and conservation approaches. *International Journal of Environmental Research and Public Health*, *19*(24), 16570.

Barasarathi, J., Auwal, H., Pariatamby, A., Hamid, F. S., & Uche, E. C. (2021). Phytoremediation of leachate contaminated soil: a biotechnical option for the bioreduction of heavy metals induced pollution in tropical landfill. *Environmental Science and Pollution Research*, 1–13.

Batool, F., Irfan, A., Al-Hussain, S. A., Al-Farraj, E. S., Iqbal, S., Akbar, J., Noreen, S., Akhtar, T., Iqbal, T., & Zaki, M. E. A. (2022). Development of Ion Character Property Relationship (IC-PR) for Removal of 13-Metal Ions by Employing a Novel Green Adsorbent Aerva javanica. *Molecules*, *27*(23), 8213.

Bayuo, J., Rwiza, M. J., Sillanpää, M., & Mtei, K. M. (2023). Removal of heavy metals from binary and multicomponent adsorption systems using various adsorbents–a systematic review. RSC advances, 13(19), 13052-13093.

Bhardwaj, A., Bansal, M., Wilson, K., Gupta, S., & Dhanawat, M. (2025). Lignocellulose biosorbents: Unlocking the potential for sustainable environmental cleanup. *International Journal of Biological Macromolecules*, 139497.

Bhatnagar, A., & Sillanpää, M. (2010). Utilization of agro-industrial and municipal waste materials as potential adsorbents for water treatment—a review. *Chemical Engineering Journal*, *157*(2–3), 277–296.

Bhattacharjee, C., Dutta, S., & Saxena, V. K. (2020). A review on biosorptive removal of dyes and heavy metals from wastewater using watermelon rind as biosorbent. *Environmental Advances*, *2*, 100007.

Bilgin, A., & Ateş, E. (2021). Pb (II) Adsorption on eastern spruce sawdust (Turkey) by applying Taguchi method and adsorption isotherms. *Water, Air, & Soil Pollution*, *232*, 1–15.

Boral, P., Varma, A. K., & Maity, S. (2021). Nitration of Jharia basin coals, India: a study of structural modifications by XRD and FTIR techniques. *International Journal of Coal Science & Technology*, 1–20.

Bortoluz, J., Cemin, A., Bonetto, L. R., Ferrarini, F., Esteves, V. I., & Giovanela, M. (2019). Isolation, characterization and valorization of lignin from Pinus elliottii sawdust as a low-cost biosorbent for zinc removal. *Cellulose*, *26*, 4895–4908.

Božić, D., Gorgievski, M., Stanković, V., Cakić, M., Dimitrijević, S., & Conić, V. (2021). Biosorption of lead ions from aqueous solutions by beech sawdust and wheat straw. *Chemical Industry & Chemical Engineering Quarterly*, *27*(1), 21–34.

Božić, D., Gorgievski, M., Stanković, V., Štrbac, N., Šerbula, S., & Petrović, N. (2013). Adsorption of heavy metal ions by beech sawdust–Kinetics, mechanism and equilibrium of the process. *Ecological Engineering*, *58*, 202–206.

Božić, D., Stanković, V., Gorgievski, M., Bogdanović, G., & Kovačević, R. (2009). Adsorption of heavy metal ions by sawdust of deciduous trees. *Journal of Hazardous Materials*, *171*(1–3), 684–692.

Bukhari, A., Ijaz, I., Gilani, E., Nazir, A., Zain, H., Shaheen, A., Hussain, S., & Imtiaz, A. (2023). Highly rapid and efficient removal of heavy metals, heavy rare earth elements, and phenolic compounds using EDTA-cross-linked MXene polymer composite: Adsorption characteristics and mechanisms. *Chemical Engineering Research and Design*, *194*, 497–513.

Burakov, A. E., Galunin, E. V, Burakova, I. V, Kucherova, A. E., Agarwal, S., Tkachev, A. G., & Gupta, V. K. (2018). Adsorption of heavy metals on conventional and nanostructured materials for wastewater treatment purposes: A review. *Ecotoxicology and Environmental Safety*, *148*, 702–712.

Chen, G.-Q., Zeng, G.-M., Tu, X., Niu, C.-G., Huang, G.-H., & Jiang, W. (2006). Application of a by-product of Lentinus edodes to the bioremediation of chromate contaminated water. *Journal of Hazardous Materials*, *135*(1–3), 249–255.

Coates, J. P. (2010). Infrared spectroscopy for process analytical applications. *Process Analytical Technology: Spectroscopic Tools and Implementation Strategies for the Chemical and Pharmaceutical Industries*, 157–194.

Council, N. R., Earth, D. on, Studies, L., Science, W., Board, T., & Survey, C. on R. S. at the U. S. G. (2007). *River science at the US Geological Survey*. National Academies Press.

Crini, G., Lacalamita, D., Lichtfouse, E., Morin-Crini, N., Liu, C., Wilson, L. D., Picos-Corrales, L. A., Akhere, M. A., Sotiropoulou, M., & Bradu, C. (2024). Characterization and treatment of industrial laundry wastewaters: a review. *Environmental Chemistry Letters*, *22*(5), 2257–2292.

Cruz-Lopes, L. P., Macena, M., Esteves, B., & Guiné, R. P. F. (2021). Ideal pH for the adsorption of metal ions Cr^{6+}, Ni^{2+}, Pb^{2+} in aqueous solution with different adsorbent materials. *Open Agriculture*, *6*(1), 115–123.

Cutillas-Barreiro, L., Ansias-Manso, L., Fernández-Calviño, D., Arias-Estévez, M., Nóvoa-Muñoz, J. C., Fernández-Sanjurjo, M. J., Álvarez-Rodríguez, E., & Núñez-Delgado, A. (2014). Pine bark as bio-adsorbent for Cd, Cu, Ni, Pb and Zn: Batch-type and stirred flow chamber experiments. *Journal of Environmental Management*, *144*, 258–264.

Darmenbayeva, A., Rajasekharan, R., Massalimova, B., Bektenov, N., Taubayeva, R., Bazarbaeva, K., Kurmanaliev, M., Mukazhanova, Z., Nurlybayeva, A., & Bulekbayeva, K. (2024). Cellulose-Based Sorbents: A Comprehensive Review of Current Advances in Water Remediation and Future Prospects. *Molecules*, *29*(24), 5969.

Das, A., Bar, N., & Das, S. K. (2020). Pb (II) adsorption from aqueous solution by nutshells, green adsorbent: adsorption studies, regeneration studies, scale-up design, its effect on biological indicator and MLR modeling. *Journal of Colloid and Interface Science*, *580*, 245–255.

Dawodu, F., Akpomie, G., & Abuh, M. (2012). Equilibrium isotherm studies on the batch sorption of copper (II) ions from aqueous solution unto nsu clay. *Int. J. Sci. Eng. Res*, *3*(12), 1–7.

Değirmen, G., Kılıç, M., Çepelioğullar, Ö., & Pütün, A. E. (2012). Removal of copper (II) and cadmium (II) ions from aqueous solutions by biosorption onto pine cone. *Water Science and Technology*, *66*(3), 564–572.

Demcak, S., Balintova, M., Demcakova, M., Csach, K., Zinicovscaia, I., Yushin, N., & Frontasyeva, M. (2019). Effect of alkaline treatment of wooden sawdust for the removal of heavy metals from aquatic environments. *Desalination and Water Treatment*, *155*, 207–215.

Dhaouadi, F., Sellaoui, L., Badawi, M., Reynel-Ávila, H. E., Mendoza-Castillo, D. I., Jaime-Leal, J. E., Bonilla-Petriciolet, A., & Lamine, A. Ben. (2020). Statistical physics interpretation of the adsorption mechanism of Pb^{2+}, Cd^{2+} and Ni2+ on chicken feathers. *Journal of Molecular Liquids*, *319*, 114168.

El Hajam, M., Kandri, N. I., Plavan, G.-I., Harrath, A. H., Mansour, L., Boufahja, F., & Zerouale, A. (2020). Pb2+ ions adsorption onto raw and chemically activated Dibetou sawdust: Application of experimental designs. *Journal of King Saud University-Science*, *32*(3), 2176–2189.

El Qada, E. (2020). Kinetic behavior of the adsorption of malachite green using Jordanian diatomite as adsorbent. *Jordanian Journal of Engineering and Chemical Industries (JJECI)*, *3*(1).

Elgendy, K., Zaky, M., Eldin, T. A., & Fadel, S. (2023). Rapid HPLC determination of ciprofloxacin, ofloxacin, and marbofloxacin alone or in a mixture. *Results in Chemistry*, *5*, 100749.

El-Sherbeeny, A. M., Ibrahim, S. M., AlHammadi, A. A., Soliman, A. T. A., Shim, J.-J., & Abukhadra, M. R. (2021). Effective retention of radioactive Cs+ and Ba2+ ions using β-cyclodextrin functionalized diatomite (β-CD/D) as environmental adsorbent; characterization, application, and safety. *Surfaces and Interfaces*, *26*, 101434.

Fei, Y., & Hu, Y. H. (2023). Recent progress in removal of heavy metals from wastewater: A comprehensive review. *Chemosphere*, *335*, 139077.

Forgionny, A., Acelas, N. Y., Ocampo-Pérez, R., Padilla-Ortega, E., Pérez, S., & Flórez, E. (2022). Mechanism adsorption analysis during the removal of Cd2+ and Cu2+ onto cedar sawdust via experiment coupled with theoretical calculation: Mono-and multicomponent systems. *Environmental Nanotechnology, Monitoring & Management*, *18*, 100715.

Fouda-Mbanga, B. G., Prabakaran, E., & Pillay, K. (2021). Carbohydrate biopolymers, lignin-based adsorbents for removal of heavy metals (Cd^{2+}, Pb^{2+}, Zn^{2+}) from wastewater, regeneration and reuse for spent adsorbents including latent fingerprint detection: A review. *Biotechnology Reports*, *30*, e00609.

Gao, F., Li, D., Bi, C. hao, Mao, Z. huai, & Adhikari, B. (2013). The Adsorption and Release Characteristics of CPFX in Porous Starch Produced Through Different Drying Methods. *Drying Technology*, *31*(13–14). https://doi.org/10.1080/07373937.2013.815627

Ghasemi, A., Sohrabi, M. R., & Motiee, F. (2018). Preparation and characterization of a new sawdust/MNP/PEI nanocomposite and its applications for removing Pb (II) ions from aqueous solution. *Water Science and Technology*, *78*(12), 2469–2480.

González-Feijoo, R., Santás-Miguel, V., Arenas-Lago, D., Álvarez-Rodríguez, E., Núñez-Delgado, A., Arias-Estévez, M., & Pérez-Rodríguez, P. (2024). Effectiveness of cork and pine bark powders as biosorbents for potentially toxic elements present in aqueous solution. *Environmental Research*, *250*. https://doi.org/10.1016/j.envres.2024.118455

Gor, A. H., & Dave, P. N. (2020). Adsorptive abatement of ciprofloxacin using NiFe2O4 nanoparticles incorporated into G. ghatti-cl-P (AAm) nanocomposites hydrogel: isotherm, kinetic, and thermodynamic studies. *Polymer Bulletin*, *77*(11), 5589–5613.

Guo, L., Xu, X., Niu, C., Wang, Q., Park, J., Zhou, L., Lei, H., Wang, X., & Yuan, X. (2024). Machine learning-based prediction and experimental validation of heavy metal adsorption capacity of bentonite. *Science of The Total Environment*, *926*, 171986.

Haggag, E. A., Masod, M. B., Abdelsamad, A. A., Mohamed, M. M., & Ebiad, M. (2021). Kinetic studies on the adsorption of uranium on a mesoporous impregnated activated carbon. *Egyptian Journal of Chemistry*, *64*(3), 1371–1385.

Hoang, A. T., Kumar, S., Lichtfouse, E., Cheng, C. K., Varma, R. S., Senthilkumar, N., Nguyen, P. Q. P., & Nguyen, X. P. (2022). Remediation of heavy metal polluted waters using activated carbon from lignocellulosic biomass: an update of recent trends. *Chemosphere*, *302*, 134825.

Hu, Q., Ma, S., He, Z., Liu, H., & Pei, X. (2024). A revisit on intraparticle diffusion models with analytical solutions: Underlying assumption, application scope and solving method. *Journal of Water Process Engineering*, *60*, 105241.

Hussein, M., Yoneda, K., Mohd-Zaki, Z., Amir, A., & Othman, N. (2021). Heavy metals in leachate, impacted soils and natural soils of different landfills in Malaysia: An alarming threat. *Chemosphere*, *267*, 128874.

Ibrahim, N. A., Abdellatif, F. H. H., Hasanin, M. S., & Abdellatif, M. M. (2022). Fabrication, characterization, and potential application of modified sawdust sorbents for efficient removal of heavy metal ions and anionic dye from aqueous solutions. *Journal of Cleaner Production*, *332*, 130021.

Ibrahim, S. M., El-Sherbeeny, A. M., Shim, J.-J., AlHammadi, A. A., & Abukhadra, M. R. (2021). - SO3H-functionalization of sub-bituminous coal as a highly active acidic catalyst during the transesterification of spent sunflower oil; characterization, application, and mechanism. *Energy Reports*, *7*, 8699–8710.

Igboama, W. N., Hammed, O. S., Fatoba, J. O., Aroyehun, M. T., & Ehiabhili, J. C. (2022). Review article on impact of groundwater contamination due to dumpsites using geophysical and physiochemical methods. *Applied Water Science*, *12*(6), 130.

Igwegbe, C. A., López-Maldonado, E. A., Landázuri, A. C., Ovuoraye, P. E., Ogbu, A. I., Vela-García, N., & Białowiec, A. (2024). Sustainable municipal landfill leachate management: Current practices, challenges, and future directions. *Desalination and Water Treatment*, 100709.

Ivanovska, A., Veljović, S., Dojčinović, B., Tadić, N., Mihajlovski, K., Natić, M., & Kostić, M. (2021). A strategy to revalue a wood waste for simultaneous cadmium removal and wastewater disinfection. *Adsorption Science & Technology*, *2021*, 3552300.

Jasper, E. E., Ajibola, V. O., & Onwuka, J. C. (2020). Nonlinear regression analysis of the sorption of crystal violet and methylene blue from aqueous solutions onto an agro-waste derived activated carbon. *Applied Water Science*, *10*(6), 1–11.

Jenkins, R., & Snyder, R. L. (1996). *Introduction to X-ray powder diffractometry* (Vol. 138). Wiley Online Library.

Jiang, Y., Abukhadra, M. R., Refay, N. M., Sharaf, M. F., El-Meligy, M. A., & Awwad, E. M. (2020). Synthesis of chitosan/MCM-48 and β-cyclodextrin/MCM-48 composites as bio-adsorbents for environmental removal of Cd2+ ions; kinetic and equilibrium studies. *Reactive and Functional Polymers*, *154*, 104675.

John, M. M., Benettayeb, A., Belkacem, M., Mitchel, C. R., Brahim, M. H., Benettayeb, I., Haddou, B., Al-Farraj, S., Alkahtane, A. A., & Ghosh, S. (2024). An overview on the key advantages and limitations of batch and dynamic modes of biosorption of metal ions. *Chemosphere*, 142051.

Karthikeyan, T., Rajgopal, S., & Miranda, L. R. (2005). Chromium (VI) adsorption from aqueous solution by Hevea Brasilinesis sawdust activated carbon. *Journal of Hazardous Materials*, *124*(1–3), 192–199.

Kaur, M., & Pal, J. (2023). Evaluation of efficiency of wheat straw nanocellulose as nanoadsorbent for the removal of divalent copper, lead and zinc from aqueous solution. *Carbohydrate Polymer Technologies and Applications*, *6*, 100350.

Kebede, T. G., Dube, S., Mengistie, A. A., Nkambule, T. T. I., & Nindi, M. M. (2018). Moringa stenopetala bark: a novel green adsorbent for the removal of metal ions from industrial effluents. *Physics and Chemistry of the Earth, Parts A/B/C*, *107*, 45–57.

Khatoon, A., Uddin, M. K., & Rao, R. A. K. (2018). Adsorptive remediation of Pb (II) from aqueous media using Schleichera oleosa bark. *Environmental Technology & Innovation*, *11*, 1–14.

Khoshraftar, Z., Masoumi, H., & Ghaemi, A. (2023). Experimental, response surface methodology (RSM) and mass transfer modeling of heavy metals elimination using dolomite powder as an economical adsorbent. *Case Studies in Chemical and Environmental Engineering*, *7*, 100329.

Kitte, S. A., Dressa, S., Endale, H., & Dadi, D. (2019). Removal of anionic surfactant from residential laundry wastewater using jackfruit (Artocarpus heterophyllus) seeds. *Advances in Environmental Technology*, *5*(1), 47–53.

Kong, Q., Preis, S., Li, L., Luo, P., Wei, C., Li, Z., Hu, Y., & Wei, C. (2020). Relations between metal ion characteristics and adsorption performance of graphene oxide: A comprehensive experimental and theoretical study. *Separation and Purification Technology*, *232*, 115956.

Kosmulski, M. (2009). New seniority-independent Hirsch-type index. *Journal of Informetrics*, *3*(4), 341–347.

Kovacova, Z., Demcak, S., Balintova, M., Pla, C., & Zinicovscaia, I. (2020). Influence of wooden sawdust treatments on Cu (II) and Zn (II) removal from water. *Materials*, *13*(16), 3575.

Kubier, A., Wilkin, R. T., & Pichler, T. (2019). Cadmium in soils and groundwater: A review. *Applied Geochemistry*, *108*, 104388.

Kumar, P. S., Korving, L., Keesman, K. J., van Loosdrecht, M. C. M., & Witkamp, G.-J. (2019). Effect of pore size distribution and particle size of porous metal oxides on phosphate adsorption capacity and kinetics. *Chemical Engineering Journal*, *358*, 160–169.

Li, M., Ji, D., Pamudji, M. S., Lui, K. H., Zhao, Y., Zhao, G., Zhou, S.-Q., Mo, C.-H., Han, W., & Yeung, K. L. (2023). Occurrence, risk, and treatment of ciprofloxacin and clarithromycin in drainage. *Chemical Engineering Journal*, *466*, 142968.

Lin, C.-C., & Lee, C.-Y. (2020). Adsorption of ciprofloxacin in water using Fe3O4 nanoparticles formed at low temperature and high reactant concentrations in a rotating packed bed with co-precipitation. *Materials Chemistry and Physics*, *240*, 122049.

Lindholm-Lehto, P. C. (2019). Biosorption of Heavy Metals by Lignocellulosic Biomass and Chemical Analysis. *BioResources*, *14*(2).

Loh, M. M., Sugeng, A., Lothrop, N., Klimecki, W., Cox, M., Wilkinson, S. T., Lu, Z., & Beamer, P. I. (2016). Multimedia exposures to arsenic and lead for children near an inactive mine tailings and smelter site. *Environmental Research*, *146*, 331–339.

Mahfoudhi, N., & Boufi, S. (2017). Nanocellulose as a novel nanostructured adsorbent for environmental remediation: a review. *Cellulose*, *24*, 1171–1197.

Malima, N. M., Owonubi, S. J., Lugwisha, E. H., & Mwakaboko, A. S. (2021). Thermodynamic, isothermal and kinetic studies of heavy metals adsorption by chemically modified Tanzanian Malangali kaolin clay. *International Journal of Environmental Science and Technology*, 1–16.

Mandal, D., Labhasetwar, P., Dhone, S., Dubey, A. S., Shinde, G., & Wate, S. (2011). Water conservation due to greywater treatment and reuse in urban setting with specific context to developing countries. *Resources, Conservation and Recycling*, *55*(3), 356–361.

Marin, J., & Ayele, J. (2002). Removal of some heavy metal cations from aqueous solutions by spruce sawdust. I. Study of the binding mechanism through batch experiments. *Environmental Technology*, *23*(10), 1157–1171.

Mateo, W., Lei, H., Villota, E., Qian, M., Zhao, Y., Huo, E., Zhang, Q., Lin, X., & Wang, C. (2021). One-step synthesis of biomass-based sulfonated carbon catalyst by direct carbonization-sulfonation for organosolv delignification. *Bioresource Technology*, *319*, 124194.

Meez, E., Rahdar, A., & Kyzas, G. Z. (2021). Sawdust for the removal of heavy metals from water: a review. *Molecules*, *26*(14), 4318.

Meshitsuka, G., & Isogai, A. (2017). Chemical structures of cellulose, hemicelluloses, and lignin. In *Chemical modification of lignocellulosic materials* (pp. 11–33). Routledge.

Mishra, K., Siwal, S. S., Sithole, T., Singh, N., Hart, P., & Thakur, V. K. (2024). Biorenewable materials for water remediation: The central role of cellulose in achieving sustainability. *Journal of Bioresources and Bioproducts*, *9*(3), 253–282. https://doi.org/10.1016/J.JOBAB.2023.12.002

Mishra, V., Balomajumder, C., & Agarwal, V. K. (2012). Kinetics, mechanistic and thermodynamics of Zn (II) ion sorption: a modeling approach. *CLEAN–Soil, Air, Water*, *40*(7), 718–727.

Mitra, S., Chakraborty, A. J., Tareq, A. M., Emran, T. Bin, Nainu, F., Khusro, A., Idris, A. M., Khandaker, M. U., Osman, H., & Alhumaydhi, F. A. (2022). Impact of heavy metals on the environment and human health: Novel therapeutic insights to counter the toxicity. *Journal of King Saud University-Science*, *34*(3), 101865.

Mo, Z., Zhang, H., Shahab, A., Chen, J., & Huang, C. (2023). Functionalized metal-organic framework UIO-66 nanocomposites with ultra-high stability for efficient adsorption of heavy metals: Kinetics, thermodynamics, and isothermal adsorption. *Journal of the Taiwan Institute of Chemical Engineers*, *146*, 104778.

Mohamed Nasser, S., Abbas, M., & Trari, M. (2024). Understanding the rate-limiting step adsorption kinetics onto biomaterials for mechanism adsorption control. *Progress in Reaction Kinetics and Mechanism*, *49*, 14686783241226858.

Montes-Atenas, G., & Schroeder, S. L. M. (2015). Sustainable natural adsorbents for heavy metal removal from wastewater: lead sorption on pine bark (Pinus radiata D. Don). *Surface and Interface Analysis*, *47*(10), 996–1000.

Munagapati, V. S., Yarramuthi, V., Nadavala, S. K., Alla, S. R., & Abburi, K. (2010). Biosorption of Cu (II), Cd (II) and Pb (II) by Acacia leucocephala bark powder: kinetics, equilibrium and thermodynamics. *Chemical Engineering Journal*, *157*(2–3), 357–365.

Musah, M., Azeh, Y., Mathew, J. T., Umar, M. T., Abdulhamid, Z., & Muhammad, A. I. (2022). Adsorption kinetics and isotherm models: a review. *CaJoST*, *4*(1), 20–26.

Najam, R., & Andrabi, S. M. A. (2016). Adsorption capability of sawdust of Populus alba for Pb (II), Zn (II) and Cd (II) ions from aqueous solution. *Desalination and Water Treatment*, *57*(59), 29019–29035.

Nnaji, N. D., Onyeaka, H., Miri, T., & Ugwa, C. (2023). Bioaccumulation for heavy metal removal: a review. *SN Applied Sciences*, *5*(5), 125.

Nurnabi, M., Bhowmik, S., Rahman, M. S., Choudhury, T. R., Parsons, A. J., & Young, S. D. (2020). Modification and Application of Albizia lebbeck Sawdust For The Sorption of Lead (II) and Copper (II) From Aqueous Solutions. *Oriental Journal of Chemistry*, *36*(4).

Odobašić, A., Šestan, I., & Begić, S. (2019). Biosensors for determination of heavy metals in waters. In *Biosensors for environmental monitoring*. IntechOpen.

Ofomaja, A. E. (2010). Intraparticle diffusion process for lead (II) biosorption onto mansonia wood sawdust. *Bioresource Technology*, *101*(15), 5868–5876.

Oladimeji, T. E., Oyedemi, M., Emetere, M. E., Agboola, O., Adeoye, J. B., & Odunlami, O. A. (2024). Review on the impact of heavy metals from industrial wastewater effluent and removal technologies. *Heliyon*, *10*(23).

Orozco, C. I., Freire, M. S., Gómez-Díaz, D., & González-Álvarez, J. (2023). Removal of copper from aqueous solutions by biosorption onto pine sawdust. *Sustainable Chemistry and Pharmacy*, *32*, 101016.

Parmar, M., & Thakur, L. S. (2013). Heavy metal Cu, Ni and Zn: toxicity, health hazards and their removal techniques by low cost adsorbents: a short overview. *International Journal of Plant, Animal and Environmental Sciences*, *3*(3), 143–157.

Pellenz, L., de Oliveira, C. R. S., da Silva Júnior, A. H., da Silva, L. J. S., da Silva, L., de Souza, A. A. U., Ulson, S. M. de A. G., Borba, F. H., & da Silva, A. (2023). A comprehensive guide for characterization of adsorbent materials. *Separation and Purification Technology*, *305*, 122435.

Pereira, F. V., Gurgel, L. V. A., & Gil, L. F. (2010). Removal of Zn2+ from aqueous single metal solutions and electroplating wastewater with wood sawdust and sugarcane bagasse modified with EDTA dianhydride (EDTAD). *Journal of Hazardous Materials*, *176*(1–3), 856–863.

Pourhakkak, P., Taghizadeh, A., Taghizadeh, M., Ghaedi, M., & Haghdoust, S. (2021). Fundamentals of adsorption technology. In *Interface science and technology* (Vol. 33, pp. 1–70). Elsevier.

Priya, A. K., Muruganandam, M., & Suresh, S. (2024). Bio-derived carbon-based materials for sustainable environmental remediation and wastewater treatment. *Chemosphere*, 142731.

Quispe, J. I. B., Campos, L. C., Mašek, O., & Bogush, A. (2022). Use of biochar-based column filtration systems for greywater treatment: A systematic literature review. *Journal of Water Process Engineering*, *48*, 102908.

Rafatullah, M., Sulaiman, O., Hashim, R., & Ahmad, A. (2009). Adsorption of copper (II), chromium (III), nickel (II) and lead (II) ions from aqueous solutions by meranti sawdust. *Journal of Hazardous Materials*, *170*(2–3), 969–977.

Rahman, M. S., & Sathasivam, K. V. (2015). Heavy metal adsorption onto Kappaphycus sp. from aqueous solutions: the use of error functions for validation of isotherm and kinetics models. *BioMed Research International*, *2015*(1), 126298.

Rai, P. K., Lee, S. S., Zhang, M., Tsang, Y. F., & Kim, K.-H. (2019). Heavy metals in food crops: Health risks, fate, mechanisms, and management. *Environment International*, *125*, 365–385.

Rind, I. K., Khuhawar, M. Y., Jahangir, T. M., Memon, N., Habib, A., Lanjwani, M. F., Soomro, W. A., Suther, G., & Liu, W. (2024). Risk identification of salts and heavy metals in water by multivariate statistical techniques and GIS based interpolation: A case study of Saeedabad, Sindh, Pakistan. *Regional Studies in Marine Science*, *73*, 103492.

Rocky, M. M. H., Rahman, I. M. M., Biswas, F. B., Rahman, S., Endo, M., Wong, K. H., Mashio, A. S., & Hasegawa, H. (2023). Cellulose-based materials for scavenging toxic and precious metals from water and wastewater: A review. *Chemical Engineering Journal*, *472*, 144677.

Rosales, E., Ferreira, L., Sanromán, M. Á., Tavares, T., & Pazos, M. (2015). Enhanced selective metal adsorption on optimised agroforestry waste mixtures. *Bioresource Technology*, *182*, 41–49.

Saha, L., Kumar, V., Tiwari, J., Rawat, S., Singh, J., & Bauddh, K. (2021). Electronic waste and their leachates impact on human health and environment: Global ecological threat and management. *Environmental Technology & Innovation*, *24*, 102049.

Salazar-Rabago, J. J., Leyva-Ramos, R., Rivera-Utrilla, J., Ocampo-Perez, R., & Cerino-Cordova, F. J. (2017). Biosorption mechanism of Methylene Blue from aqueous solution onto White Pine (Pinus durangensis) sawdust: Effect of operating conditions. *Sustainable Environment Research*, *27*(1), 32–40.

Salman, M., Athar, M., & Farooq, U. (2015). Biosorption of heavy metals from aqueous solutions using indigenous and modified lignocellulosic materials. *Reviews in Environmental Science and Bio/Technology*, *14*, 211–228.

Sandulovici, R. C., Gălăţanu, M. L., Cima, L. M., Panus, E., Truţă, E., Mihăilescu, C. M., Sârbu, I., Cord, D., Rîmbu, M. C., & Anghelache, Ş. A. (2024). Phytochemical Characterization, Antioxidant, and Antimicrobial Activity of the Vegetative Buds from Romanian Spruce, Picea abies (L.) H. Karst. *Molecules*, *29*(9), 2128.

Satyam, S., & Patra, S. (2024). Innovations and challenges in adsorption-based wastewater remediation: a comprehensive review. *Heliyon*.

Sayed, I. R., Farhan, A. M., AlHammadi, A. A., El-Sayed, M. I., Abd El-Gaied, I. M., El-Sherbeeny, A. M., Al Zoubi, W., Ko, Y. G., & Abukhadra, M. R. (2022). Synthesis of novel nanoporous zinc phosphate/hydroxyapatite nano-rods (ZPh/HPANRs) core/shell for enhanced adsorption of Ni2+ and Co2+ ions: Characterization and application. *Journal of Molecular Liquids*, *360*, 119527.

Sellaoui, L., Guedidi, H., Reinert, L., Knani, S., Duclaux, L., & Lamine, A. Ben. (2016). Experimental and theoretical studies of adsorption of ibuprofen on raw and two chemically modified activated carbons: new physicochemical interpretations. *RSC Advances*, *6*(15), 12363–12373.

Semerjian, L. (2018). Removal of heavy metals (Cu, Pb) from aqueous solutions using pine (Pinus halepensis) sawdust: Equilibrium, kinetic, and thermodynamic studies. *Environmental Technology & Innovation*, *12*, 91–103.

Shankar, R., Pandiyan, P., & Malini, T. P. (2024). Study on the adsorption and photodegradation of ciprofloxacin using mesoporous Nd2O3/maleic hydrazide doped gC3N4 nanocomposite. *Diamond and Related Materials*, *149*, 111586.

Sherlala, A. I. A., Raman, A. A. A., Bello, M. M., & Buthiyappan, A. (2019). Adsorption of arsenic using chitosan magnetic graphene oxide nanocomposite. *Journal of Environmental Management*, *246*, 547–556.

Shi, K., Tao, X., Hong, F., He, H., Ji, Y., & Li, J. (2012). Mechanism of oxidation of low rank coal by nitric acid. *Journal of Coal Science and Engineering (China)*, *18*, 396–399.

Shukla, S. R., & Pai, R. S. (2005). Adsorption of Cu (II), Ni (II) and Zn (II) on modified jute fibres. *Bioresource Technology*, *96*(13), 1430–1438.

Singh, A., Chauhan, S., Varjani, S., Pandey, A., & Bhargava, P. C. (2022). Integrated approaches to mitigate threats from emerging potentially toxic elements: A way forward for sustainable environmental management. *Environmental Research*, *209*, 112844.

Song, S., Li, Q., Leslie, G., & Shen, Y. (2024). Water treatment methods in heavy metals removal during photovoltaic modules recycling: a review. *Resources, Conservation and Recycling*, *208*, 107701.

Taty-Costodes, V. C., Fauduet, H., Porte, C., & Delacroix, A. (2003). Removal of Cd (II) and Pb (II) ions, from aqueous solutions, by adsorption onto sawdust of Pinus sylvestris. *Journal of Hazardous Materials*, *105*(1–3), 121–142.

TOFAN, L., PĂDURARU, C., BUNIA, I. O. N., AMĂLINEI, R. L. M., & MIRON, A. (n.d.). *Pb (II) REMOVAL FROM AQUEOUS SOLUTIONS BY USING WASTES OF PINUS STROBUS BARK*.

Van Brahana, J. (2020). Hydrologic cycle. In *Fresh Water and Watersheds* (pp. 65–67). CRC Press.

Vishan, I., Saha, B., Sivaprakasam, S., & Kalamdhad, A. (2019). Evaluation of Cd (II) biosorption in aqueous solution by using lyophilized biomass of novel bacterial strain Bacillus badius AK: Biosorption kinetics, thermodynamics and mechanism. *Environmental Technology & Innovation*, *14*, 100323.

Wang, J., & Guo, X. (2020). Adsorption isotherm models: Classification, physical meaning, application and solving method. *Chemosphere*, *258*, 127279.

Wang, X. S., Li, Z. Z., & Sun, C. (2009). A comparative study of removal of Cu (II) from aqueous solutions by locally low-cost materials: marine macroalgae and agricultural by-products. *Desalination*, *235*(1–3), 146–159.

Weber Jr, W. J., & Morris, J. C. (1963). Kinetics of adsorption on carbon from solution. *Journal of the Sanitary Engineering Division*, *89*(2), 31–59.

Weber, W. J., & DiGiano, F. A. (1996). Process dynamics in environmental systems. *(No Title)*.

Weyrich, J. N., Mason, J. R., Bazilevskaya, E. A., & Yang, H. (2023). Understanding the mechanism for adsorption of Pb (II) ions by Cu-BTC metal–organic frameworks. *Molecules*, *28*(14), 5443.

Xu, D., Xu, Y., Zhao, A., Ke, H., Zhang, J., & Chen, H. (2011). Study on temporal cumulative effect of Cd content of soil under mining activity. *2011 International Symposium on Water Resource and Environmental Protection*, *3*, 1873–1876.

Yang, J.-S., Park, Y.-T., Baek, K., & Choi, J. (2010). Removal of metal ions from aqueous solutions using sawdust modified with citric acid or tartaric acid. *Separation Science and Technology*, *45*(12–13), 1963–1974.

Yao, C., & Zhu, C. (2021). A new multi-mechanism adsorption kinetic model and its relation to mass transfer coefficients. *Surfaces and Interfaces*, *26*, 101422.

Yu, H., Niu, S., Bai, T., Tang, X., & Lu, C. (2018). Microwave-assisted preparation of coal-based heterogeneous acid catalyst and its catalytic performance in esterification. *Journal of Cleaner Production*, *183*, 67–76.

Zaimee, M. Z. A., Sarjadi, M. S., & Rahman, M. L. (2021). Heavy metals removal from water by efficient adsorbents. Water, 13(19), 2659.

Zamora-Ledezma, C., Negrete-Bolagay, D., Figueroa, F., Zamora-Ledezma, E., Ni, M., Alexis, F., & Guerrero, V. H. (2021). Heavy metal water pollution: A fresh look about hazards, novel and conventional remediation methods. *Environmental Technology & Innovation*, *22*, 101504.

Zhang, P., Yang, M., Lan, J., Huang, Y., Zhang, J., Huang, S., Yang, Y., & Ru, J. (2023). Water quality degradation due to heavy metal contamination: Health impacts and eco-friendly approaches for heavy metal remediation. *Toxics*, *11*(10), 828.

Zheng, L., Ji, H., Gao, Y., Yang, Z., Ji, L., Zhao, Q., Liu, Y., & Pan, X. (2022). Effects of Modified Biochar on the mobility and speciation distribution of Cadmium in Contaminated Soil. *Processes*, *10*(5), 818.

Zhou, G., Li, S., Meng, Q., Niu, C., Zhang, X., & Wang, Q. (2023). A new type of highly efficient fir sawdust-based super adsorbent: Remove cationic dyes from wastewater. *Surfaces and Interfaces*, *36*, 102637.

Zhou, Y., Zhang, R., Gu, X., & Lu, J. (2015). Adsorption of divalent heavy metal ions from aqueous solution by citric acid modified pine sawdust. *Separation Science and Technology*, *50*(2), 245–252.

Zolgharnein, J., Asanjarani, N., & Shariatmanesh, T. (2013). Taguchi L16 orthogonal array optimization for Cd (II) removal using Carpinus betulus tree leaves: adsorption characterization. *International Biodeterioration & Biodegradation*, *85*, 66–77.

9. APPENDIXES

Table 9-1. Kinetic, isothermic and thermodynamics of (Cd (II), Pb (II), Cu (II), Zn (II)) ions using various types of L.C.B

Biosorbent Material	Target Metal Ion	Best-Fit Isotherm Model(s)	Best-Fit Kinetic Model	Thermodynamic Characteristics	**Reference**
Bark of *Pinus strobus* (Romania)	Pb (II)	Langmuir Freundlich	PSO	Spontaneous and endothermic	(TOFAN et al., 2009.)
Bark of *Pinus brutia*	Pb (II)	Langmuir	PSO	Endothermic	(Değirmen et al., 2012)
Bark of *Acacia leucocephala*	Cd (II) Pb (II) Cu (II)	Langmuir	PSO	Spontaneous and exothermic	(Munagapati et al., 2010)
Pinus sylvestris	Cu (II) Zn (II)	Langmuir	PSO	Spontaneous and endothermic	(Taty-Costodes et al., 2003)
Mixed agro-forestry residues	Cu (II) Zn (II)	Langmuir	PFO	Not Reported	(Rosales et al., 2015)
Pine bark wastes (Romania)	Cu (II) Zn (II)	Langmuir Freundlich	PSO	Spontaneous and endothermic	(Değirmen et al., 2012)
Pinecone biomass	Cu (II) Cd (II)	Langmuir and Freundlich	PSO	Spontaneous and endothermic	(Değirmen et al., 2012)
Peanut hull biomass	Cu (II)	Langmuir	PSO	Spontaneous and endothermic	(Adeyemo et al., 2014)
Various agricultural byproducts	Cu (II)	Langmuir	PSO	Spontaneous and endothermic	(X. S. Wang et al., 2009)
Sawdust from *Cedrus deodara*	Zn (II)	N.M	PSO	Spontaneous and endothermic	(Mishra et al., 2012)
Unmodified Pinecone	Cu (II)	Langmuir	PSO	Spontaneous and endothermic	(Adeyemo et al., 2014)
Sawdust from Beech wood	Cu (II) Zn (II)	Langmuir	PSO	Not Reported	(Božić et al., 2013)

I.M: Isotherm Model, **T.D.M**: Thermodynamic Model, **PSO:** Pseudo Second Order Kinetic Model, **SFO**: Pseudo First Order Kinetic Model, **L.C.B**: lignocellulosic Biomass, **K.M**: Kinetic Model, N.M: Not Mentioned.

Mixture of agroforestry wastes: Fern (**FE**), rice husk (**RI**) and oak leaves (**OA**), Agricultural by-products: (Laminaria japonica, P. yezoensis Ueda, rice bran, wheat bran and walnut hull).

The maximum adsorption capacities (Q) estimated from the Langmuir isotherm model for Cu (II), Pb (II) and Zn (II) were 3.89, 25.00 and 23.81 mg/g for Coconut tree sawdust (CTS), 34.48, 90.90 and 35.71 mg/g for Egg shell (ES), and 3.65, 21.28 and 40.00 mg/g on sugarcane bagasse (SB), respectively. The maximum adsorption capacity of Cu (II), Zn (II) and Cd (II) were found to be 14.53, 7.47 and 7.29 mg/g, respectively on walnut shell (Božić et al., 2009).

Table 9-2. Q_{max} values of some biomass.

Biosorbent Material	Q (mg/g)		
	Cu (II)	Pb (II)	Zn (II)
Bentonite	14.10	-	21.1
Pomegranate peel	1.31	13.87	-
Rice husk	-	0.62	19.61
Activated carbon derived from Cicer arietinum	17.77	20.69	19.93
Volcanic rock	10.87	9.52	4.46
Coir fibre	9.43	29.41	-
Phosphate rock	7.24	78.74	5.44
Poplar sawdust	3.24	-	-
Groundnut shells	4.46	-	7.62
Jute fibres	4.23		3.55
Polyporus tenoiculus	14.7	92	-
Tea waste	48	65	-
Cotton fibre	6.12	21.62	4.53
Chorella vulgaris	25.42	-	31.38
Residual biomass	28.34	92.20	25.37
*CTS	3.89	25.00	23.81
ES	34.48	90.90	35.71
SB	3.65	21.28	40.00

(CTS): Coconut tree sawdust**, (ES):** Egg shell**, (SB)**: Sugarcane Bagasse**.** (Putra et al 2014).

Various types of adsorbents and their Q_{max} values

HM & its corresponding q_{max} (mg/g)	**Adsorbent**	**Source**
Pb (II) 278	Eastern Spruce Sawdust (Turkey)	Bilgin et al.,2021
Pb (II) 17.37 Cu (II) 9.4	Albizia lebbeck Sawdust	(Nurnabi et al., 2020)
Cu (II) 4.94 Zn (II) 10.96	Dye-Unloaded Sawdust	(Shukla & Pai, 200a)
Pb (II) - Cu (II) -	(Pinus halepensis) sawdust	Semerjan, 2018
8.4, 5.95 Cu (II), Zn (II)	Modified jute fibres	(Shukla & Pai, 2005)
Cu 11 & Zn 4.9	Teakwood sawdust	(Shukla & Pai, 2005)
Pb (II) 9.9	Beech sawdust	(Božić et al., 2021)
Pb (II) 6.35 & Cd (II) 2.87	Picea smithiana sawdust	Mahmood-ul-Hassan et.al.,2018
Pb (II) 33.33	Raw Diabetou wood sawdust	(Adegoke et.al.,2022)
Pb (II) 15.5	*Algerian pine sawdust	(Nordineet.al.,2016)
Zn (II) 4.54 & Cu (II) 4.32	*Carpinus betulus	(Zolgharnein et al., 2013)
Pb (II) 10.1255 & Zn (II) 8.477 & Cd (II) 8.877	*Populus alba sawdust	(Najam & Andrabi, 2016)
Zn (II) 16.55	Lignin from Pinus elliottii sawdust	(Bortoluz et al., 2019)
Cd(II) 6.3& Cu(II) 7.9& Pb(II) 10.3 & Zn (II) 6.0	*Picea abies* (L.) Karst	**This study**

Table 9-3. Linear and nonlinear adsorption isotherm models.

Isothermal Model	Equation		Parameters	Findings
	Linear	Non-linear		
Langmuir	$\frac{C_e}{q_e} = \frac{1}{k_L q_m} + \frac{C_e}{q_m}$… [7] where q_m (mg/g) is the maximum adsorption capacity and K_L (L/mg) is Langmuir constant. q_m and K_L values can be determined from the slope and intercept of the linear plots of C_e /q_e against C_e.	$q_e = \frac{k_L q_m C_e}{(1 + k_L C_e)}$	q_e: is the equilibrium quantity of the adsorbate (mg. g-1). C_e: is the equilibrium concentration of the adsorbate (mg. L^{-1}). K_L: the constant of Langmuir isotherm. q_m: is the adsorption capacity (mg. g^{-1})	•Homogeneous surface of bio adsorbents. • Mono layer adsorption. •Adsorbate amount has no influence on the adsorption kinetic. •No interaction between the adsorbed molecules. •A dimensionless model.
Freundlich	$log q_e = log K_f + \frac{1}{n} log C_e$ …[8] K_f (mg/g) and n are Freundlich constants which are determined from the values of slope and intercept of the plots of log q_e against log C_e.	$q_e = K_F C_e^{\,1/n}$	K_f: the Freundlich isotherm constant, measured in units of mg. g^{-1}. n: denotes the adsorption intensity.	• Heterogeneous surface of biosorbent. • Multilayer adsorption with interaction between adsorbed molecules. • Used to describe the adsorption of organic and inorganic compounds on a wide variety of adsorbents. • Amount of adsorbate increases infinitely with an increase in concentration. • Used for lower concentration of metals. • A dimensionless model.
Temkin	$q_e = BlnA + BlnC_e$… [9] A is the equilibrium binding constant, and (B) is the Temkin constant being estimated from the slope and intercept of the plots of q_e against ln (C_e).	$q_e = BlnAC_e$	A: the binding constant (g^{-1}) when the system is at equilibrium. B: the adsorption heat.	• Describes adsorbate-adsorbent interaction. • Measuring binding energy. • Used to assess the relationship between the bioadsorbent surface and the adsorption heat of all molecules. • Estimate adsorption energy of all molecules in a layer. • Shows a linear decrease in heat of adsorption of all molecules with an increase in bioadsorbent surface coverage

Table 9-4. Model performance results using 6 regression models

Metal	Metric	Linear Regression	Decision Tree	Random Forest	Support Vector Regressor	Gradient Boosting	XGBoost
Cd	**MAE**	0.836	0.283	0.419	0.694	0.283	0.283
	MSE	1.166	0.161	0.401	1.284	0.161	0.162
	RMSE	1.080	0.401	0.633	1.133	0.401	0.402
	R^2 Score	0.484	0.929	0.823	0.432	0.929	0.929
Cu	**MAE**	0.885	0.359	0.519	0.924	0.359	0.359
	MSE	2.046	0.360	0.789	2.442	0.360	0.361
	RMSE	1.430	0.600	0.889	1.563	0.600	0.601
	R^2 Score	-0.021	0.820	0.606	-0.218	0.820	0.820
Pb	**MAE**	0.849	0.301	0.470	0.876	0.301	0.302
	MSE	1.819	0.270	0.659	2.176	0.270	0.270
	RMSE	1.349	0.519	0.812	1.475	0.519	0.520
	R^2 Score	0.015	0.854	0.643	-0.178	0.854	0.854
Zn	**MAE**	0.846	0.374	0.458	0.717	0.374	0.374
	MSE	1.337	0.299	0.496	1.396	0.299	0.299
	RMSE	1.156	0.546	0.704	1.182	0.546	0.547
	R^2 Score	0.428	0.872	0.788	0.403	0.872	0.872

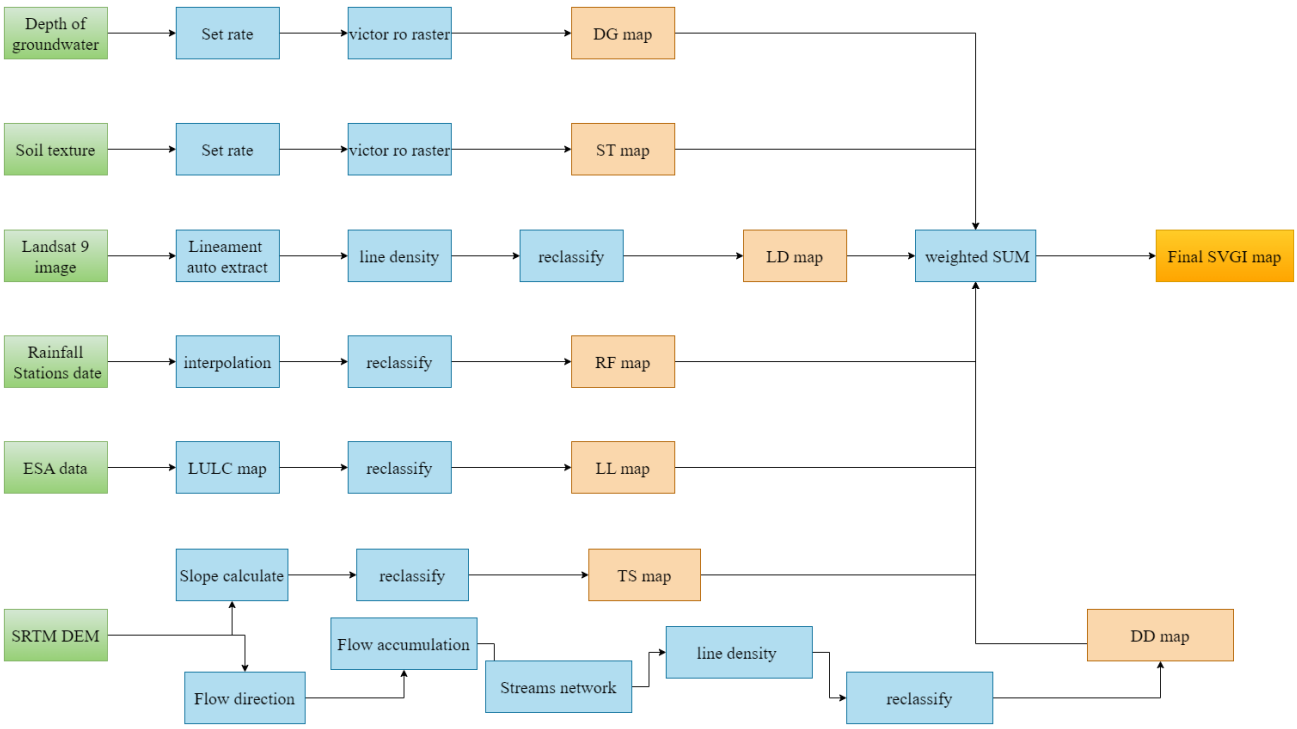

Figure A 9-1. Flowchart of the affecting parameters of SVGI.

Table 9-5. Sources of the data used in SGVI method.

Primary data	Source	Resolution
DEM	Shuttle Radar Topography Mission (SRTM)	30 m
LULC	European Space Agency (ESA)	10 m
Soil texture	The Food and Agriculture Organization (FAO)	-
Depth of Groundwater	previous study	(Assayed et al., 2022)
Rainfall	Jordan Meteorology Department records	1000m
Lineament	Landsat 9 and PCI geomatica software	-

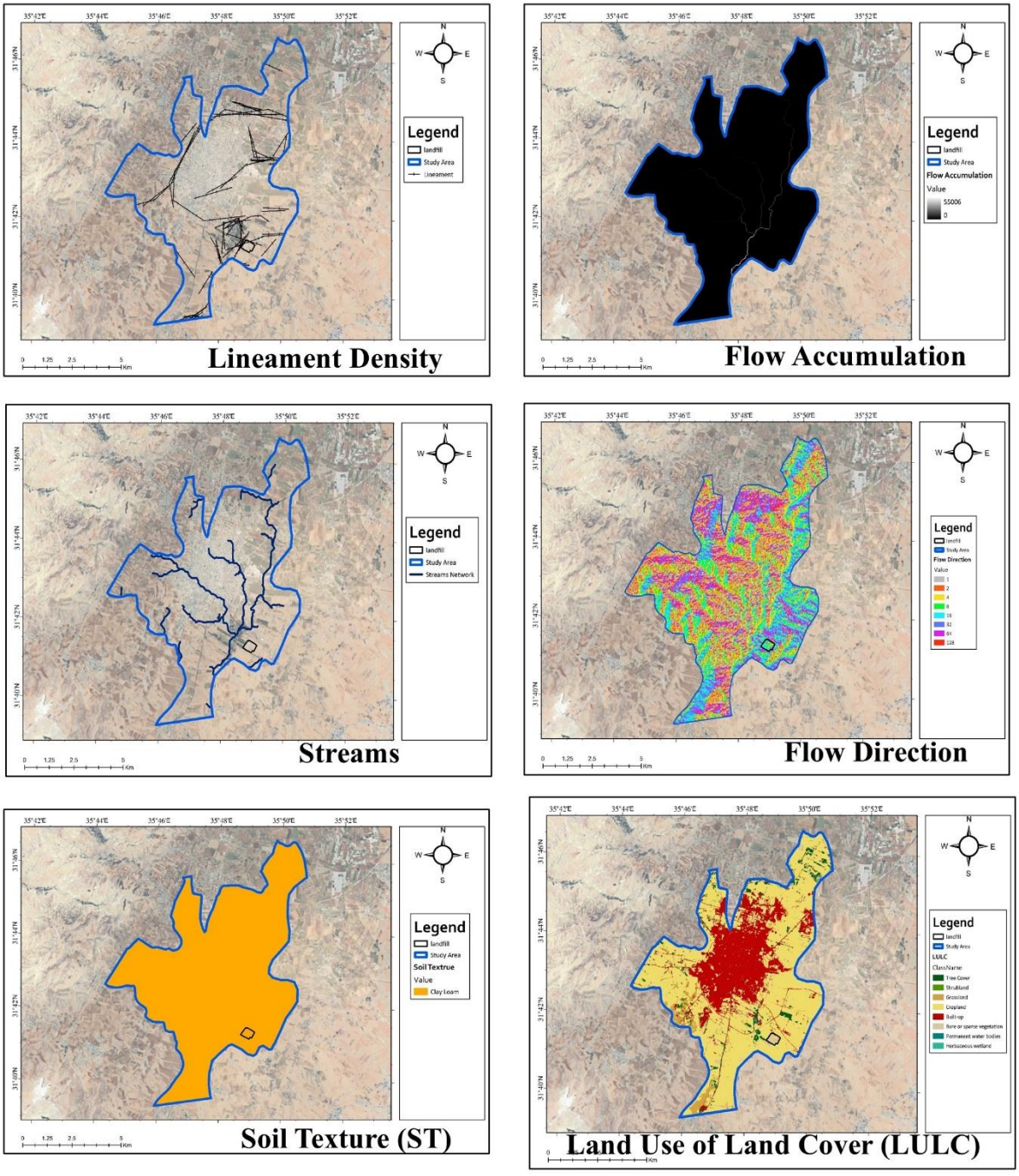

Figure A 9-2. Input thematic maps derived from GIS analysis for the Madaba landfill study area, utilized in the Simplified Groundwater Vulnerability Index (SGVI) assessment: Lineament Density, Flow Accumulation, Streams (Drainage Network), Flow Direction, Soil Texture (ST), and Land Use/Land Cover (LULC).

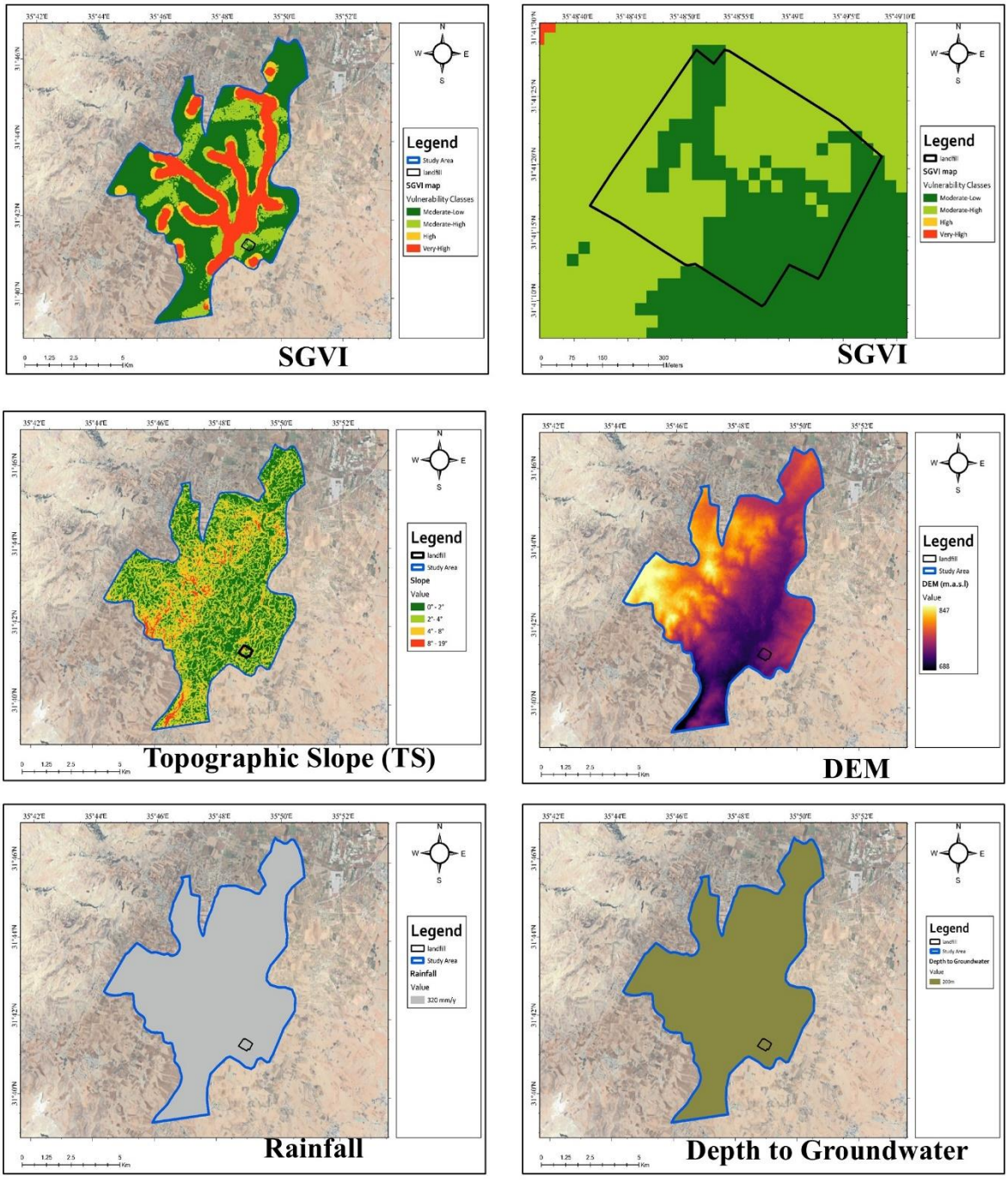

Figure A 9-3. Additional input thematic maps and the final derived Simplified Groundwater Vulnerability Index (SGVI) map for the Madaba landfill study area: Topographic Slope (TS), Digital Elevation Model (DEM), Rainfall, Depth to Groundwater, overall SGVI classification, and zoomed-in SGVI classification focused on the landfill site.

Table 9-6. Soil pollution risk assessment by PTEs

Indices	Values	Class	Pollution risk
Geoaccumulation index, Igeo	Igeo<= 0	0	Unpolluted
	0 < Igeo < 1	1	Unpolluted to moderately polluted
	1 < Igeo < 2	2	Moderately polluted
	2 < Igeo < 3	3	Moderately too strongly polluted
	3 < Igeo < 4	4	Strongly polluted
	4 < Igeo < 5	5	Strongly to extremely polluted
	5 < Igeo	6	Extremely polluted
Pollution index, PI	PI < 1	1	Unpolluted
	1 < PI < 2	2	Slightly polluted
	2 < PI < 3	3	Moderately polluted
	PI < 3	4	Extremely polluted
Integrated pollution index,	IPI < 1	1	Unpolluted
	1 < IPI < 2	2	Moderately polluted
	IPI > 2	3	Extremely polluted

Source (Hussein et al., 2021)**.**